Naval Research Laboratory

Washington, DC 20375-5320

NRL/FR/7320--99-9695

Improving the Numerics of a Third-Generation Wave Action Model

W. ERICK ROGERS

Planning Systems Inc.
MSAAP Bldg. 9121
Stennis Space Center, MS

JAMES M. KAIHATU

Oceanography Division
Naval Research Laboratory
Stennis Space Center, MS

NICO BOOIJ
LEO HOLTHUIJSEN

Delft University of Technology
Hydromechanics Section
Stevinweg 1 2628 CN Delft, the Netherlands

December 3, 1999

REPORT DOCUMENTATION PAGE

Form Approved
OMB No. 0704-0188

1. AGENCY USE ONLY (*Leave Blank*)	2. REPORT DATE	3. REPORT TYPE AND DATES COVERED
	December 3, 1999	Oct. 1, 1997 — July 31, 1999

4. TITLE AND SUBTITLE

Improving the Numerics of a Third-Generation Wave Action Model

5. FUNDING NUMBERS

6. AUTHOR(S)

W. Erick Rogers, James M. Kaihatu,* Nico Booij,** and Leo H. Holthuijsen**

7. PERFORMING ORGANIZATION NAME(S) AND ADDRESS(ES)

Planning Systems Inc.
MSAAP Bldg. 9121
Stennis Space Center, MS 39529-5004

Naval Research Laboratory
Code 7322
Stennis Space Center, MS 39529-5004

8. PERFORMING ORGANIZATION REPORT NUMBER

NRL/FR/7320--99-9695

9. SPONSORING/MONITORING AGENCY NAME(S) AND ADDRESS(ES)

Office of Naval Research
800 N. Quincy Street
Arlington, VA 22217

10. SPONSORING/MONITORING AGENCY REPORT NUMBER

11. SUPPLEMENTARY NOTES

*Oceanography Division, Code 7322, Naval Research Laboratory, Stennis Space Center, MS
**Delft University of Technology, Hydromechanics Section, Stevinweg 1 2628 CN Delft, the Netherlands

12a. DISTRIBUTION/AVAILABILITY STATEMENT

Approved for public release; distribution unlimited.

12b. DISTRIBUTION CODE

13. ABSTRACT (*Maximum 200 words*)

A higher order numerical scheme for geographic wave action propagation is chosen as a potential alternative to the existing scheme in the third-generation wave action model SWAN. The chosen scheme is a cyclic hybrid of upwind and centered differencing. The SWAN model with the new scheme (dubbed "SWAN-X") is tested against analytical solutions and experimental (lab and field) data. SWAN-X requires significantly more computational time than SWAN (primarily in stationary mode), since nonphysical oscillations are manifested with high Courant numbers despite the stability of the scheme. It is felt that the advantages of the scheme are best seen in large-scale propagation problems and in wave propagation over rugged bathymetry and/or islands. For most situations over the continental shelf and in nearshore areas, SWAN-X exhibits greater variability than SWAN — an indication of reduced numerical diffusion. Artificial diffusion techniques to combat the "garden sprinkler effect" are discussed.

14. SUBJECT TERMS

Wave action model
Model validation
Higher order numerical scheme

15. NUMBER OF PAGES

84

16. PRICE CODE

17. SECURITY CLASSIFICATION OF REPORT	18. SECURITY CLASSIFICATION OF THIS PAGE	19. SECURITY CLASSIFICATION OF ABSTRACT	20. LIMITATION OF ABSTRACT
UNCLASSIFIED	UNCLASSIFIED	UNCLASSIFIED	UL

NSN 7540-01-280-5500

Standard Form 298 (Rev. 2-89)
Prescribed by ANSI Std 239-18
298-102

CONTENTS

IMPROVING THE NUMERICS OF A THIRD-GENERATION WAVE ACTION MODEL

1. INTRODUCTION

"SWAN" (Simulated WAves Nearshore) was created at the Delft University of Technology as an extension of third-generation hyperbolic wave action models to shallow water regions (e.g., Booij et al. 1996). The model has recently become available in the public domain, although further model development and improvement continues. The numerical scheme for spatial wave action propagation used by the model is one of several aspects currently being improved. Originally, an implicit, first order, upwind numerical scheme was chosen for the model due to the stability and low computational cost of the scheme. The unconditional stability of the scheme makes the model suitable for use in shallow water, where conditionally stable models (e.g., WAM, WAMDI Group 1988) may become prohibitively expensive. The primary drawback of this scheme is its relatively high rate of numerical diffusion. This diffusion is a major obstacle to the use of SWAN for larger scale applications. We have incorporated a feature into an experimental version of the model that gives the user the option of using a higher order and less diffusive numerical scheme—a cyclic scheme taken from the work of Stelling and Leendertse (1992).

2. MODEL DESCRIPTION

Thorough description and validation of the wave model prior to the addition of the higher order numerical scheme can be found in the literature (Ris 1997, Booij et al. 1999). Herein, we will only give detailed attention to those aspects of the model that are relevant to the geographic propagation of wave action.

"SWAN" refers to the official version v30.75 of the code. "SWAN-X33" is an unofficial extension of v30.75, modified by the authors. This code allows the use of either the original propagation scheme or the higher order propagation scheme. Unless otherwise noted, "SWAN-X" or "SWAN-X33" herein refers to the unofficial model with the higher order scheme activated. The changes made by the authors are presented in Appendix A.

2.1 Governing Equation: Action Balance

SWAN is governed by a two-dimensional wave action density spectrum

$$N(x,y,\sigma,\theta) = E(x,y,\sigma,\theta) / \sigma, \tag{1}$$

Manuscript approved August 5, 1999.

where x and y denote geographic location, σ is the relative frequency, and θ is the direction of propagation. Wave action is propagated in geographic and spectral space, while source and sink terms act on the waves. The action balance equation, in horizontal Cartesian coordinates *(x,y)*, can be written as

$$\frac{\partial}{\partial t}N + \frac{\partial}{\partial x}c_x N + \frac{\partial}{\partial y}c_y N + \frac{\partial}{\partial \sigma}c_\sigma N + \frac{\partial}{\partial \theta}c_\theta N = \frac{S}{\sigma}, \tag{2}$$

(e.g., Whitham 1974; Phillips 1977; Mei 1983; Hasselmann et al. 1973). Here, t denotes time, and S denotes the total of source and sink terms. The first term represents the local rate of change; the second and third terms represent geographic propagation; the fourth term represents changes to relative frequency (e.g., by nonstationary depth or by currents); the fifth term represents refraction (by depth and currents). The four propagation speeds are shown below (as derived from linear wave theory, e.g., Whitham 1974; Mei 1983).

Propagation speed in x-space:

$$C_x = \frac{dx}{dt} = \frac{1}{2}\left[1 + \frac{2kd}{\sinh 2kd}\right]\frac{\sigma k_x}{k^2} + U_x. \tag{3}$$

Propagation speed in y-space:

$$C_y = \frac{dy}{dt} = \frac{1}{2}\left[1 + \frac{2kd}{\sinh 2kd}\right]\frac{\sigma k_y}{k^2} + U_y. \tag{4}$$

Propagation speed in sigma-space:

$$C_\sigma = \frac{d\sigma}{dt} = \frac{\partial \sigma}{\partial d}\left[\frac{\partial d}{\partial t} + \overline{U} \bullet \nabla d\right] - c_g \overline{k} \bullet \frac{\partial \overline{U}}{\partial s}. \tag{5}$$

Propagation speed in theta-space:

$$C_\theta = \frac{d\theta}{dt} = -\frac{1}{k}\left[\frac{\partial \sigma}{\partial d}\frac{\partial d}{\partial m} + \overline{k} \bullet \frac{\partial \overline{U}}{\partial m}\right]. \tag{6}$$

Here, $\overline{k} = (k_x, k_y)$ is the wave number with magnitude k (related to σ through the dispersion relationship of linear wave theory), d is water depth, $\overline{U} = (U_x, U_y)$ is the current velocity, s is the space coordinate in direction θ, and m is a coordinate normal to s. The operator d/dt denotes the total derivative along a spatial path of action propagation, and it is defined as:

$$\frac{d}{dt} = \frac{\partial}{\partial t} + C_g \bullet \nabla_{x,y}, \tag{7}$$

where $C_g = \bar{k}/k \cdot \partial\sigma/\partial k$ is the group velocity. The term *S* represents all source/sink terms that act on the action balance equation. These terms include wind input, dissipation (by whitecapping, bottom friction, and depth-induced breaking), and nonlinear wave-wave interactions (triads and quadruplets). Detailed description of these terms and how they are implemented in SWAN can be found in Ris (1997) and Booij et al. (1999).

2.2 Treatment of Wave Phase

The wave action balance equation is a phase-averaged formulation. This has the advantage of not hindering the model with the severe (subwavelength) resolution requirements that are typical of phase-resolving models. Unfortunately, use of the phase-averaged formulation means that wave diffraction cannot be treated implicitly in the model governing equation. There are tentative plans to add diffraction to a later version of SWAN in a parameterized, explicit manner (this is discussed further in Appendix B).

2.3 Numeric Formulation of Propagation

An implicit upwind difference scheme is used for geographic and spectral propagation (the latter is supplemented with a centered scheme). This scheme, also know as the Backward Space, Backward Time (BSBT) scheme, has the advantage of being unconditionally stable (i.e., no maximum time step size required for stability). This is advantageous when modeling coastal regions (where spatial resolution is typically fine), as it can be much more economical than a conditionally stable scheme.

The finite difference formulation of the governing equation is (from Booij et al. 1999):

$$\left[\frac{N^n - N^{n-1}}{\Delta t}\right]_{i_x,i_y,i_\sigma,i_\theta} + \left[\frac{[c_x N]_{i_x} - [c_x N]_{i_x-1}}{\Delta x}\right]_{i_y,i_\sigma,i_\theta} + \left[\frac{[c_y N]_{i_y} - [c_y N]_{i_y-1}}{\Delta y}\right]_{i_x,i_\sigma,i_\theta}$$
$$+\left[\frac{(1+\upsilon)[c_\sigma N]_{i_\sigma+1} - 2\upsilon[c_\sigma N]_{i_\sigma} - (1-\upsilon)[c_\sigma N]_{i_\sigma-1}}{2\Delta\sigma}\right]^n_{i_x,i_y,i_\theta} + \left[\frac{(1+\eta)[c_\theta N]_{i_\theta+1} - 2\eta[c_\theta N]_{i_\theta} - (1-\eta)[c_\theta N]_{i_\theta-1}}{2\Delta\theta}\right]^n_{i_x,i_y,i_\sigma} \quad (8)$$
$$= \left[\frac{S}{\sigma}\right]^n_{i_x,i_y,i_\sigma,i_\theta},$$

where *n* is a time-level index; i_x, i_y, i_σ, and i_θ are grid counters; and Δx, Δy, $\Delta\sigma$, and $\Delta\theta$ are increments in time, geographic space, and spectral space, respectively.

In spectral space, the user has the option of supplementing the implicit upwind scheme with an implicit centered difference scheme. The result is a less diffusive propagation in spectral space, but a greater likelihood of spurious oscillations. The coefficients υ and η are weighting factors, controlling the relative weight of the two finite difference schemes in frequency and directional space, respectively.

2.4 Model Execution

2.4.1 Nonstationary Mode

Running SWAN in nonstationary mode is a simple matter of time stepping. The user specifies time step increment, simulation begin-time, and end-time. Each time step involves simple sweeping in geographic space and solution of a matrix for $N(\sigma,\theta)$ at each geographic grid location. The simple sweeping in geographic space can be used with the upwind implicit numerical scheme because $N(x_i,y_j,t_n) = f\,[N(x_{i-1},y_j,t_n)$,

$N(x_i,y_{j-1},t_n)$, $N(x_i,y_j,t_{n-1})$], all three of which are known. Directional space is divided into four quadrants that are solved independently (except for interactions across the quadrant boundaries, which must be accounted for). If currents are present or if depth is not stationary, solution of a banded matrix is required. Otherwise, a simple tridiagonal matrix is solved. The user has the option of using a set number of iterations at each time step; using these iterations, the model more accurately accounts for interactions across the internal boundaries in spectral space. Multiple iterations at each time step are generally not used in nonstationary mode, under the assumption that large changes do not occur from one time step to the next.

The sequence of operations in nonstationary mode can be summarized in pseudo-code as:

```
DO TIME LOOP
DO ITERATION LOOP (generally one iteration only)
        DO QUADRANT LOOP (4 times, once per quadrant/sweep direction)
            DO GEOGRAPHIC SPACE LOOPS
                Calculate propagation and source terms.
                Solve matrix for N(σ,θ).
(END LOOPS)
```

2.4.2 Stationary Mode

The stationary mode of SWAN differs from the nonstationary mode in two respects. Firstly, there is no time stepping (the solution is steady state). Secondly, iterations are required in stationary mode.

In stationary mode, the model is solved by simply sweeping through the geographic grid, with spectral propagation being solved independently at each grid point. As in nonstationary mode, directional space is divided into four quadrants. Multiple iterations are necessary to fully propagate energy in spectral space. Iterations allow transfer of energy across sector boundaries and facilitate the migration of energy in frequency space due to nonlinear interactions.

Convergence criteria are used to determine when to stop the iterations. Convergence criteria are based on a) relative and absolute changes in wave height between iterations, and b) relative and absolute changes in mean wave period. If convergence is not reached in a user-specified maximum number of iterations, the program terminates.

2.5 Model Limitations

2.5.1 Deficiencies of SWAN at Oceanic Scales

The SWAN model has a few noteworthy shortcomings, which tend to prohibit its use as a general-purpose wave model, suitable for both shelf-scale applications *O* (10 km) and ocean-scale applications *O* (1000 km).

2.5.1.1 Diffusion

The low computational cost and the unconditional stability of the upwind implicit scheme that SWAN uses for geographic propagation comes at a price—namely, a high degree of numerical diffusion. The term "diffusion" is used herein to describe the smoothing of wave action in space. "Numerical diffusion" refers to diffusion caused by inaccuracy of a numerical scheme. "Physical diffusion" does not exist in SWAN, as the governing equations are equations of advection rather than advection-diffusion; thus all diffusion in SWAN is numerical. In this report, we are primarily concerned with the numerical diffusion by SWAN in geo-

graphic space (as opposed to spectral space). It should be noted that the numerical diffusion in SWAN is a mass-conserving process: wave action is not lost through diffusion, except in cases where wave action moves out of the system through the open boundaries as a result of diffusion.

Figure 1 shows a severe example of this numerical diffusion. As evidenced by the scale of Fig. 1, this diffusion is not, strictly speaking, related to scale. However, two factors make diffusion a greater concern at oceanic scales than at shelf scales:

1. Diffusion is exacerbated by nonstationary input conditions, which are more typical for larger-scale applications.
2. Grid point-to-grid point variations in wave energy, either locally generated or specified at the boundaries, are typically greater for larger scale applications. This results in a higher rate of diffusion.

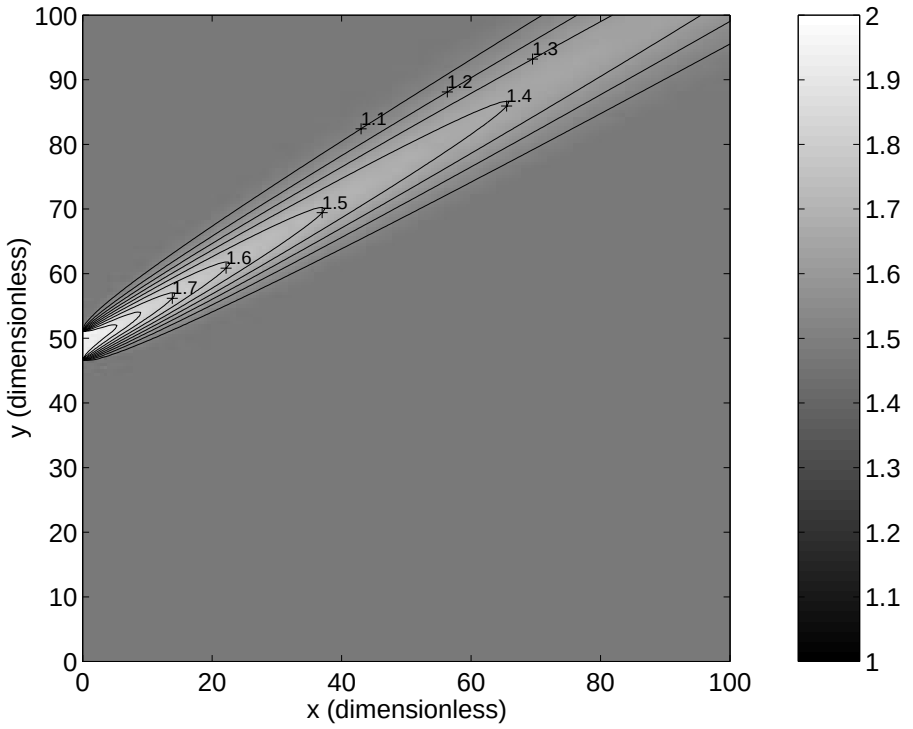

Fig. 1 — Idealized test case: propagation of wave energy past a submerged breakwater with a gap using the diffusive first order upwind scheme. Wave energy is shown. Energy is specified at the left ($x = 0$) boundary: energy = 2 at gap, energy = 1 elsewhere. Energy is propagated at an angle with the grid. Model parameters: CFL = 1.4; $C_g = 8.0$ (dimensionless); $dx = dy = 0.5$ (dimensionless); direction of transport theta = 35 degrees from x axis; and 201 grid points in x; and 201 grid points in y. Distance is nondimensionalized by Courant number.

Increasing the applicability of SWAN by reducing this numerical diffusion is the primary focus of this report.

2.5.1.2 Nonstationary Input at Boundaries

Nonstationary input at boundaries has not yet been implemented in SWAN (except in the context of nested simulations). At the large time scales of oceanic applications, this is a rather severe omission. Currently, there are plans to implement nonstationary boundary input in a public version to be released in 1999.

2.5.1.3 Spherical Coordinates

The curvature of the Earth becomes important at larger geographic scales. Therefore, ocean-scale wave models (e.g., WAMDI 1988) are typically calculated in spherical coordinates. The present version of SWAN does not allow for spherical coordinates, although there are plans for a future version that will.

2.5.2 Other Limitations

2.5.2.1 Diffraction

As stated in Section 2.2, diffraction cannot be included implicitly in the governing equation of a hyperbolic wave model such as SWAN. The developers of SWAN are, however, investigating the possibility of including diffraction in parameterized form in a later release of SWAN.

2.5.2.2 Open Boundaries

Boundary conditions in both geographic and spectral space are fully absorbing. Wave energy enters the domain along the open boundaries only if specified by the user. Thus, when the lateral boundaries are not specified, this generally results in a shadow-region adjacent to one or both of the lateral boundaries.

Awareness of this feature is especially important for coastal simulations. In a typical coastal simulation, the model user prescribes wave conditions along only the offshore boundary of a rectangular grid domain (e.g., Fig. 2). In order to prevent the shadow-region from influencing the region of interest (which is often close to shore), the user must increase the lateral extent of the domain. Specifying wide directional spectra (e.g., -80° to +80°) as model input along a single open boundary would require the use of a domain with a wide aspect ratio.

2.5.2.3 Hydrodynamics

SWAN does not attempt to quantify the effect of wave climate on circulation in the domain. This is well beyond the scope of the model. Currents are present as input only.

3. CHOOSING THE NEW SCHEME

The purpose of this study is to reduce the artificial numerical diffusion in SWAN by replacing the diffusive, upwind, implicit scheme (used for geographic propagation of wave energy) with a less diffusive, higher-order numerical scheme. To this end, we have evaluated the capabilities of various potential replacement schemes. First, we compared a range of schemes in one-dimensional mode. Then we conducted two-dimensional tests using several of the more promising schemes.

3.1 Tests of One-Dimensional Propagation

3.1.1 Description of One-Dimensional Tests

Two basic types of one-dimensional tests were performed:

1. A spike of wave energy defined as the initial condition of the model:

$$N(x) = \{64 \times [(x - 0.5)^2 - 1/64]\}^2 \text{ if } 3/8 \le x \le 5/8,$$
$$N(x) = 0 \text{ otherwise.} \tag{9}$$

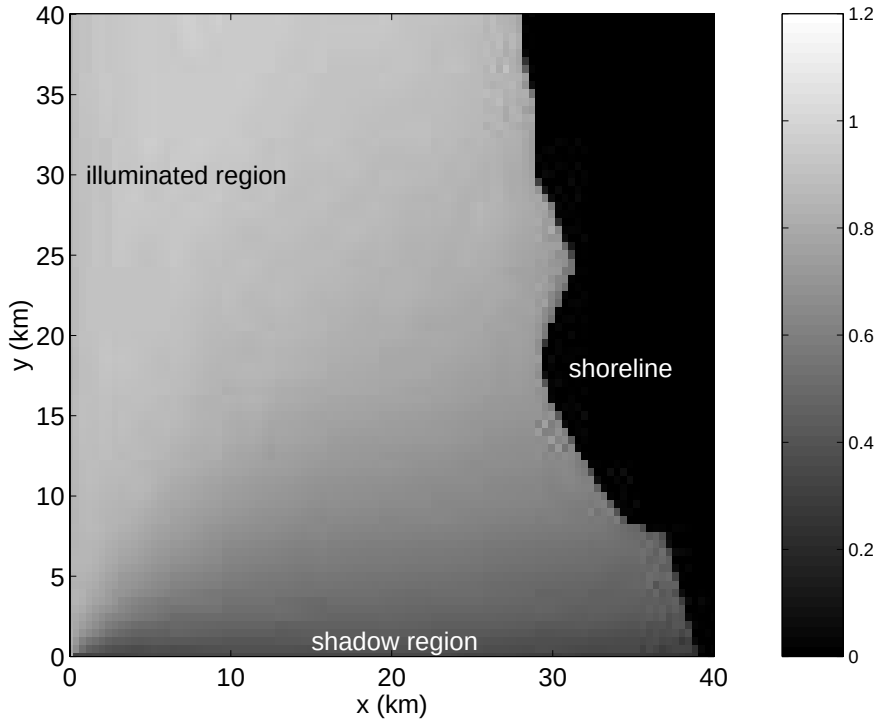

Fig. 2 — An example of the shadow region created if wave energy is not specified along the lateral boundaries. Waveheight, H_{mo}, is shown. Here, input is specified at the left ($x = 0$) boundary, and is not specified at the (y = 0) boundary or the (y = 40 km) boundary. The (x = 40 km) boundary lies on land. There is a gradual transition between the illuminated region and shadow region due to the broadness of the input directional spectra and, to a lesser extent, numerical diffusion.

A single group velocity, C_g, is specified and the spike is then propagated by time stepping. N at the two boundaries is set to zero for all time steps.

2. A sinusoidal variation of wave energy is defined as an unsteady open boundary condition:

$$N_{x=0} = 1 + 0.1 \times \sin(\omega t). \tag{10}$$

The initial condition is a state of rest ($N(x)$=1 for all x).

3.1.2 Scheme Descriptions and Observations of Performance

The numerical schemes are described in the following paragraphs. The advantages and disadvantages of each scheme are listed. These are based on preliminary knowledge of accuracy and stability conditions, as well as observations of one-dimensional test results.

Where possible, the finite difference approximations of spatial and temporal derivatives are given separately. In the context of the one-dimensional tests, these approximations are used in the one-dimensional hyperbolic simple wave equation:

$$\frac{\partial N}{\partial t} + C_g \frac{\partial N}{\partial x} = 0. \tag{11}$$

Stability requirements stated in this section are only applicable to the one-dimensional simple wave equation.

3.1.2.1 BSBT (Backward Space, Backward Time)

Also known as the first-order, upwind implicit scheme, this is the numerical scheme used for geographic propagation in SWAN. Approximations to the derivatives using this scheme are:

$$\frac{\partial N}{\partial t} \approx \frac{N_i^n - N_i^{n-1}}{\Delta t} \tag{12}$$

and

$$\frac{\partial N}{\partial x} \approx \frac{N_i^n - N_{i-1}^n}{\Delta x}. \tag{13}$$

Advantages:

- Compact: requires only three points (ideal for use at boundaries)
- Fast computationally
- Unconditionally stable

Disadvantages:

- Severe numerical diffusion

3.1.2.2 Second-Order, Upwind, Implicit

This scheme is the second-order extension of the BSBT scheme (e.g., Roache 1972). Applied to the one-dimensional simple wave equation, the scheme gives:

$$N_i^n \approx N_i^{n-1} - \mu(N_i^n - N_{i-1}^n) - \tfrac{1}{2}\mu(\mu+1)(N_i^n - 2N_{i-1}^n + N_{i-2}^n). \tag{14}$$

Advantages:

- Unconditionally stable
- Less diffusive than BSBT scheme

Disadvantages:

- High rate of diffusion relative to most other higher-order schemes
- Unlike the first-order scheme, creates nonphysical oscillations

3.1.2.3 SL1: Stelling and Leendertse (q_0= 0, q_1= 1/6)

This scheme is taken from the work of Stelling and Leendertse (1992), using the parameters q_0 = 0 and q_1 = 1/6 in the derivation. The scheme uses a four-point upwind differencing at time level t_n and a three point centered differencing at time level t_{n-1}:

$$\frac{\partial N}{\partial t} \approx \frac{N_i^n - N_i^{n-1}}{\Delta t} \tag{15}$$

and

$$\frac{\partial N}{\partial x} \approx \frac{1}{2}\left(\frac{N_{i+1}^{n-1} - N_{i-1}^{n-1}}{2\Delta x} + \frac{10N_i^n - 15N_{i-1}^n + 6N_{i-2}^n - N_{i-3}^n}{6\Delta x} \right). \tag{16}$$

Advantages:

- Unconditionally stable
- Less diffusive than BSBT scheme

Disadvantages:

- Some numerical diffusion (increasing with higher Courant numbers and lower resolution). At higher Courant numbers, this diffusion is large relative to most other schemes tested.
- Some nonphysical oscillations.

Figure 3 shows example comparisons of BSBT and SL1 solutions.

3.1.2.4 SL2: Stelling and Leendertse (q_0= 0, q_1= 0)

This scheme employs a three-point upwind differencing at time level t_n and a three-point centered differencing at time level t_{n-1}:

$$\frac{\partial N}{\partial t} \approx \frac{N_i^n - N_i^{n-1}}{\Delta t} \tag{17}$$

and

$$\frac{\partial N}{\partial x} \approx \frac{1}{2}\left(\frac{N_{i+2}^{n-1} + 4N_{i+1}^{n-1} - 4N_{i-1}^{n-1} - N_{i-2}^{n-1}}{12\Delta x} + \frac{3N_i^n - 4N_{i-1}^n + N_{i-2}^n}{2\Delta x} \right). \tag{18}$$

Advantages:

- Unconditionally stable
- Fewer nonphysical oscillations than SL1 at higher Courant numbers

Disadvantages:

- Some numerical diffusion (more than the SL1 scheme)

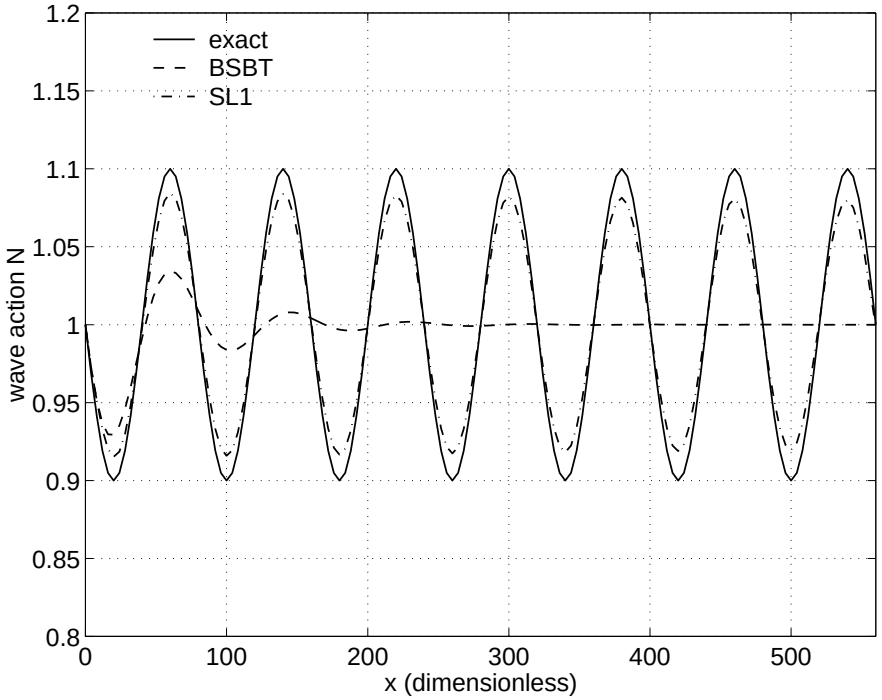

Fig. 3 — A one-dimensional sinusoidal test case comparing the BSBT and SL1 schemes. Model parameters: CFL= 0.5; C_g = 8.0 (dimensionless); Δx = 4 (dimensionless); 20 points per wavelength.

3.1.2.5 SL3: Stelling and Leendertse (q_0= -1/6, q_1= 0)

This scheme employs a three-point upwind differencing at time level t_n and a five-point centered differencing at time level t_{n-1}:

$$\frac{\partial N}{\partial t} \approx \frac{N_i^n - N_i^{n-1}}{\Delta t} \tag{19}$$

and

$$\frac{\partial N}{\partial x} \approx \frac{1}{2}\left(\frac{N_{i+1}^{n-1} - N_{i-1}^{n-1}}{2\Delta x} + \frac{3N_i^n - 4N_{i-1}^n + N_{i-2}^n}{2\Delta x} \right). \tag{20}$$

Advantages:

- Unconditionally stable
- Fewer nonphysical oscillations than SL1 at higher Courant numbers

Disadvantages:

- Some numerical diffusion (more than the SL1 scheme)

Figure 4 shows some example comparisons of the Stelling and Leendertse schemes.

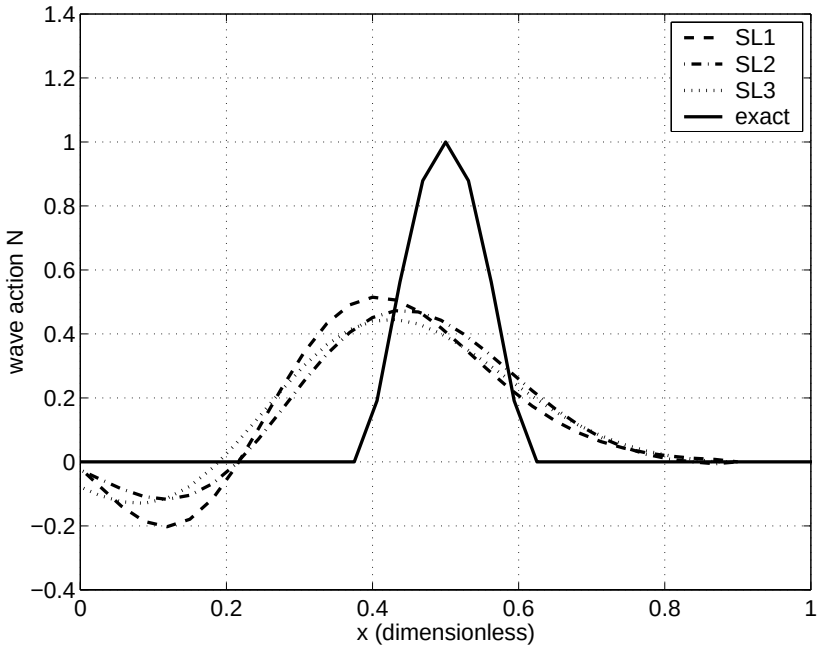

Fig. 4 — A one-dimensional spike propagation test case comparing the three Stelling and Leendertse schemes. Model parameters: CFL = 1.6; C_g = 8 (dimensionless); Δx = 1/32 (dimensionless).

3.1.2.6 Box

The Box scheme (e.g., Petit 1997) is a compact scheme which uses a two-point upwind differencing at both time level t_n and at time level t_{n-1}:

$$\frac{\partial N}{\partial t} \approx \frac{1}{2}\left(\frac{N_i^n - N_i^{n-1}}{\Delta t} + \frac{N_{i-1}^n - N_{i-1}^{n-1}}{\Delta t} \right) \tag{21}$$

and

$$\frac{\partial N}{\partial x} \approx \frac{1}{2}\left(\frac{N_i^n - N_{i-1}^n}{\Delta x} + \frac{N_i^{n-1} - N_{i-1}^{n-1}}{\Delta x} \right). \tag{22}$$

Advantages:

- Unconditionally stable
- Good diffusion characteristics at all resolutions; in general, less diffusive than the SL1 scheme
- Compact (ideal for use at boundaries)

Disadvantages:

- Relatively high amount of nonphysical oscillation, especially at higher Courant numbers
- Phase speed error is significant at lower Courant numbers

3.1.2.7 Theta-Box

Theta-Box (e.g., Petit 1997) is a generalized form of the Box scheme, weighting the (t_n) differencing and the (t_{n-1}) differencing in the spatial derivative using a coefficient θ:

$$\frac{\partial N}{\partial t} \approx \frac{1}{2}\left(\frac{N_i^n - N_i^{n-1}}{\Delta t} + \frac{N_{i-1}^n - N_{i-1}^{n-1}}{\Delta t} \right) \tag{23}$$

and

$$\frac{\partial N}{\partial x} \approx \frac{1}{2}\left(\theta \frac{N_i^n - N_{i-1}^n}{\Delta x} + (1-\theta) \frac{N_i^{n-1} - N_{i-1}^{n-1}}{\Delta x} \right). \tag{24}$$

Advantages:

- In general, less diffusive than the SL1 scheme
- Compact (ideal for use at boundaries)
- Unconditionally stable for θ ≥ 0.5

Disadvantages:

- Relatively high amount of nonphysical oscillation
- At θ ≠ 0.5, this scheme generally performed worse than the standard Box scheme (θ = 0.5)

3.1.2.8 Crank-Nicholson

The Crank-Nicholson scheme (e.g., Roache 1972) is a computationally implicit scheme (*N* values at time level t_n cannot be solved independently), the components of which are:

$$\frac{\partial N}{\partial t} \approx \frac{N_i^n - N_i^{n-1}}{\Delta t} \tag{25}$$

and

$$\frac{\partial N}{\partial x} \approx \frac{1}{2}\left(\frac{N_{i+1}^n - N_{i-1}^n}{2\Delta x} + \frac{N_{i+1}^{n-1} - N_{i-1}^{n-1}}{2\Delta x} \right). \tag{26}$$

Advantages:

- Unconditionally stable

Disadvantages:

- Very slow. Because Crank-Nicholson is a computationally implicit scheme, a matrix solver is required.
- Moderate amount of diffusion
- Large amount of nonphysical oscillation

3.1.2.9 Borsboom

The Borsboom scheme (e.g., Petit 1997) is another computationally implicit scheme. It is similar to the Crank-Nicholson scheme, with a time derivative that is spatially weighted:

$$\frac{\partial N}{\partial t} \approx \frac{1}{6}\left(\frac{N_{i+1}^{n} - N_{i+1}^{n-1}}{\Delta t}\right) + \frac{4}{6}\left(\frac{N_{i}^{n} - N_{i}^{n-1}}{\Delta t}\right) + \frac{1}{6}\left(\frac{N_{i-1}^{n} - N_{i-1}^{n-1}}{\Delta t}\right) \tag{27}$$

and

$$\frac{\partial N}{\partial x} \approx \frac{1}{2}\left(\frac{N_{i+1}^{n} - N_{i-1}^{n}}{2\Delta x} + \frac{N_{i+1}^{n-1} - N_{i-1}^{n-1}}{2\Delta x}\right). \tag{28}$$

Advantages:

- Unconditionally stable
- Less diffusive than Crank-Nicholson or SL1

Disadvantages:

- Very slow (in terms of CPU time, it is the most expensive of all schemes tested here)
- Moderate nonphysical oscillation

Figure 5 compares the SL1 scheme to the two computationally implicit schemes.

3.1.2.10 NISL: Non-Interpolating Semi-Lagrangian

This scheme, from Olim (1994), is a modification of the Lax-Wendroff method. It uses a finite differencing based on three centered upwind points at a distance in the grid determined by the Courant number. At time level t_n, the scheme "looks back" along the characteristic line to three neighboring points at time level t_{n-1}. The application of the scheme to the one-dimensional simple wave equation is written as:

$$N_i^n \approx N_{i-p}^{n-1} - \tfrac{1}{2}(\mu - p)(N_{i-p+1}^{n-1} - N_{i-p-1}^{n-1}) + \tfrac{1}{2}(\mu - p)^2(N_{i-p+1}^{n-1} - 2N_{i-p}^{n-1} - N_{i-p-1}^{n-1}), \tag{29}$$

where μ is the Courant number, $C\,\Delta t/\Delta x$, and p is the nearest integer to μ.

Advantages:

- Unconditionally stable
- No inherent upper limit to Courant number
- Exceptional performance at higher CFLs (e.g., at $\mu > 2$, performs better than any other scheme tested)

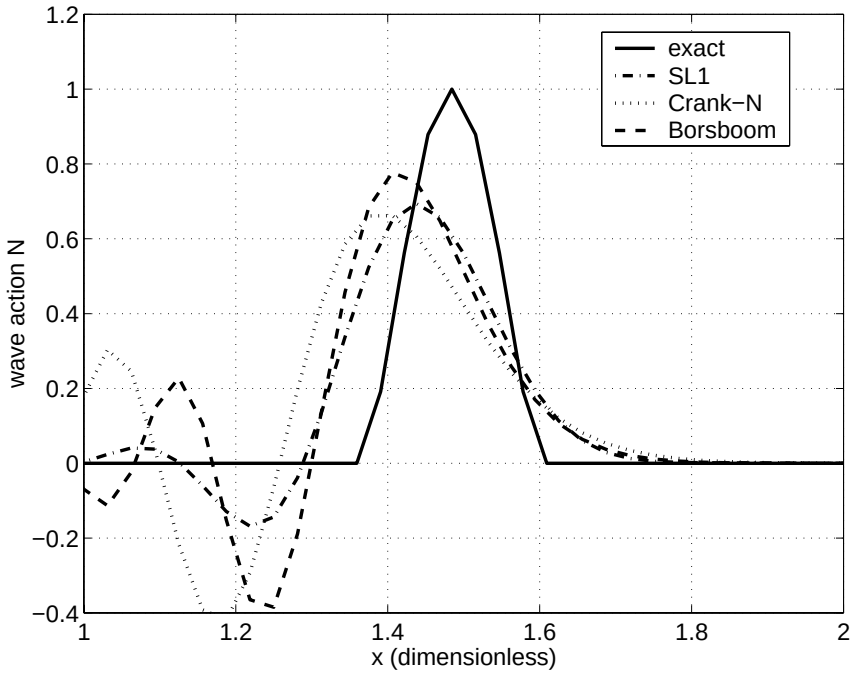

Fig. 5 — A one-dimensional spike propagation test case comparing the SL1 scheme to the two computationally implicit schemes. Model parameters: CFL = 1.5; C_g = 1 (dimensionless); Δx = 1/32 (dimensionless).

Disadvantages:

- At lower Courant numbers, exhibits significant diffusion and nonphysical oscillation (compared to comparable schemes)
- The numeric stencil (the points that the scheme uses) varies according to Courant number, which could be inconvenient when coding a model

3.1.2.11 BSFT (Backward Space, Forward Time)

This first-order, upwind, explicit scheme is stated as (e.g., Roache 1972):

$$\frac{\partial N}{\partial t} \approx \frac{N_i^n - N_i^{n-1}}{\Delta t} \tag{30}$$

and

$$\frac{\partial N}{\partial x} \approx \frac{N_i^{n-1} - N_{i-1}^{n-1}}{\Delta x}. \tag{31}$$

This is the primary numerical scheme used in the third-generation hyperbolic wave model WAM (WAMDI Group 1988).

Advantages:

- Compact: requires only three points
- Exceptionally fast computationally (the fastest of all the schemes tested here)

Disadvantages:

- Severe numerical diffusion (although generally less than BSBT scheme)
- Conditionally stable (stable for Courant number, $\mu \leq 1.0$)
- Generally performs well only when Courant number is one or slightly less than one

3.1.2.12 Lax

The Lax scheme is (Roache 1972):

$$\frac{\partial N}{\partial t} \approx N_i^n - \frac{1}{2}\left(\frac{N_{i+1}^{n-1} - N_{i-1}^{n-1}}{\Delta t}\right) \tag{32}$$

and

$$\frac{\partial N}{\partial x} \approx \frac{N_{i+1}^{n-1} - N_{i-1}^{n-1}}{2\Delta x}. \tag{33}$$

Advantages:

- Fast computationally

Disadvantages:

- Conditionally stable
- High diffusion, especially at lower Courant numbers
- Worst performer of all explicit schemes tested: generally, performs well only when Courant number is one or slightly less than one

3.1.12.13 BCMLn3: Backward Characteristic Method, Lagrangian Interpolation (n = 3)

The formulation of this method is similar to that of NISL in that it tracks the solution backward along characteristic rays. The BCMLn3 scheme interpolates to the surrounding points at the end of the backward projection using Lagrangian interpolation functions. The approximation of the one-dimensional hyperbolic wave equation using this method is (e.g., Petit 1997):

$$\begin{aligned} N_i^n = {} & \tfrac{1}{120}(\mu-2)(\mu-1)(\mu)(\mu+1)(\mu+2)N_{i-3}^{n-1} \\ & -\tfrac{1}{24}(\mu-3)(\mu-1)(\mu)(\mu+1)(\mu+2)N_{i-2}^{n-1} \\ & +\tfrac{1}{12}(\mu-3)(\mu-2)(\mu)(\mu+1)(\mu+2)N_{i-1}^{n-1} \\ & -\tfrac{1}{12}(\mu-3)(\mu-2)(\mu-1)(\mu+1)(\mu+2)N_i^{n-1} \\ & +\tfrac{1}{24}(\mu-3)(\mu-2)(\mu-1)(\mu)(\mu+2)N_{i+1}^{n-1} \\ & -\tfrac{1}{120}(\mu-3)(\mu-2)(\mu-1)(\mu)(\mu+1)N_{i+2}^{n-1} \end{aligned} \tag{34}$$

Advantages:

- At lower Courant numbers (e.g., $\mu < 2$), is generally more accurate than any other scheme tested here

Disadvantages:

- Conditionally stable: $\mu \leq 1$ (calculated); $\mu \leq 2$ (observed)

3.1.2.14 Fromm

The Fromm scheme (Fromm 1968) uses one point at time level (t_n) and four points at time level (t_{n-1}). The one-dimensional wave equation is:

$$N_i^n \approx N_i^{n-1} - \tfrac{1}{2}\mu(N_{i+1}^{n-1} - N_{i-1}^{n-1}) + \tfrac{1}{2}\mu^2(N_{i+1}^{n-1} - 2N_i^{n-1} + N_{i-1}^{n-1}) - \tfrac{1}{4}\mu(\mu-1)(N_{i+1}^{n-1} - 3N_i^{n-1} + 3N_{i-1}^{n-1} - N_{i-2}^{n-1}). \quad (35)$$

Advantages:

- Generally less diffusive than SL1 scheme (although more diffusive than BCMLn3)
- Zero phase error

Disadvantages:

- Conditionally stable: $\mu \leq 1$

3.1.2.15 QUICKEST: Backward Characteristic Method, Lagrangian Interpolation ($n = 2$)

This scheme is stated as (Leonard 1979):

$$N_i^n \approx N_i^{n-1} - \tfrac{1}{6}\mu(2N_{i+1}^{n-1} + 3N_i^{n-1} - 6N_{i-1}^{n-1} + N_{i-2}^{n-1}) + \tfrac{1}{2}\mu^2(N_{i+1}^{n-1} - 2N_i^{n-1} + N_{i-1}^{n-1}) + \tfrac{1}{6}\mu^3(N_{i-2}^{n-1} - 3N_{i-1}^{n-1} + 3N_i^{n-1} - N_{i+1}^{n-1}). \quad (36)$$

This scheme is used by the third-generation hyperbolic wave model WAVEWATCH (Tolman 1995).

Advantages:

- Generally less diffusive than SL1 scheme (although more diffusive than BCMLn3)

Disadvantages:

- Conditionally stable: $\mu \leq 1$ (calculated); $\mu \leq 2$ (observed)

Figure 6 shows an example of a comparison of the SL1 to the five conditionally stable schemes tested, including QUICKEST. In this case, and in most other cases, the higher-order conditionally stable schemes (QUICKEST, Fromm, and BCMLn3) are more accurate than SL1.

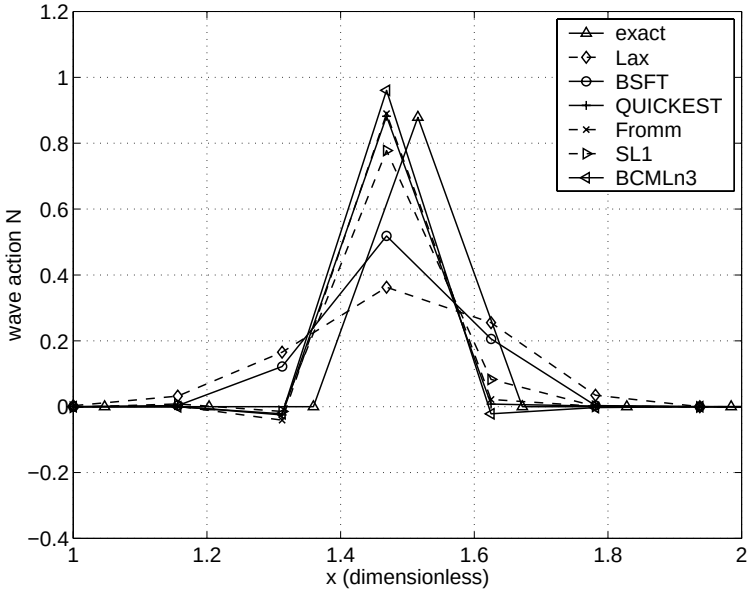

Fig. 6 ——A one-dimensional spike propagation test case comparing the SL1 scheme to the five conditionally stable schemes. Model parameters: CFL = 0.75; C_g = 1 (dimensionless); Δx = 1/32 (dimensionless).

3.2 Tests of Two-Dimensional Propagation

After the one-dimensional tests were conducted, most of the schemes were eliminated as candidates for the new model. In order to preserve the unconditional stability of the model, the conditionally stable schemes were eliminated. Due to consideration of computational costs, the two computationally implicit schemes were eliminated. The theta-Box scheme was also eliminated, as it offered little apparent advantage over the Box scheme. The second-order, upwind, implicit scheme was eliminated due to poor performance in the one-dimensional tests. The following schemes were, therefore, tested in two dimensions: BSBT, SL1, SL2, SL3, Box, and NISL. The SL2 and SL3 schemes were included in only two of the two-dimensional tests. These two schemes were subsequently eliminated, as performance was consistently inferior to that of the SL1 scheme.

The NISL scheme, in two dimensions, is stated by Olim (1994) as:

$$
\begin{aligned}
N_{i,j}^{n} \approx\ & N_{i-p,j-q}^{n-1}(1-\mu_{rx}^{2}-\mu_{ry}^{2})+\frac{\mu_{rx}\mu_{ry}}{4}(N_{i-p-1,j-q-1}^{n-1}+N_{i-p+1,j-q+1}^{n-1}-N_{i-p+1,j-q-1}^{n-1}-N_{i-p-1,j-q+1}^{n-1}) \\
&+\frac{\mu_{rx}}{2}[N_{i-p-1,j-q}^{n-1}(1+\mu_{rx})-N_{i-p+1,j-q}^{n-1}(1-\mu_{rx})] \\
&+\frac{\mu_{ry}}{2}[N_{i-p,j-q-1}^{n-1}(1+\mu_{ry})-N_{i-p,j-q+1}^{n-1}(1-\mu_{ry})],
\end{aligned}
\tag{37}
$$

where μ_{rx} is the residual Courant number in x-space, $(C_x \Delta t/\Delta x - p)$; p is the nearest integer to $\mu_x = (C_x \Delta t/\Delta x)$; μ_{ry} is the residual Courant number in y-space, $(C_y \Delta t/\Delta y - q)$; and q is the nearest integer to $\mu_y = (C_y \Delta t/\Delta y)$.

The Box scheme was extended to two-dimensional space by rewriting it as a "cube" scheme, where each derivative is calculated from the eight points on an upwind-oriented cube:

$$\frac{\partial N}{\partial t} \approx \frac{1}{4}\left(\frac{N_{i,j}^{n} - N_{i,j}^{n-1}}{\Delta t} + \frac{N_{i-1,j}^{n} - N_{i-1,j}^{n-1}}{\Delta t} + \frac{N_{i,j-1}^{n} - N_{i,j-1}^{n-1}}{\Delta t} + \frac{N_{i-1,j-1}^{n} - N_{i-1,j-1}^{n-1}}{\Delta t} \right), \tag{38}$$

$$\frac{\partial N}{\partial x} \approx \frac{1}{4}\left(\frac{N_{i,j}^{n} - N_{i-1,j}^{n}}{\Delta x} + \frac{N_{i,j}^{n-1} - N_{i-1,j}^{n-1}}{\Delta x} + \frac{N_{i,j-1}^{n} - N_{i-1,j-1}^{n}}{\Delta x} + \frac{N_{i,j-1}^{n-1} - N_{i-1,j-1}^{n-1}}{\Delta x} \right), \tag{39}$$

and

$$\frac{\partial N}{\partial y} \approx \frac{1}{4}\left(\frac{N_{i,j}^{n} - N_{i,j-1}^{n}}{\Delta y} + \frac{N_{i,j}^{n-1} - N_{i,j-1}^{n-1}}{\Delta y} + \frac{N_{i-1,j}^{n} - N_{i-1,j-1}^{n}}{\Delta y} + \frac{N_{i-1,j}^{n-1} - N_{i-1,j-1}^{n-1}}{\Delta y} \right). \tag{40}$$

In the cases of the other four schemes (BSBT, SL1, SL2, SL3), the equations for partial derivatives given in Section 3.1.2 were applied directly to the two-dimensional simple wave equation:

$$\frac{\partial N}{\partial t} + C_x \frac{\partial N}{\partial x} + C_y \frac{\partial N}{\partial y} = 0. \tag{41}$$

3.2.1 Nonstationary, Nonuniform Input

3.2.1.1 Two-Dimensional Propagation of a Spike

A spike of the following form was propagated using the six models described above:

$$N(x,y) = [\cosh(\psi * \Gamma)]^{-1}, \tag{42}$$

where ψ is a narrowness coefficient, and Γ is the distance from the spike center. Examples of results are shown in Figs. 7 through 10. Several observations were made:

- As expected, relative performance of the schemes was a function of Courant number, and (to a lesser degree) spatial resolution. The NISL scheme is clearly superior at larger Courant numbers (e.g., $\mu > 1$), while the Box and the Stelling and Leendertse schemes do best at lower Courant numbers (e.g., $\mu < 0.5$).

- As in the one-dimensional tests, the SL1 scheme generally creates less diffusion than the other two Stelling and Leendertse schemes.

- SL1 generally has slightly greater diffusion than the Box scheme.

- Box exhibited more problems with nonphysical oscillation than SL1.

- The NISL scheme sometimes becomes unstable in cases where ($\mu_{xr} \approx \mu_{yr} \approx 0.5$). Explanation for this phenomenon could not be found via stability analysis.

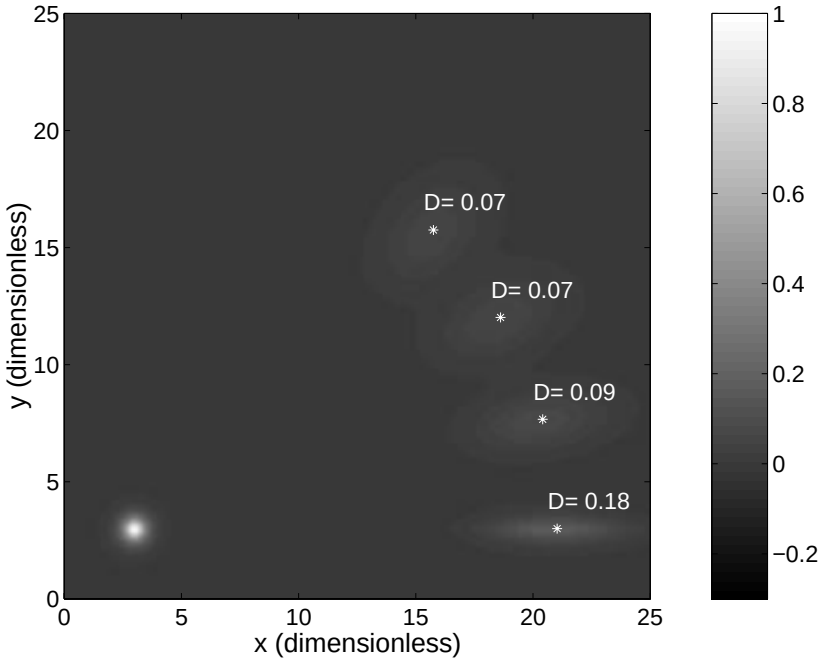

Fig. 7 — Results of two-dimensional spike propagation test using the BSBT scheme. The initial shape and location of the four spikes is shown in the lower left corner. The four spikes are propagated at angles of 0, 15, 30, and 45 degrees. The parameter "D" (shown above the end location of each of the four spikes) indicates the fraction of spike amplitude retained, a rough measure of diffusion (lower D = greater diffusion). Model parameters: CFL = 0.75; $\Delta x = \Delta y = 0.1$ (dimensionless); $C_g = 0.18$ (dimensionless).

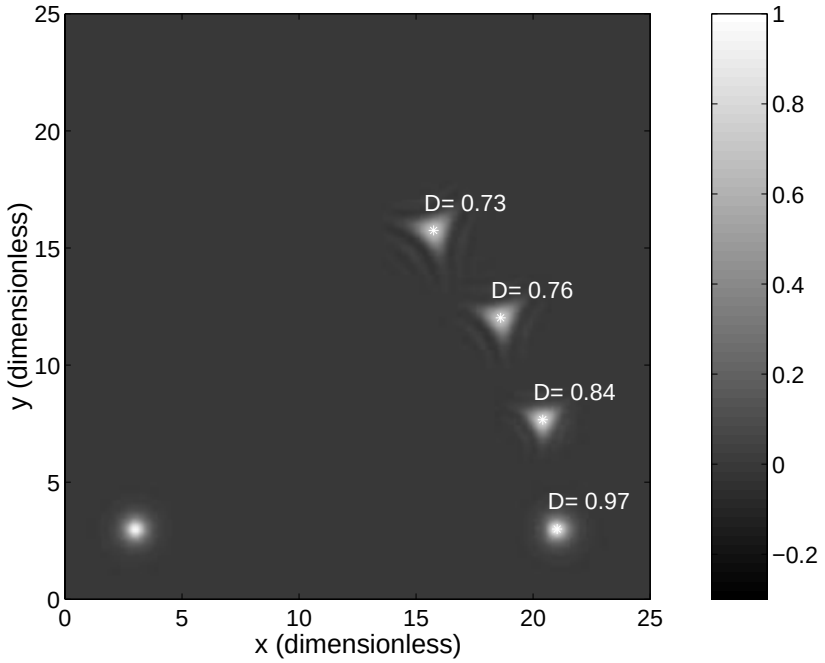

Fig. 8 — Results of two-dimensional spike propagation test using the Box scheme. Model setup is identical to that of the BSBT test case described in Fig. 7.

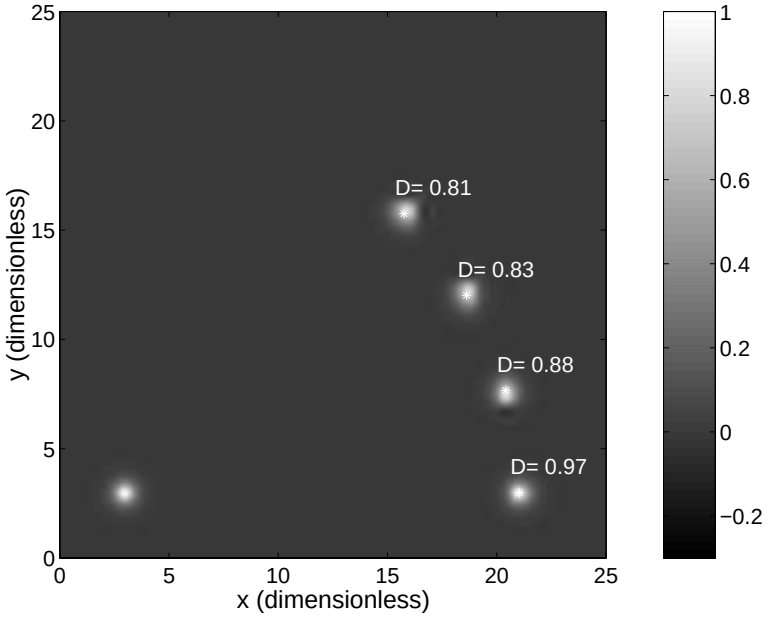

Fig. 9 — Results of two-dimensional spike propagation test using the NISL scheme. Model setup is identical to that of the BSBT test case described in Fig. 7.

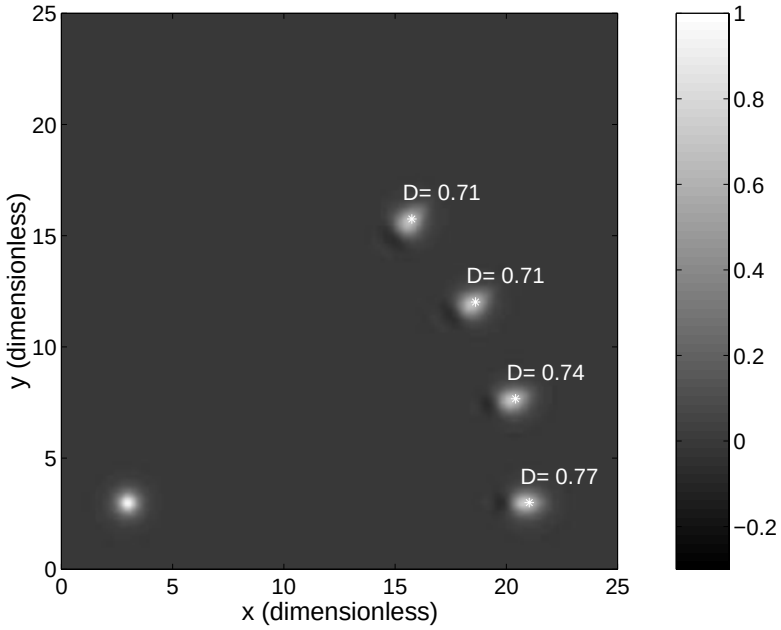

Fig. 10 — Results of two-dimensional spike propagation test using the SL1 scheme. Model setup is identical to that of the BSBT test case described in Fig. 7.

3.2.1.2 Sine Wave Propagation Test

Two-dimensional "waves of wave energy" were simulated in these tests. Conditions were specified along the ($x = 0$) and ($y = 0$) boundaries:

$$N_{x=0}(y) = 1.0 + \sin(y \times k_y - \sigma \times t) \tag{43}$$

and

$$N_{y=0}(x) = 1.0 + \sin(x \times k_x - \sigma \times t). \tag{44}$$

Figure 11 shows the results from one of these simulations, and Figs. 12 and 13 show transects of wave energy along the direction of energy propagation.

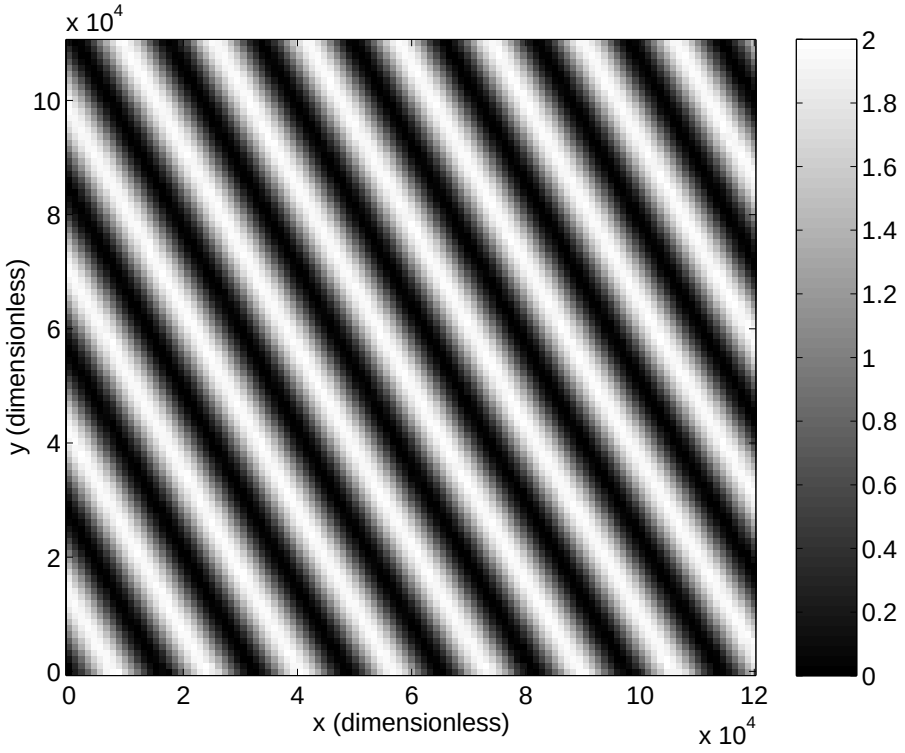

Fig. 11 — Example result of the two-dimensional sine wave propagation test for the Box scheme. Global wave action is shown. Model parameters: CFL = 0.75; direction of transport theta = 30 degrees from *x* axis; 15 points per wavelength.

Unlike the spike propagation tests, these tests showed a marked difference in diffusion characteristics between the Box and SL1 schemes. The SL1 scheme often exhibited severe diffusion, especially at higher Courant numbers, whereas diffusion levels were generally low with the Box scheme.

Just as in the one-dimensional tests, the SL2 and SL3 schemes exhibited greater diffusion than the SL1 scheme, while offering only a minor decrease in nonphysical oscillations.

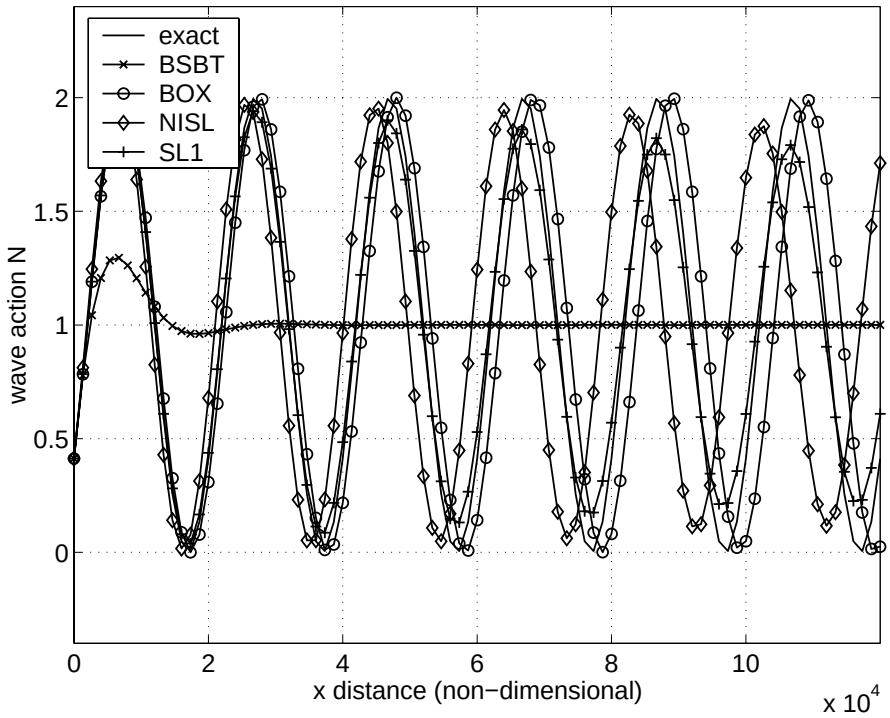

Fig. 12 — A two-dimensional sine wave propagation test: wave action along the direction of propagation. Model parameters: CFL = 0.25; direction of transport theta = 45 degrees from *x* axis; 15 points per wavelength.

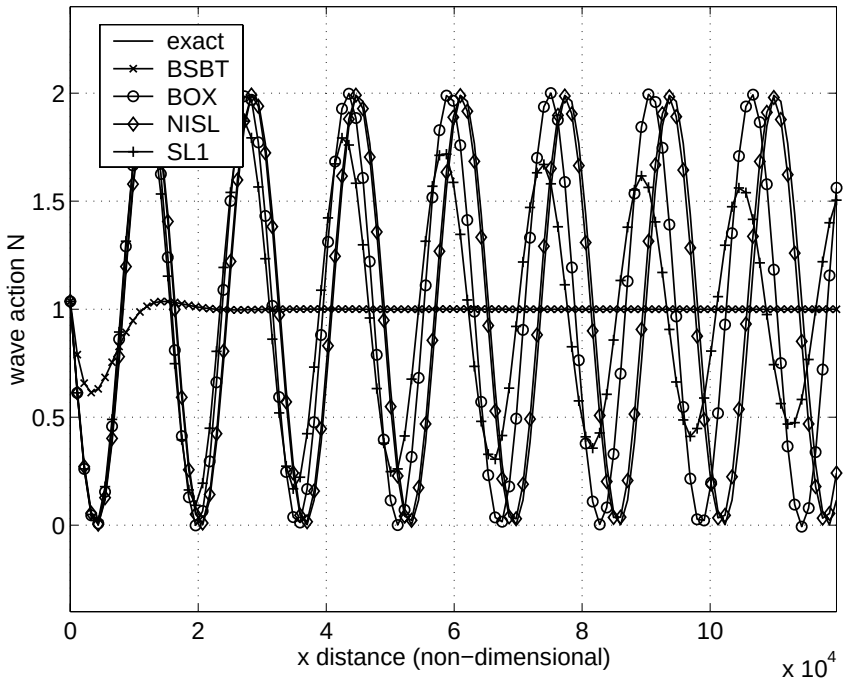

Fig. 13 — A two-dimensional sine wave propagation test: wave action along the direction of propagation. Model parameters: CFL = 1.0; direction of transport theta = 30 degrees from *x* axis; 15 points per wavelength.

The sine wave tests provided greater insight into errors in propagation speed caused by inadequate spatial resolution, unfavorable Courant numbers, or both. Observations of nonphysical oscillation showed a similar trend to that of diffusion: the NISL scheme excels at higher Courant numbers, while Box and SL1 do best at lower numbers.

3.2.2 Stationary, Uniform Input: Test of Leading Oscillations

This is a very simple test with constant and uniform input along the offshore ($x = 0$) boundary. The initial condition is a state of zero energy throughout the grid. Thus, the test is similar to the shock propagation tests often used for computational fluid mechanics codes. In order to study oscillations at the leading edge of the energy front, the simulations were not run to steady state. Results were compared along transects in the direction of energy propagation. Figures 14 and 15 show some of the results of these tests. Because of the emphasis on nonphysical oscillation, observations were very favorable toward the SL1 scheme. The NISL scheme and Box scheme exhibited severe oscillations, with no significant advantage over the SL1 scheme at any spatial resolution or time step increment.

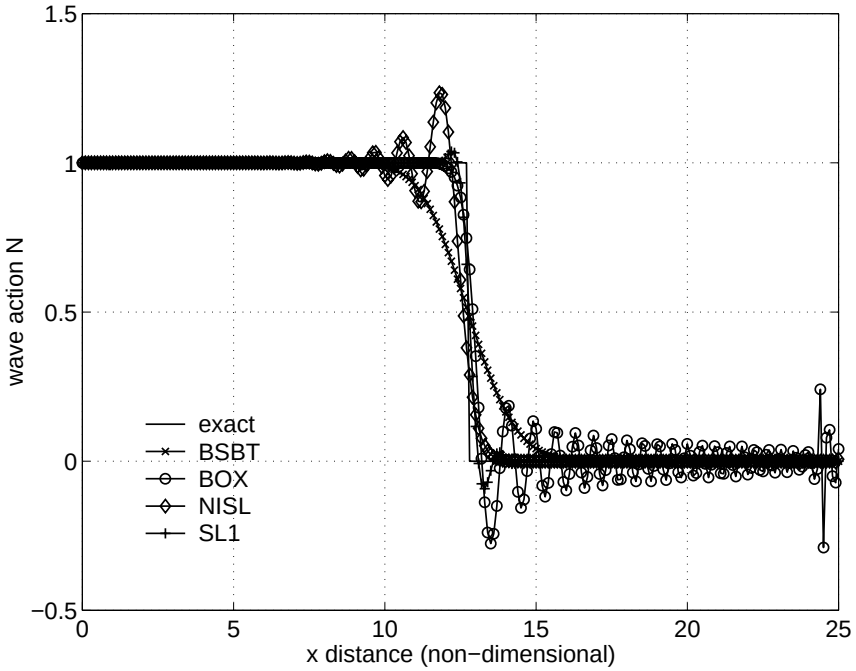

Fig. 14 — A two-dimensional test of leading oscillations: wave action along the direction of propagation. Model parameters: CFL = 0.25; direction of transport theta = 45 degrees from x axis; $\Delta x = \Delta y = 0.1$ (dimensionless).

3.2.3 Stationary, Nonuniform Input: Submerged Breakwater Tests

A submerged breakwater was crudely simulated by specifying wave heights at the offshore boundary:

$H_{mo}(x = 0) =$ 2.0 m, where 4700 m < y < 5100 m, and
$H_{mo}(x = 0) =$ 1.0 m, where y ≤ 4700 m and $y \geq$ 5100 m.

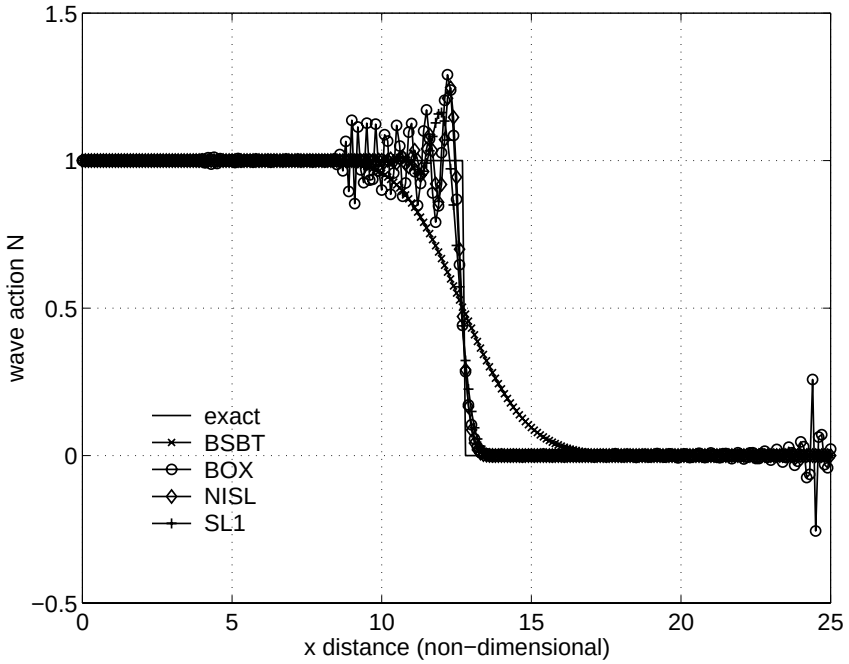

Fig. 15 — A two-dimensional test of leading oscillations: wave action along the direction of propagation. Model parameters: CFL = 1.2; direction of transport theta = 45 degrees from x axis; $\Delta x = \Delta y = 0.1$ (dimensionless).

This input was stationary (constant in time), but the simulations were not run to steady state. As with the previous test case, nonphysical oscillation is a major concern. The SL1 scheme generated much less oscillatory output than did the NISL and Box schemes. Diffusion characteristics of Box, SL1, and NISL are all favorable compared to the BSBT scheme. Figures 16 through 23 show a few comparisons of the BSBT, BOX, NISL, and SL1 schemes. The SL2 and SL3 schemes were also tested. These schemes proved to be less accurate than the SL1 scheme, consistent with previous experiments.

3.3 Computation Timings

The computational expense of the BSBT, SL1, Box, and NISL schemes were compared using timing analysis for simple cases. The computational costs of the four schemes, normalized by the BSBT results, are:

- BSBT: 1.0
- Box: 1.1
- SL1: 1.5
- NISL: 1.5

Note that for these tests, almost all the computation time is spent calculating geographic propagation. By contrast, within SWAN, most computation time is spent solving the matrix required due to finite differencing in spectral space. A relatively small percent of time is spent on the finite differencing of geographic partial derivatives. Therefore, a 50% increase in expense of the geographic propagation scheme results in a much smaller — approximately 5% — increase in total computation time.

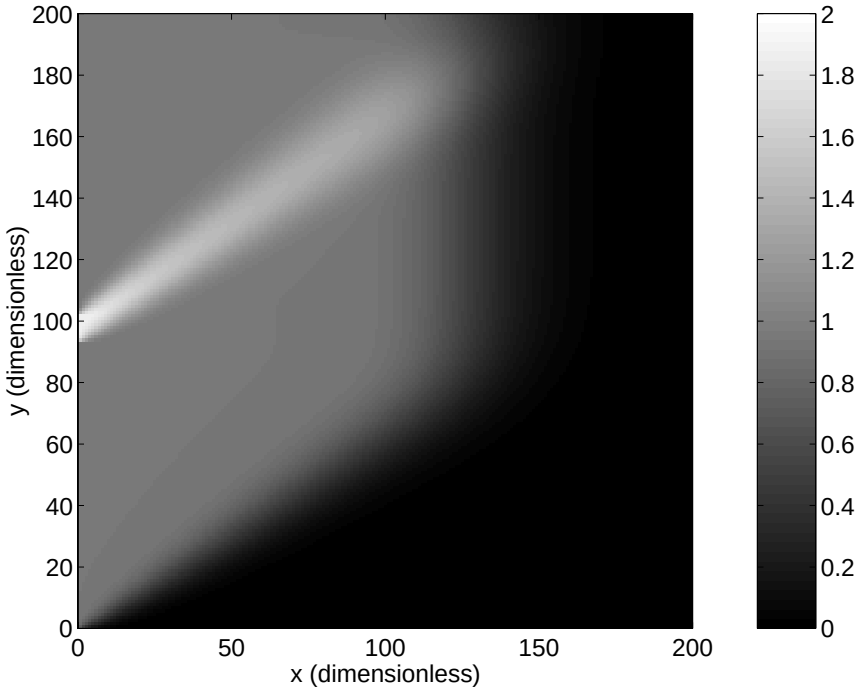

Fig. 16 — Submerged breakwater with gap; BSBT scheme. Wave action is specified at the left (x = 0) boundary and propagated through the domain. Model parameters: CFL = 0.7; direction of transport theta = 35 degrees from x axis; $\Delta x = \Delta y = 1$ (dimensionless).

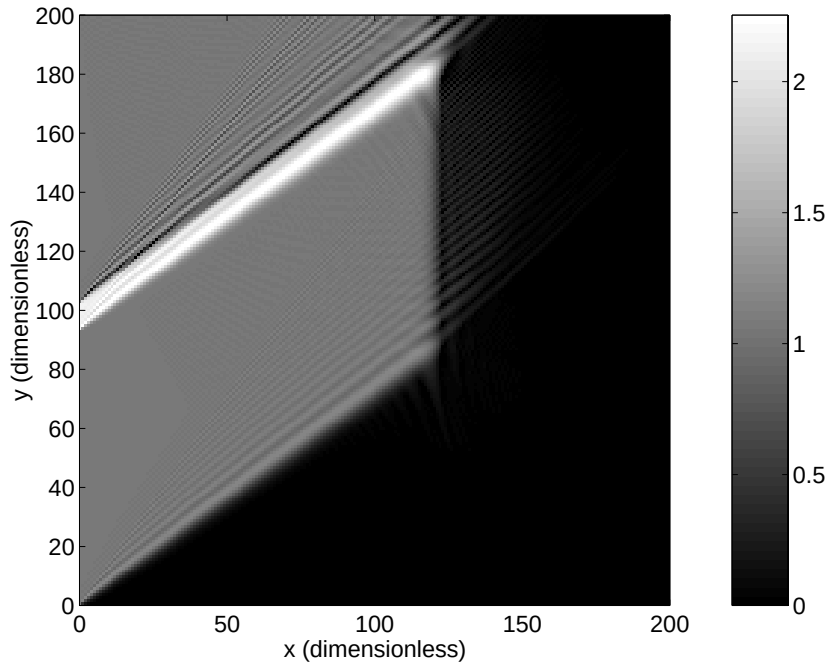

Fig. 17 — Submerged breakwater with gap; Box scheme. Model setup is identical to that of the BSBT test case described in Fig. 16.

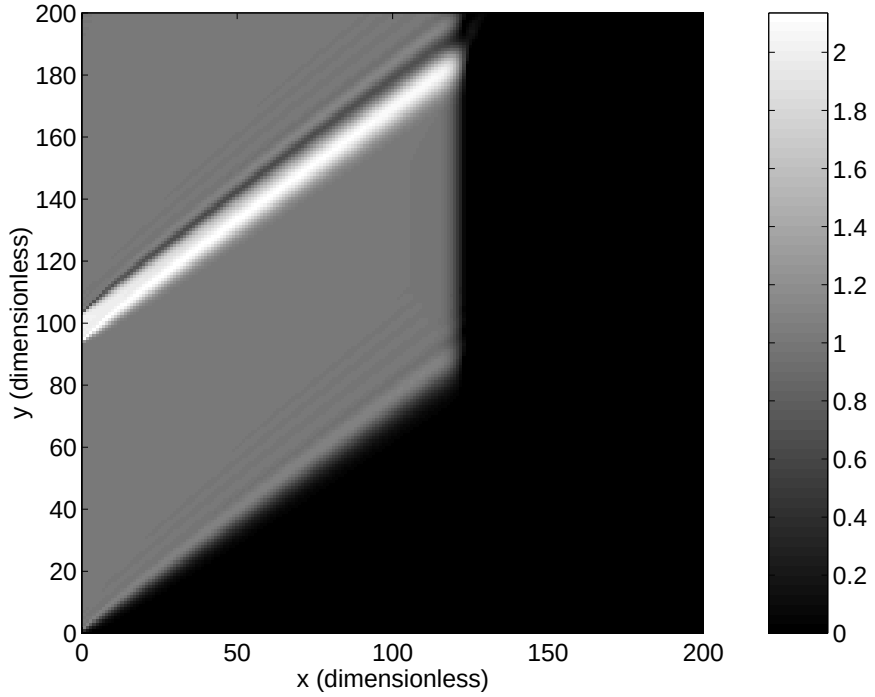

Fig. 18 — Submerged breakwater with gap; NISL scheme. Model setup is identical to that of the BSBT test case described in Fig. 16.

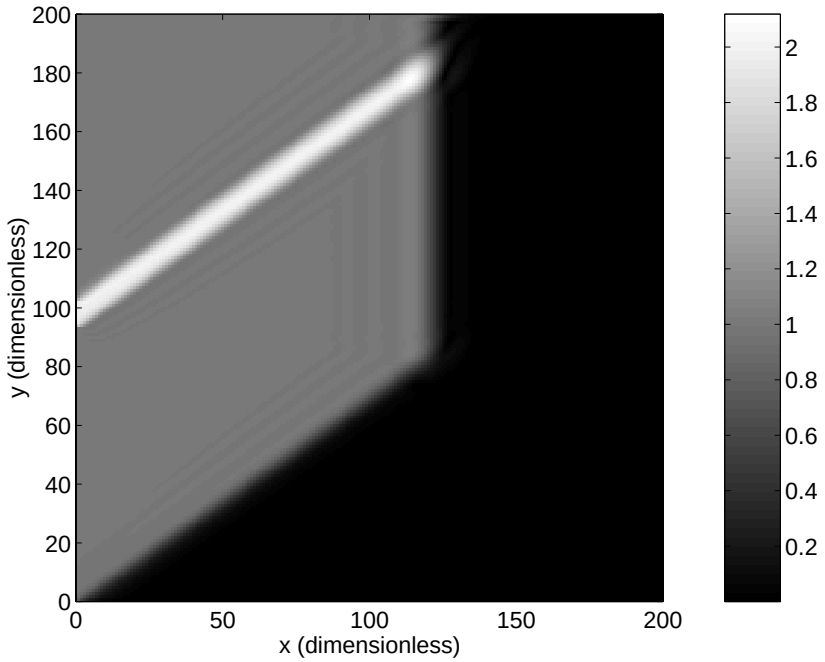

Fig. 19 — Submerged breakwater with gap; SL1 scheme. Model setup is identical to that of the BSBT test case described in Fig. 16.

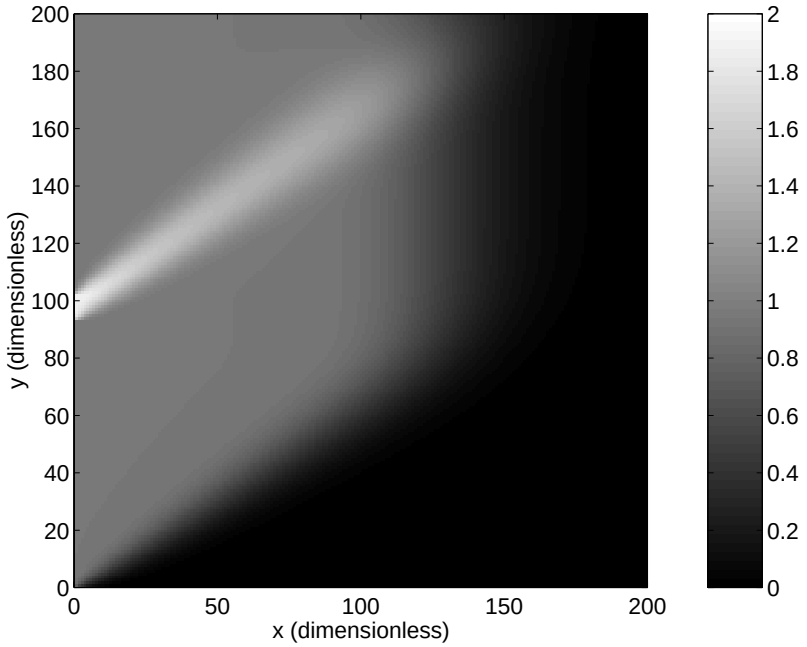

Fig. 20 — Submerged breakwater with gap; BSBT scheme. Wave action is specified at the left ($x = 0$) boundary and propagated through the domain. Model parameters: CFL = 1.4; direction of transport theta = 35 degrees from x axis; $\Delta x = \Delta y = 1$ (dimensionless).

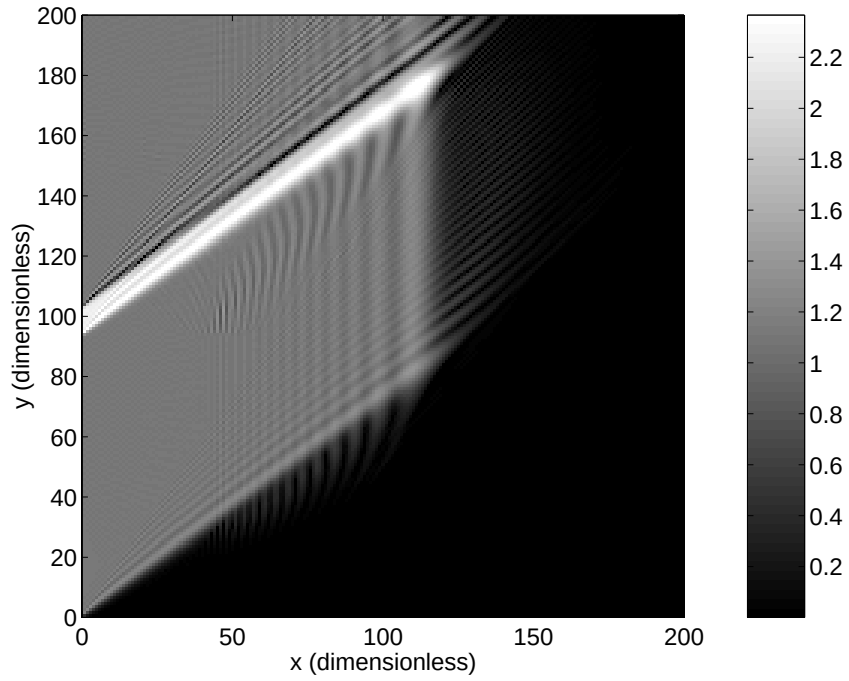

Fig. 21 — Test case: submerged breakwater with gap; Box scheme. Model setup is identical to that of the BSBT test case described in Fig. 20.

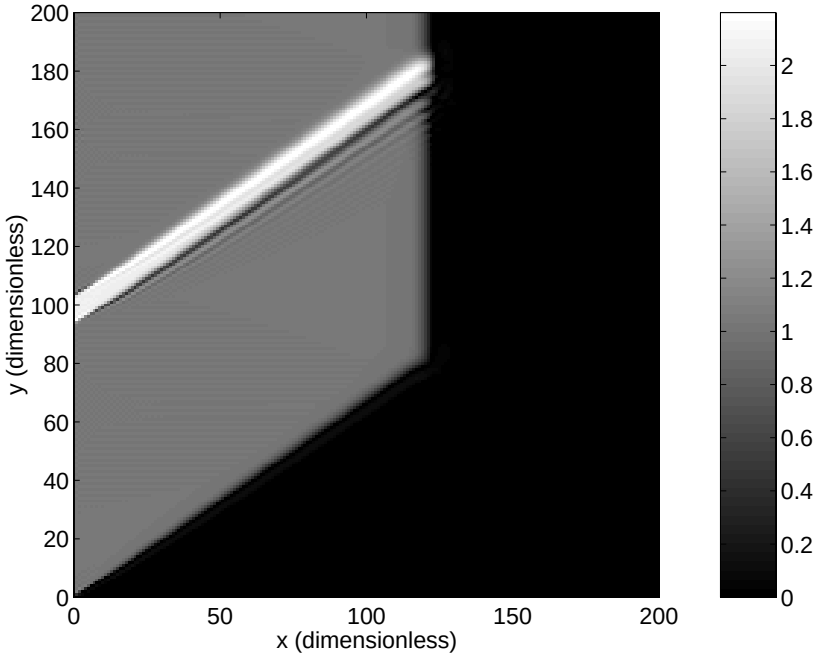

Fig. 22 — Test case: submerged breakwater with gap; NISL scheme. Model setup is identical to that of the BSBT test case described in Fig. 20.

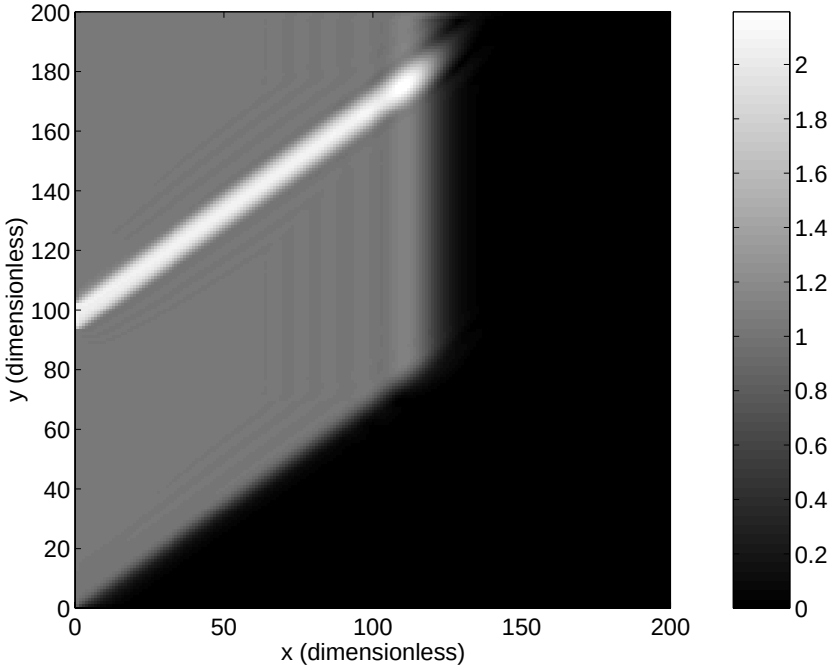

Fig. 23 — Test case: submerged breakwater with gap; SL1 scheme. Model setup is identical to that of the BSBT test case described in Fig. 20.

3.4 Conclusions

The SL1 scheme was chosen for implementation in SWAN. The advantages of this scheme are:

- Numerical diffusion is low compared to the BSBT scheme. SL1 is also less diffusive than the other two Stelling and Leendertse schemes that were tested. Though most of the other numerical schemes tested exhibited less diffusion than SL1, it is thought that the diffusion characteristics of SL1 are acceptable for the vast majority of applications.
- The scheme is unconditionally stable, unlike, e.g., the more accurate Backward Characteristic Method (Lagrangian Interpolation) schemes.
- The scheme has an acceptable computation cost, unlike, e.g., the Borsboom scheme.
- The scheme exhibited relatively few problems with nonphysical oscillation, making it favorable over the Box scheme and several others.

4. IMPLEMENTING THE NEW SCHEME

The spatial propagation routine in SWAN-X33 was supplemented with the SL1 scheme. Details of changes to the code can be found in Appendix A. A version of the code that employs the Box scheme had been created previously, but development of this code was discontinued when it became clear that the SL1 scheme would be used in SWAN-X33.

4.1 Scheme Usage

Within three nodal points of the geographic grid boundaries, the BSBT scheme is used. At the interior grid points, the user has the option of using either the BSBT scheme or the SL1 scheme.

The possibility of using the Box scheme at the grid boundaries (rather than the BSBT scheme) was briefly considered. However, since the impact of this change would be relatively minor (it would directly influence only the boundary nodes), this alteration of the model was not made.

4.2 Nonstationary Mode

In nonstationary mode, the sequence of operations in SWAN-X33 is identical to that of SWAN. The BSBT scheme is replaced by the SL1 scheme at the appropriate grid locations. In one dimension, the simple wave equation approximated with the SL1 scheme is

$$N_i^n \approx N_i^{n-1} - \frac{\mu}{4}(N_{i+1}^{n-1} - N_{i-1}^{n-1}) - \frac{\mu}{12}(10N_i^n - 15N_{i-1}^n + 6N_{i-2}^n - N_{i-3}^n). \tag{45}$$

Simple stepping in i solves the N^n matrix. A specialized matrix solver is not required, as all the N^n terms are oriented in an upwind direction, and can therefore be treated independently.

4.3 Stationary Mode

4.3.1 Time-Stepping Method

Stationary mode in SWAN-X33 cannot function as it does in SWAN (simple sweeping), since the SL1 scheme is not entirely upwind, but is centered at the explicit time level. Therefore, the stationary model time-steps until the simulation reaches steady state (convergence). The user specifies the time increment, the

maximum number of time steps, and the convergence criteria. The user must consider the possibility of nonphysical oscillatory behavior at Courant numbers significantly greater than unity, and balance this with consideration of computational cost. This is the method currently being used by SWAN-X33. Alternative methods were investigated.

4.3.2 Alternative Methods

Two alternatives to the time-stepping method used in the stationary mode of SWAN-X33 were investigated: solution of the problem matrix by Gauss-Seidel method and by relaxation method. Setting the $\partial/\partial t$ terms in the simple wave equation to zero, Eq. (45) becomes

$$\frac{10}{12}N_i^n \approx -\frac{1}{4}(N_{i+1}^{n-1} - N_{i-1}^{n-1}) - \frac{1}{12}(-15N_{i-1}^n + 6N_{i-2}^n - N_{i-3}^n). \tag{46}$$

The Gauss-Seidel method uses a slightly modified form of this equation — the time level of the third N term is changed from (n-1) to (n); since the solution is a steady-state solution, the most current time level available is used for all terms:

$$\frac{10}{12}N_i^n \approx -\frac{1}{4}(N_{i+1}^{n-1} - N_{i-1}^{n}) - \frac{1}{12}(-15N_{i-1}^n + 6N_{i-2}^n - N_{i-3}^n). \tag{47}$$

Using the Gauss-Seidel method, the matrix solution did not converge for a simple, two-dimensional test case.

In the relaxation method, as in the other two methods, the matrix is solved by simple stepping in i. Using the SL1 scheme for the simple, one-dimensional wave equation, this method is stated as

$$\frac{10}{12}N_i^n \approx \frac{10}{12}N_i^{n-1} - \omega\left[\frac{1}{4}N_{i+1}^{n-1} + \frac{10}{12}N_i^{n-1} - \frac{1}{4}N_{i-1}^n - \frac{15}{12}N_{i-1}^n + \frac{6}{12}N_{i-2}^n - \frac{1}{12}N_{i-3}^n\right], \tag{48}$$

where ω is a user-defined relaxation parameter. This method was also tested using a simple, two-dimensional case. Using an optimal relaxation parameter, convergence was achieved more rapidly than with the time-stepping method. However, the complexities of choosing the optimal relaxation parameter made the use of this method in SWAN-X33 impractical.

5. VERIFYING THE NEW MODEL

The accuracy and robustness of the model were verified in a series of tests.

5.1 Submerged Breakwater Test

As a "sanity check" on the new model, SWAN-X33 was compared to the simple, two-dimensional SL1-scheme model described in Section 3.2.3. The models were compared in both stationary and nonstationary mode. The model output was nearly identical (e.g,. see Fig. 24).

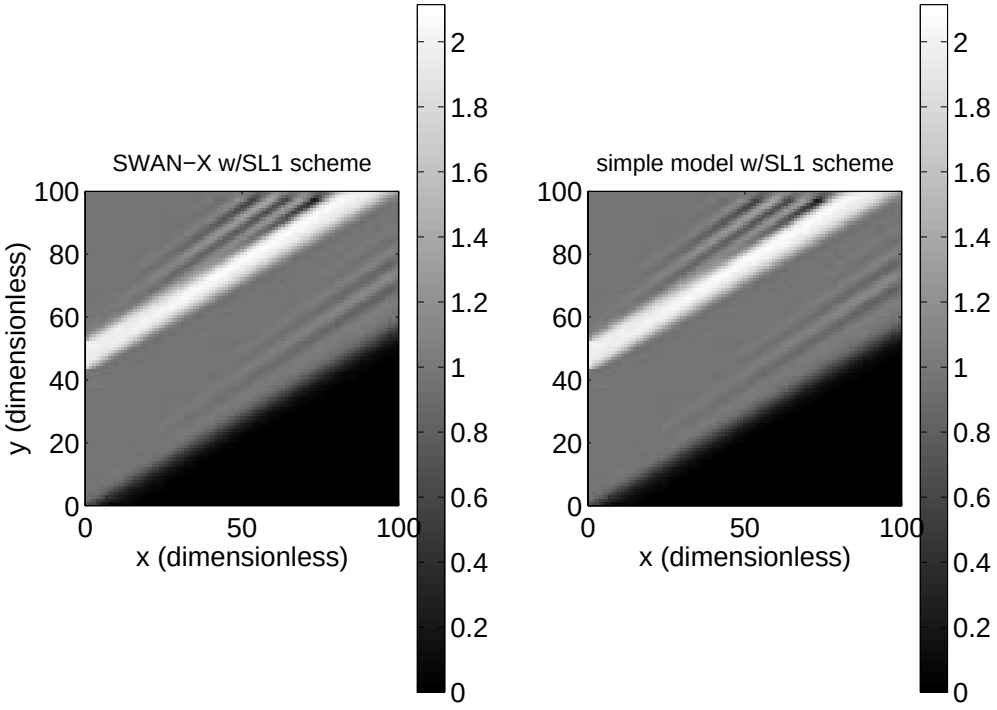

Fig. 24 — Test case: submerged breakwater with gap; SL1 scheme; SWAN-X is compared to the simple model used in the scheme comparisons. Wave action is specified at the left ($x = 0$) boundary and propagated through the domain. Model parameters: CFL = 8e-3; direction of transport theta = 30 degrees from x axis; $\Delta x = \Delta y = 1$ (dimensionless).

5.2 Planar Slope Test

Depth-induced refraction and shoaling in the new model were tested using a planar slope test case. A 1/125 slope was used with a variety of wave conditions. Results were good (e.g., Fig. 25).

5.3 Tests with Currents

Current-induced refraction and shoaling were tested using the same series of experiments used by Ris (1997):

1. Following current: a flow parallel to the wave direction increasing from 0 to 2 m/s.
2. Opposing current: a flow parallel to the wave direction increasing from 0 to –2 m/s.
3. Slanting current ($\theta = 30°$): a flow increasing from 0 to 2 m/s; wave angle of approach is 30°, where $\theta = –90°$ is a following current (in the direction of flow) and $\theta = 0$ is cross-flow.
4. Slanting current ($\theta = –30°$): a flow increasing from 0 to 2 m/s; wave angle of approach is –30°.

Analytical solutions for cases (1) and (2) are given by

$$\frac{H^2}{H_o^2} = \frac{c_o^2}{c(c+2U)} \tag{49}$$

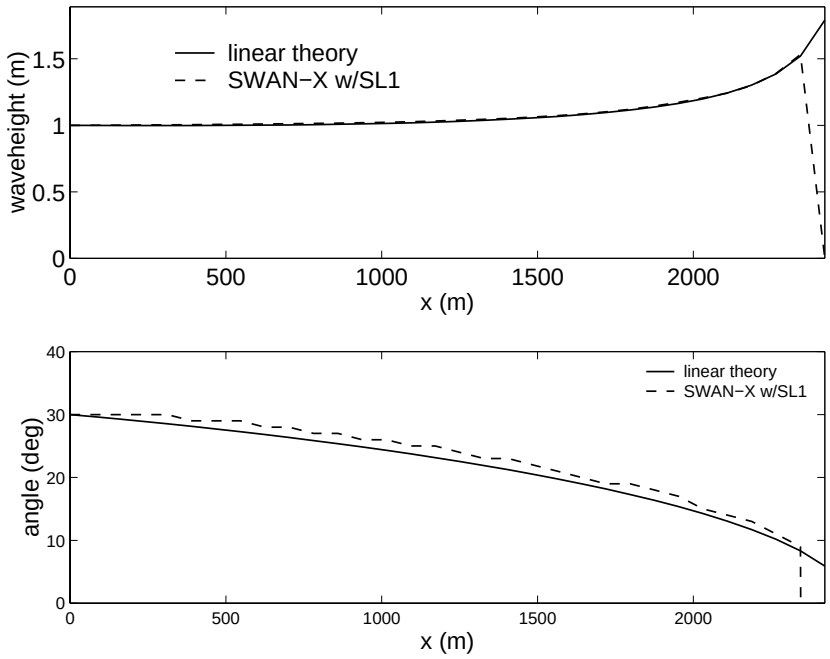

Fig. 25 — A planar slope test case. Model parameters: wave direction at offshore boundary = 30 degrees; wave period = 9.65 s.

and

$$\frac{c}{c_o} = \frac{1}{2} + \frac{1}{2}\sqrt{1 + 4\frac{U}{c_o}}, \tag{50}$$

(e.g., Philips 1977). In the slanting current case, H is calculated using a conservation of energy relation:

$$H = H_o \sqrt{\frac{\sin(2\theta_o)}{\sin(2\theta)}}. \tag{51}$$

An analytical solution for θ was derived. Starting with the relations given by Johnson (1947) that assume that a wave crest is continuous across a discontinuity in the current field, we have

$$\frac{C_o}{\sin\theta_o} = U + \frac{C}{\sin\theta} \tag{52}$$

and

$$k = k_o \frac{\sin(\theta_o)}{\sin(\theta)}, \tag{53}$$

and from the dispersion relation in deep water,

$$C = \sqrt{\frac{g}{k}}. \tag{54}$$

Substituting Eq. (53) into Eq. (54) gives

$$C = \sqrt{\frac{g\sin(\theta)}{k_o \sin(\theta_o)}}. \tag{55}$$

Substituting Eq. (55) into Eq. (52) gives

$$\frac{C_o}{\sin\theta_o} = U + \sqrt{\frac{g}{k_o \sin(\theta_o)\sin(\theta)}} \text{ or } \theta = \arcsin\left\{\left[\left(\frac{C_o^2}{\sin^2\theta_o} - \frac{2UC_o}{\sin\theta_o} + U^2\right)\frac{k_o \sin\theta_o}{g}\right]^{-1}\right\}. \tag{56}$$

Agreement with these analytical solutions is good (see Figs. 26 through 28).

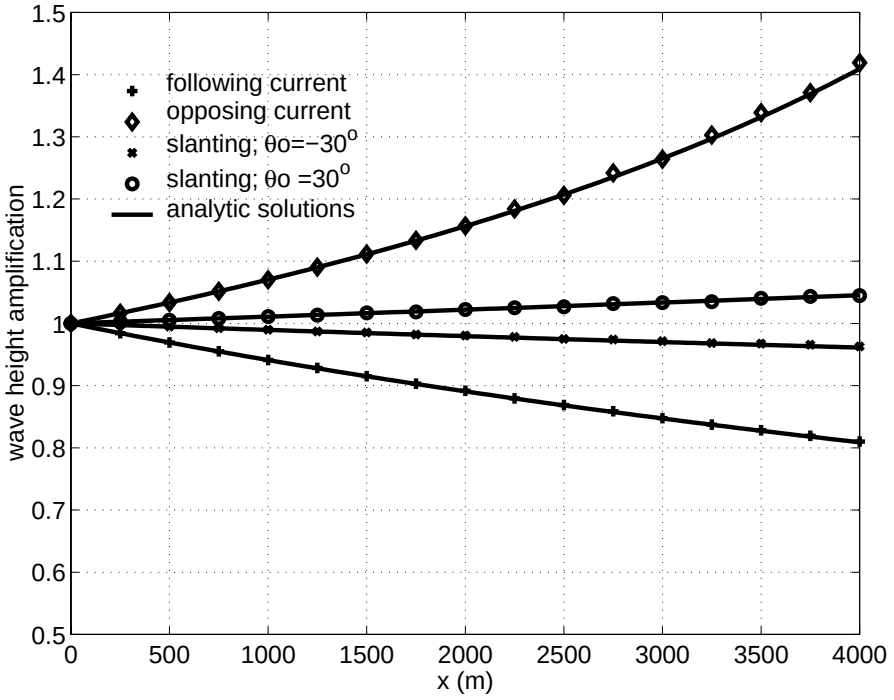

Fig. 26 — Current-induced refraction and shoaling. Solid lines indicate analytical solutions; "+" indicates model output.

Results from the tests of SWAN and SWAN-X with current input suggest that the models are highly sensitive to frequency resolution (e.g., for the cases described here, 162 frequency bins were used). This sensitivity is thought to be due to the nonzero $C\sigma$ in the presence of currents. With propagation occurring in σ-space, the finite differencing of the $\partial/\partial\sigma$ terms is sensitive to $\Delta\sigma$.

5.4 Validation of Generation by Wind

Wave generation by wind in the modified model was validated by comparison to analytical solutions and to the original (BSBT-based) model. Tests are intentionally similar to those that were used by Ris (1997) to validate the original model. All simulations used stationary, uniform wind fields of U_{10} = 20 m/s, identical to conditions used for the SWAMP (1985) tests.

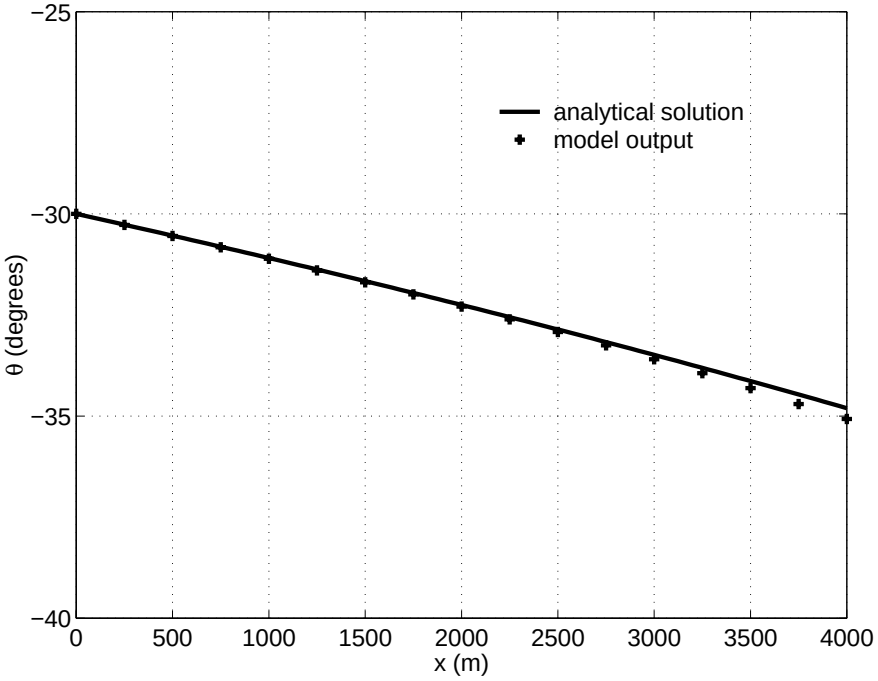

Fig. 27 — Current-induced refraction and shoaling; offshore wave angle = –30 degrees. Effect of nonuniform current on wave direction is shown.

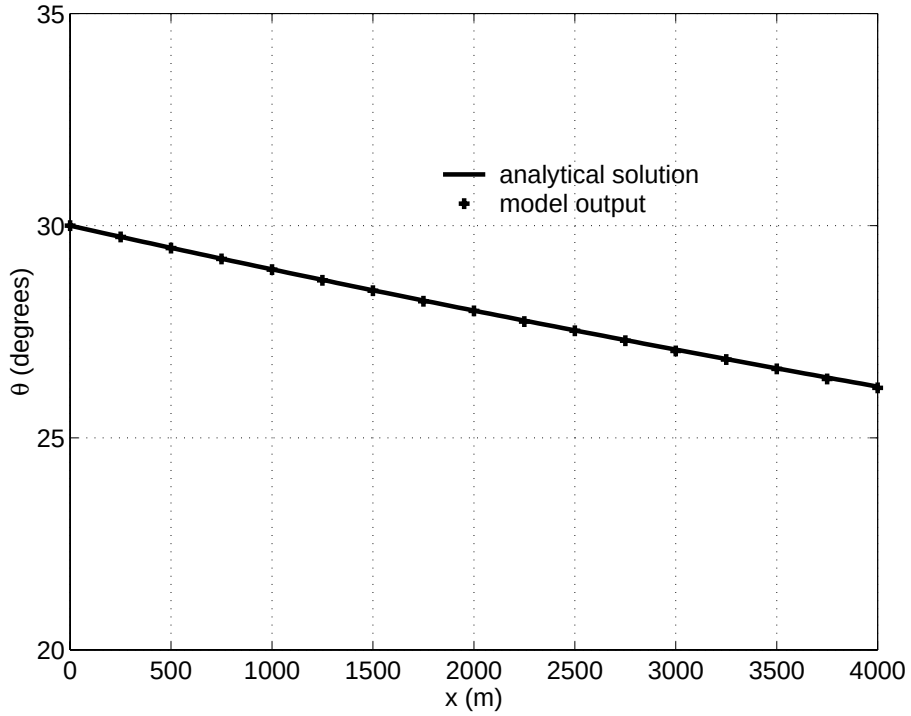

Fig. 28 — Current-induced refraction and shoaling; offshore wave angle = +30 degrees. Effect of nonuniform current on wave direction is shown.

5.4.1 Fetch-Limited Wave Growth

The model was tested for cases of finite fetch lengths, nominally infinite depth, and nominally infinite duration. Nine simulations, each with a different fetch, were conducted: 1124 km, 562 km, 281 km, 141 km, 70 km, 35 km, 18 km, 8.8 km, and 4.4 km. Note that the different fetch lengths could have been modeled using a single simulation, but separate simulations were conducted to have higher geographic resolution for the shorter fetches.

Values were nondimensionalized by the friction velocity as in the SWAMP tests of wind generation in numerical models (SWAMP Group 1985):

$$X^* = \frac{gX}{U_*^2} E^* = \frac{gE_{tot}}{U_*^4} f_p^* = \frac{f_p U_*}{g} \tag{57}$$

where X^* is the dimensionless fetch; X is the fetch; U^* is the friction velocity: $U_* = \sqrt{C_D u^2}$, $C_D = (0.8 + 0.065 \times U_{10}) \times 0.001$ (Wu 1980; Wu 1982); E_{tot} is the total energy: $E_{tot} = \left[H_{mo} / 4 \right]^2$; E^* is the dimensionless total energy; and f^*_p is the dimensionless peak frequency.

The geographic grid for each of the nine simulations was 300 × 300 grid points. A relatively coarse spectral grid was used: 10 frequency bins and a directional resolution of 10.3°.

Results from the two models were compared to empirical expressions formulated by Kahma and Calkoen (1992):

$$E^* = (6.5 \times 10^{-3}) \times (X^*)^{0.9} \text{ and } f_p^* = 0.5281 \times (X^*)^{-0.27}. \tag{58}$$

Agreement is fair (see Figs. 29 and 30); it is likely that agreement would have been better if a finer spectral resolution had been used (this was not done due to computational cost).

Implementation of the new scheme seems to have no deleterious effect on the growth curve prediction relative to that of SWAN.

5.4.2 Depth-Limited Wave Growth

A second set of tests involved finite depth, nominally infinite duration, and nominally infinite fetch. Values were nondimensionalized by the U_{10} velocity:

$$\tilde{d} = \frac{gd}{U_{10}^2}, \tilde{E} = \frac{g^2 E_{tot}}{U_{10}^4}, \text{and } \tilde{f}_p = \frac{f_p U_{10}}{g}. \tag{59}$$

Two expressions for $\tilde{E}$ and $\tilde{f}_p$ were available for comparison: an analytical expression from Bretschneider (1973):

$$\tilde{E} = 5 \times 10^{-3} \times \left[\tanh(0.53 \tilde{d}^{0.75}) \right]^2, \tilde{f}_p = 0.133 \times \left[\tanh(0.833 \tilde{d}^{0.375}) \right]^{-1}, \tag{60}$$

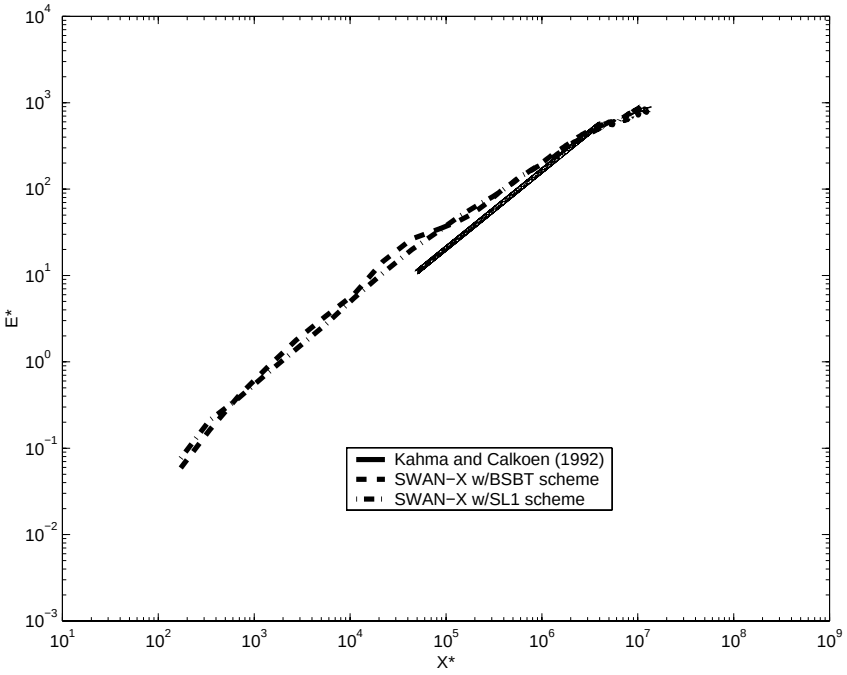

Fig. 29 — Fetch-limited wave generation by wind. Nondimensionalized energy. The BSBT- and SL1-based models are compared to an empirical growth curve from Kahma and Calkoen (1992).

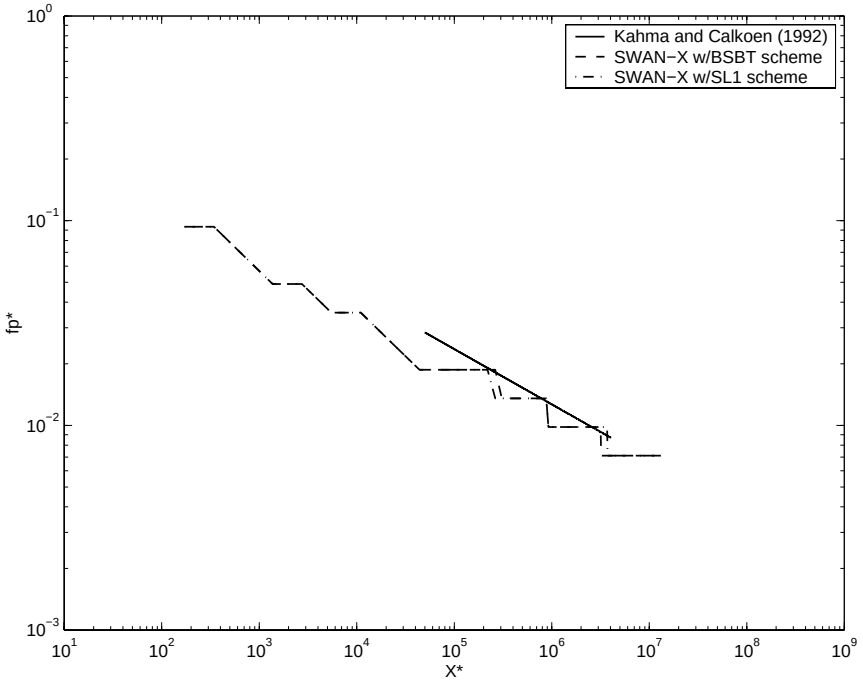

Fig. 30 — Fetch-limited wave generation by wind. Nondimensionalized frequency. The BSBT- and SL1-based models are compared to an empirical growth curve from Kahma and Calkoen (1992).

and an empirical expression by Young and Verhagen (1996), which, given infinite fetch, is written as:

$$\tilde{E} = 3.64 \times 10^{-3} \times \left[\tanh(0.493\tilde{d}^{0.75})\right]^{1.74}, \tilde{f}_p = 0.133 \times \left[\tanh(0.331\tilde{d}^{1.01})\right]^{-0.37}. \quad (61)$$

The latter set of equations was derived for $(6 \times 10^{-2}) < \tilde{d} < 2.$

Seven simulations were conducted (see Table 1). The time step used in SL1 computations is also shown. Note that the Courant numbers for these simulations were high [$O(100)$]. Large time steps were required to approximate infinite duration while keeping computational time reasonable. Due to the uniform and steady model input (both wind field and bathymetry), the oscillations in the wave field (resulting from high Courant number) were not severe.

Table 1 — Simulation Parameters for Depth-Limited Wave Growth

Depth (m)	**Δx (m)**	**Δt (s) (SL1 only)**	**Approximate C_g (m/s)**
0.45	10	2000	1
1.33	30	2000	2
4	60	2000	4
12	375	3000	7
36	1250	15000	10
108	2500	25000	11
324	3750	40000	11.5

The Hasselmann (1973) formulation for bottom friction, with a JONSWAP friction coefficient of C_{JON}=0.038m^{2}s^{-3} was used for all simulations. Hasselmann (1973) suggests a C_{JON} of 0.038m^{2}s^{-3} for swell conditions and Bouws and Komen (1983) propose a C_{JON} of 0.067m^{2}s^{-3} for wind sea conditions. For these simulations, C_{JON} was not varied, as Ris (1997) observed that these tests are not sensitive to friction coefficient. Comparisons of both models to the analytical and empirical solutions are good (see Figs. 31 and 32).

5.4.3 Duration-Limited Wave Growth

For duration-limited wave growth, both infinite depth and infinite fetch are approximated for several simulation durations: 83 min, 3 hr, 14 hr, 28 hr, 56 hr, and 139 hr. The two models are compared to verify that the higher-order scheme does not have any impact on growth rate. Indeed, this is the case (see Fig. 33).

5.5 Berkhoff-Booij-Radder (BBR) Shoal

Berkhoff et al. (1982) conducted a series of experiments of wave propagation over a submerged elliptical shoal superimposed on a plane beach. This experimental setup provides a scenario where both refraction and diffraction are significant.

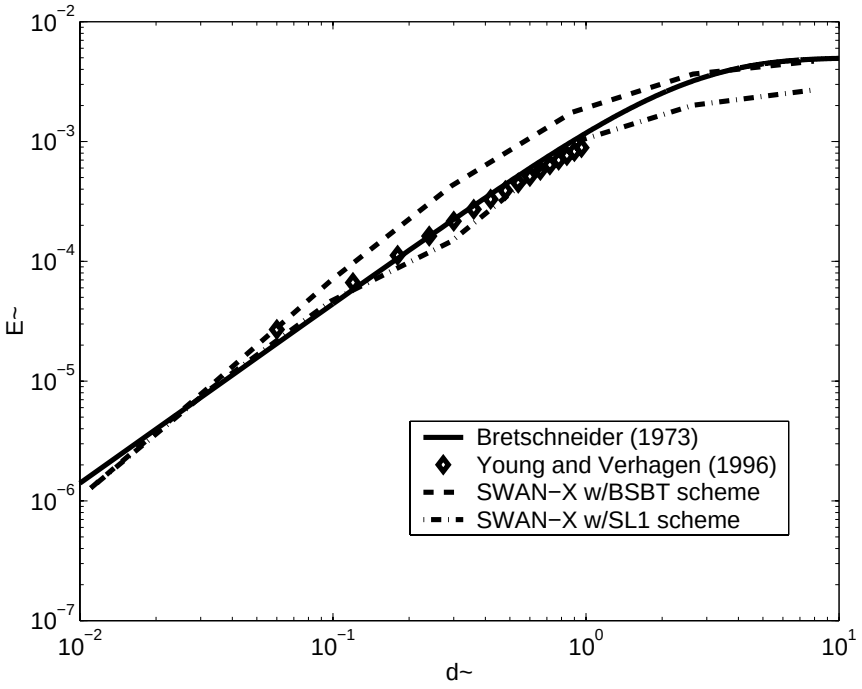

Fig. 31 — Fetch-limited wave generation by wind. Nondimensionalized energy. The BSBT- and SL1-based models are compared to growth curves taken from Bretschneider (1973) and Young and Verhagen (1996).

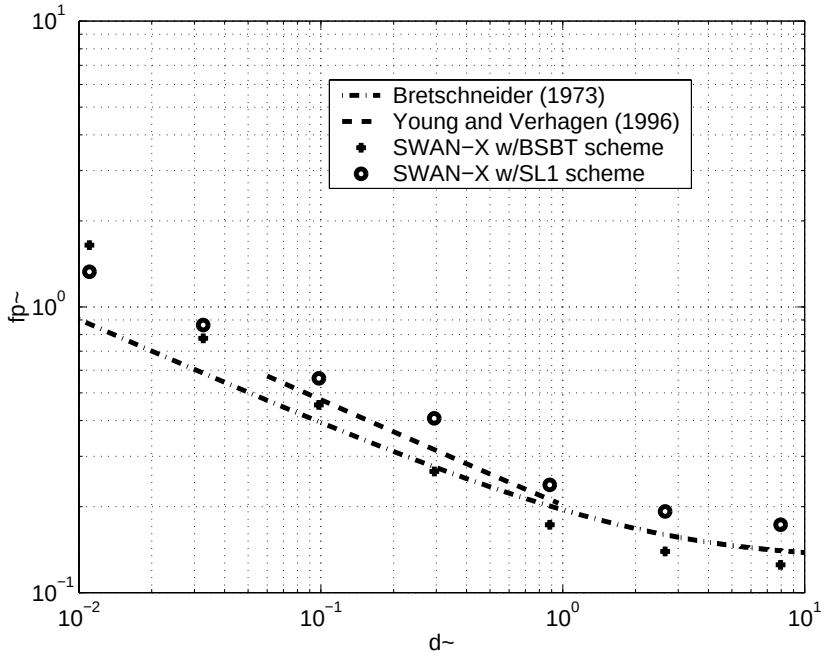

Fig. 32 — Fetch-limited wave generation by wind. Nondimensionalized frequency. The BSBT- and SL1-based models are compared to growth curves taken from Bretschneider (1973) and Young and Verhagen (1996).

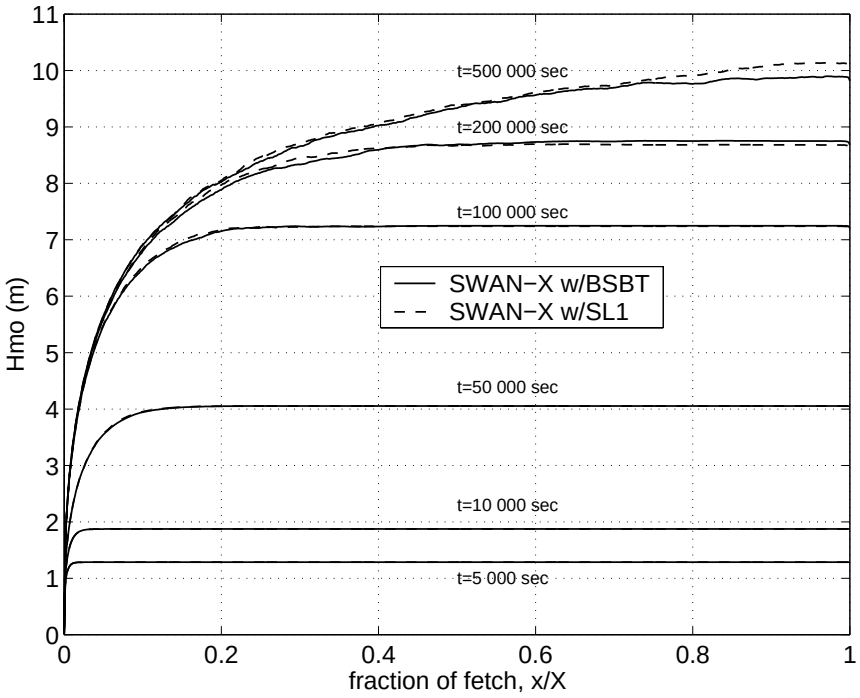

Fig. 33 — Duration-limited wave generation by wind. Wave heights are plotted. The BSBT- and SL1-based models are compared.

Domain size: 25 × 25 m
Grid resolution: $\Delta x = \Delta y = 0.25$ m
Wave height at boundary: $H_{mo} = 0.0464$ m
Wave period: $T = 1$ s (monochromatic)
Wave angle at input boundary: $\theta = 0°$ (unidirectional)

Figure 34 shows the experimental layout. Data from the experiment were compared to results from SWAN, SWAN-X33, and REF/DIF1 (Kirby and Dalrymple 1993) — a phase-resolving, monochromatic wave model based on the parabolic approximation of the mild-slope equation. Unlike the two SWAN models, REF/DIF1 has no diffusion and includes the effects of both refraction and diffraction (implicitly). In these simulations, refraction creates a feature in the wave height field that is prone to diffusion in the hyperbolic models. SWAN-X33 results show significantly less diffusion than SWAN. Figures 35 and 36 show results along two transects where the difference between the two models is greatest (transect nos. 3 and 7). Note the absence of diffraction-induced oscillations in *H(y)* output from the SWAN models.

5.6 DELILAH

5.6.1 Introduction

The DELILAH (Duck Experiment on Low-frequency and Incident-band Longshore and Across-shore Hydrodynamics) (Birkemeier 1991) was conducted at the U.S. Army Corps of Engineers Field Research Facility at Duck, North Carolina during October, 1990 in order to investigate many aspects of surf zone physics. Numerous measurement instruments were employed and several research entities participated.

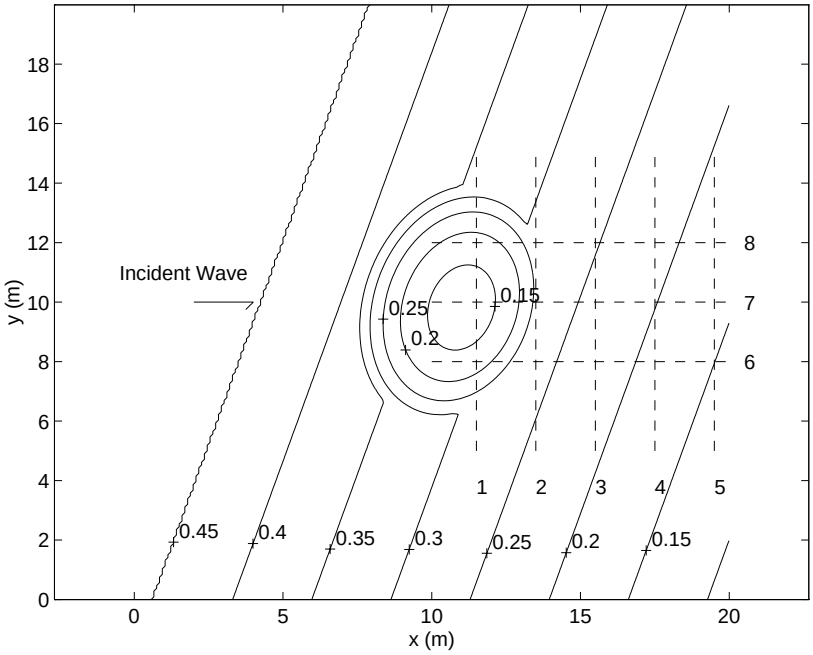

Fig. 34 — Layout of the Berkhoff-Booij-Radder lab experiment

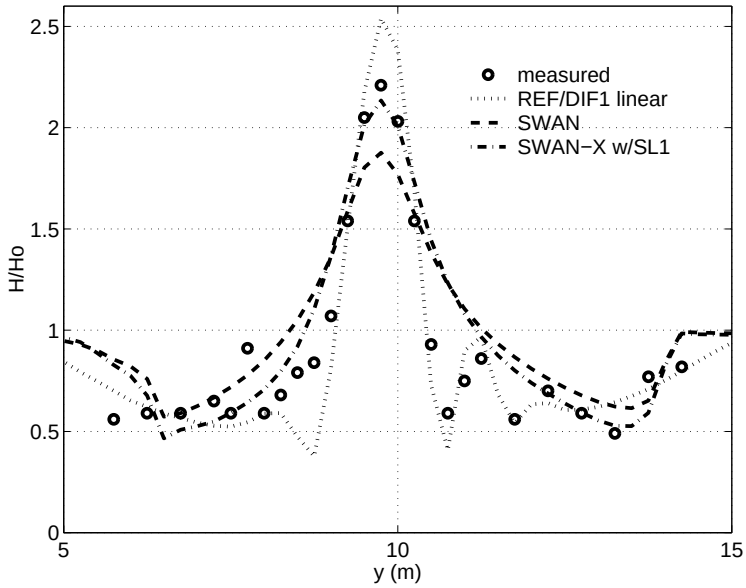

Fig. 35 — The BBR test case: comparison of data to the phase-resolving model REF/DIF1 and the two SWAN models along transect 3 (a lateral transect)

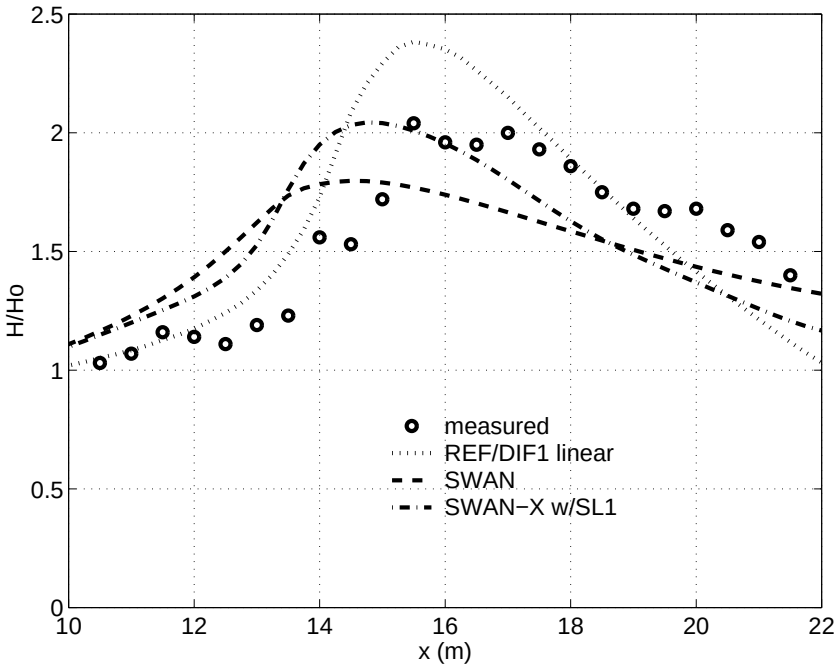

Fig. 36 — The BBR test case: comparison of data to the phase-resolving model REF/DIF1 and the two SWAN models along transect 7 (a longitudinal transect)

5.6.2 Available Data

Daily surveys of a 550 m by 375 m minigrid area were combined with a single, larger (1590 m × 1640 m) regional grid, providing model bathymetries for each day of the experiment. Bathymetric contours are approximately straight and parallel, except near a pier (which is outside the minigrid area). At Duck, sand bar features are often formed near the shoreline during storm events.

Nearshore wave gauges and current meters collected data inside the minigrid area. The nearshore wave gauges provide directional spectra. However, because of less than optimal placement of the wave gauges, the nearshore spectra are, for practical purposes, nondirectional. The nearshore gauges also provide waveheight data along one cross-shore transect and two longshore transects.

High-quality directional spectra data were available for the permanent 8-m depth "Linear Array" and for the 13-m depth SAMSON array. The models were initialized using two-dimensional spectra that had been calculated from the SAMSON array measurements. Data were taken at 2 Hz and samples were taken for 2 hr, 16 min. periods. These samples represented 3 hr time spans, with the remaining 44 min. taken for data analysis and processing.

Figure 37 shows the wave gauge arrangements and a general map of the experiment area.

5.6.3 Model Results

SWAN and SWAN-X33 were each run for 15 of the 3-hr periods between October 6 and 27, 1990, to test a full range of wave conditions. The bathymetry itself also changed considerably during this time. In

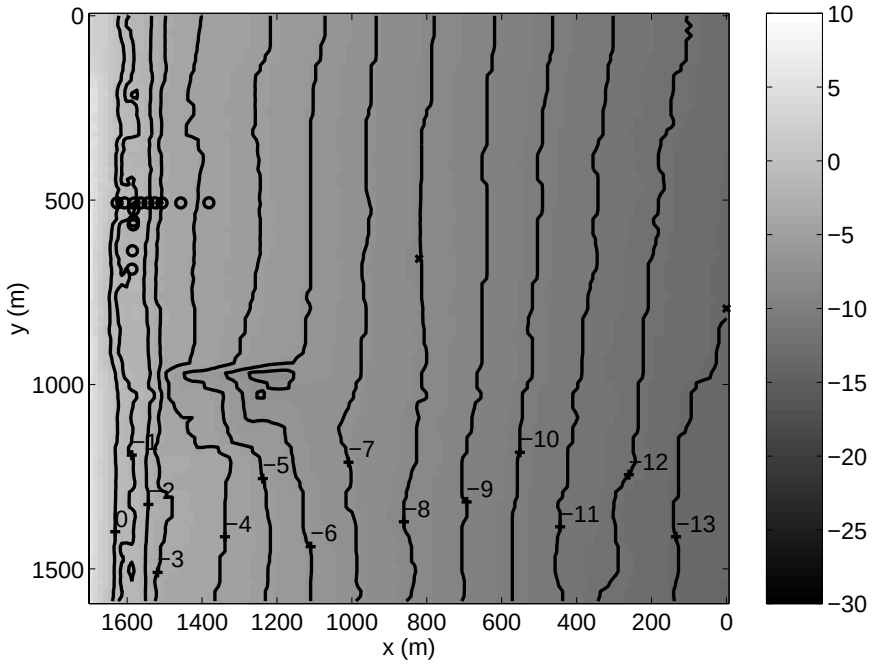

Fig. 37 — Layout of the DELILAH simulations. Locations of spectral data are shown as x's. Locations of nearshore gauges are denoted with o's. Depth contours are in meters. NNW is up.

both models, nonlinear wave-wave interactions were turned off and wave generation by wind was not included. Dissipation by bottom friction was also omitted (this is the default setting of the model).

These 15 cases were also modeled using the spectral parabolic wave model REF/DIF-S (Kirby and Ozkan 1994) and a simple model that calculates wave transformation using the approximation of straight and parallel contours. In general, all four wave models provided very similar results: model-to-model differences were typically much smaller than model-to-data differences.

5.6.3.1 Global Waveheights

The difference between SWAN and SWAN-X caused by diffusion is most easily visualized by comparing global waveheights. Refraction-induced features are evident, especially those created by the scour hole in the vicinity of the Field Research Facility pier (see Fig. 38). These features are visibly diffused by the BSBT scheme. Note that even without diffusion, these refraction features are fairly smooth due to the averaging effect of a full wave spectrum. Spatial gradients and the resulting diffusion are both reduced by the broadness of the input spectra. For more unidirectional and monochromatic wave conditions, the impact of the numerical diffusion would be much greater.

5.6.3.2 Waveheights at Cross-Shore Transects

Because diffusion tends to act perpendicularly to the axis of wave when computations are stationary, comparisons of the two SWAN models along a cross-shore transect do not effectively illustrate diffusion. However, since high-quality data were available along such a transect, comparisons were made as a validation of the two models. Agreement with data is generally good for the models (e.g., see Fig. 39), though SWAN overpredicts waveheights in the nearshore for most of the cases. This can be partially attributed to

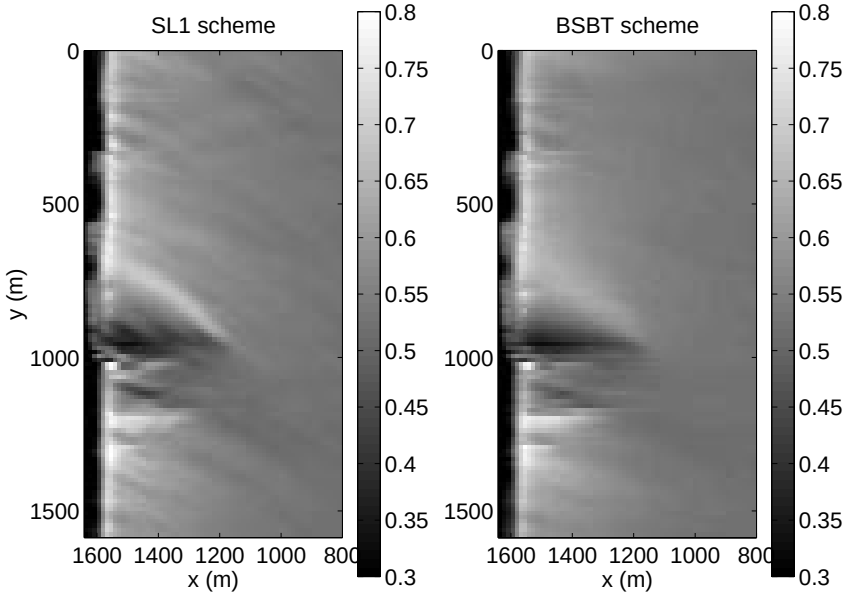

Fig. 38 — Global waveheight comparison for DELILAH simulation of 10-07-90@1600 (EST). Zero moment waveheights are shown in meters.

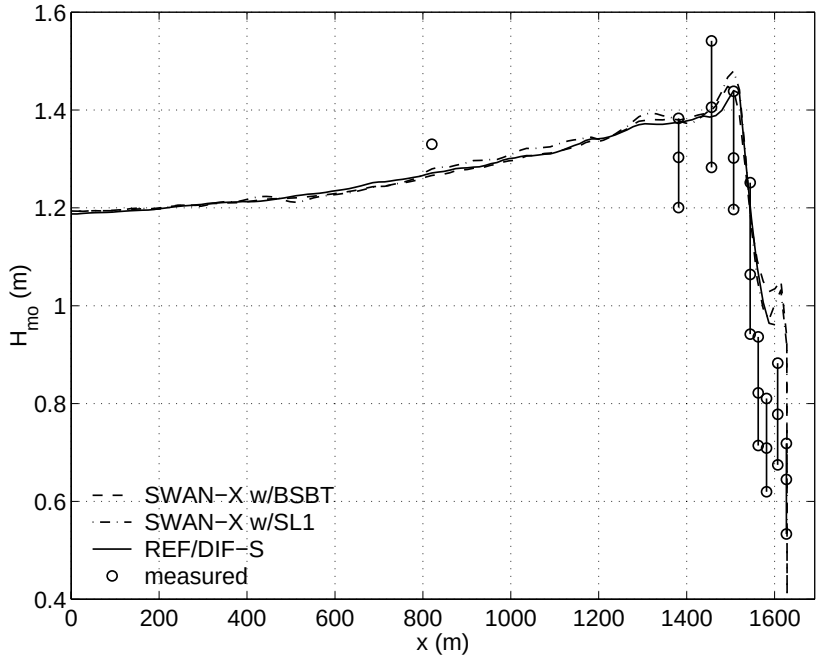

Fig. 39 — Zero moment waveheights are compared along a cross-shore transect: DELILAH simulation of 10-14-90@1900 (EST)

the omission of bottom friction, although other factors may have been equally important (e.g., possible deficiencies of SWAN's breaking mechanism).

5.6.3.3 Directional Spectra at 8-m Contour

Model output was compared to data from the 8-m gauge location. As one might expect, the degree of wave transformation between the 13-m depth contour and 8-m depth contour is generally quite small. Figures 40 through 43 show the spectral comparisons for two simulations with a typical error level (error in terms of H_{mo}, measured vs computed). Both models compare well with the data. SWAN and SWAN-X33 show very similar results, except at one end of the directional spectra, where the SWAN-X spectra are somewhat irregular. This irregularity is typical of the 15 SWAN-X simulations conducted. The irregularity is caused by interaction of the SL1 scheme in geographic space with the centered difference scheme in directional space. It is thought that this irregularity has minimal deleterious impact on model results, particularly in regards to quantities like waveheights.

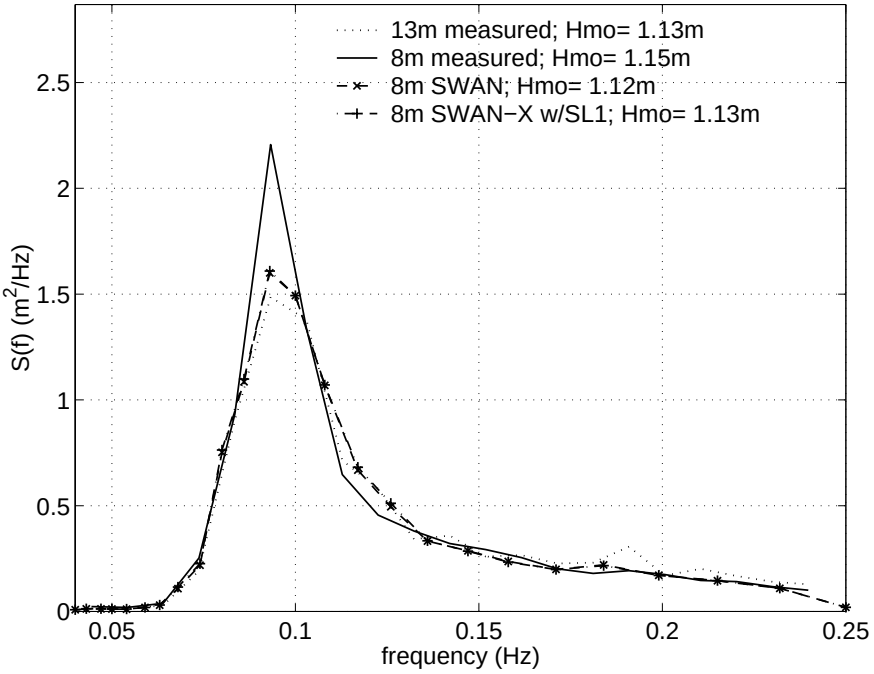

Fig. 40 — Comparison of frequency spectra for the two models and data at the 8 m array for DELILAH simulation of 10-10-90@0100 (EST)

5.6.3.4 Nondirectional Spectra at Nearshore Gauges

Measured frequency spectra from the two nearshore arrays were compared to model results. Figures 44 and 45 show typical results for the (seaward) bar crest and the (landward) bar trough array, respectively. Comparisons of the SWAN models—BSBT mode vs SL1 mode—show an expected outcome: similar S(f) distributions with small differences in waveheight due to decreased diffusion of refraction-focusing in the SL1-based model.

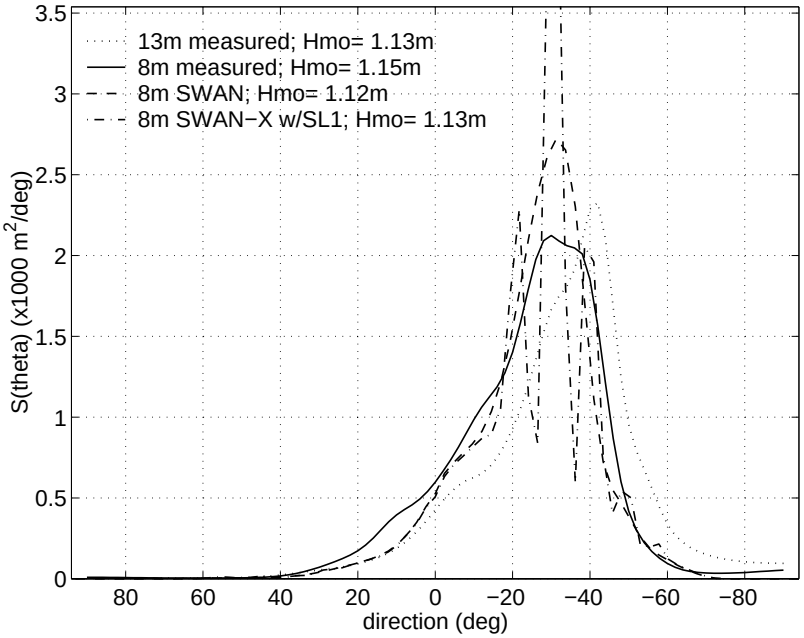

Fig. 41 — Comparison of directional spectra for the two models and data at the 8-m array for DELILAH simulation of 10-10-90@0100 (EST)

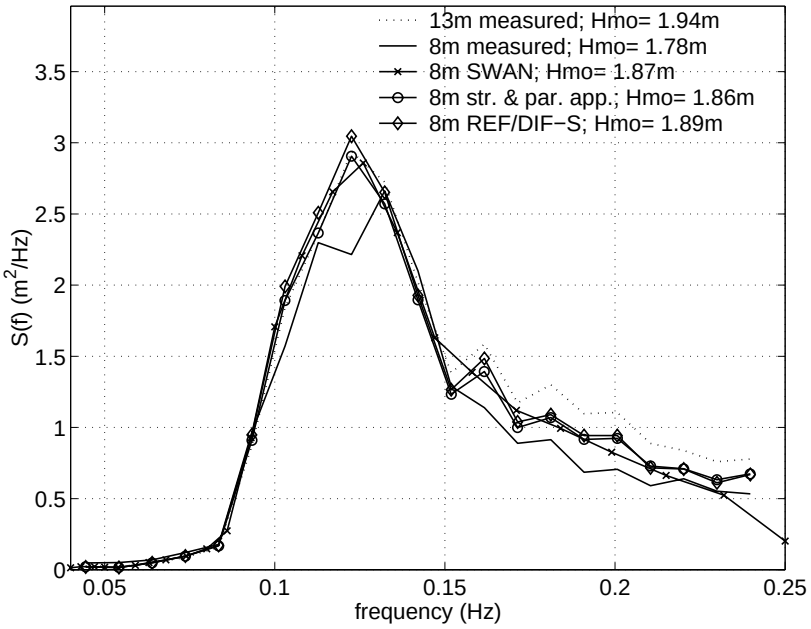

Fig. 42 — Comparison of frequency spectra at the 8-m array for DELILAH simulation of 10-11-90@0100 (EST): data vs SWAN, REF/DIF-S, and simplified model

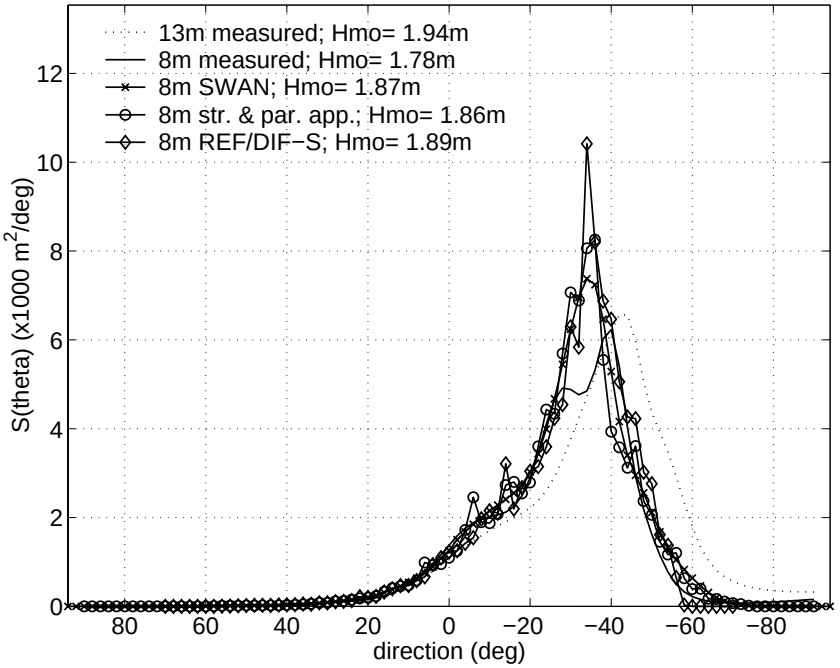

Fig. 43 — Comparison of directional spectra at the 8-m array for DELILAH simulation of 10-11-90@0100 (EST): data vs SWAN, REF/DIF-S, and simplified model

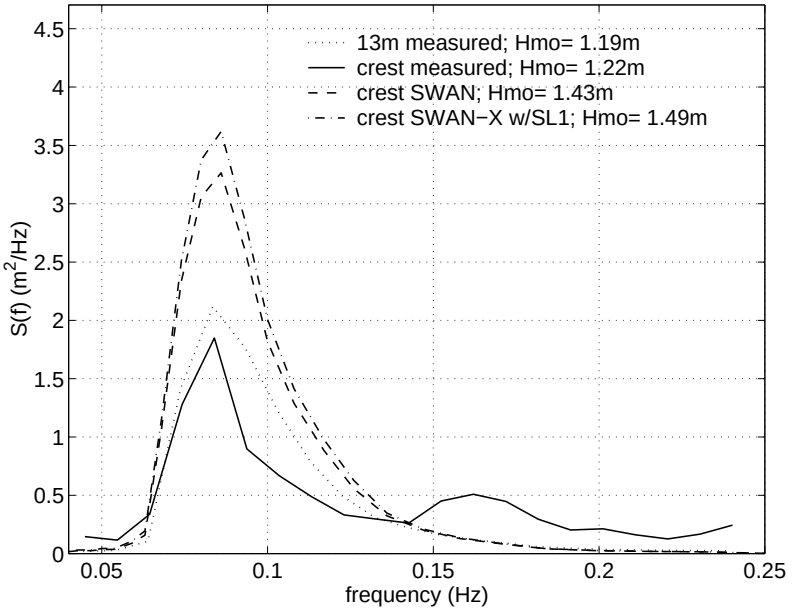

Fig. 44 — Comparison of frequency spectra at the bar crest array for DELILAH simulation of 10-14-90@1900 (EST): data vs the two SWAN models

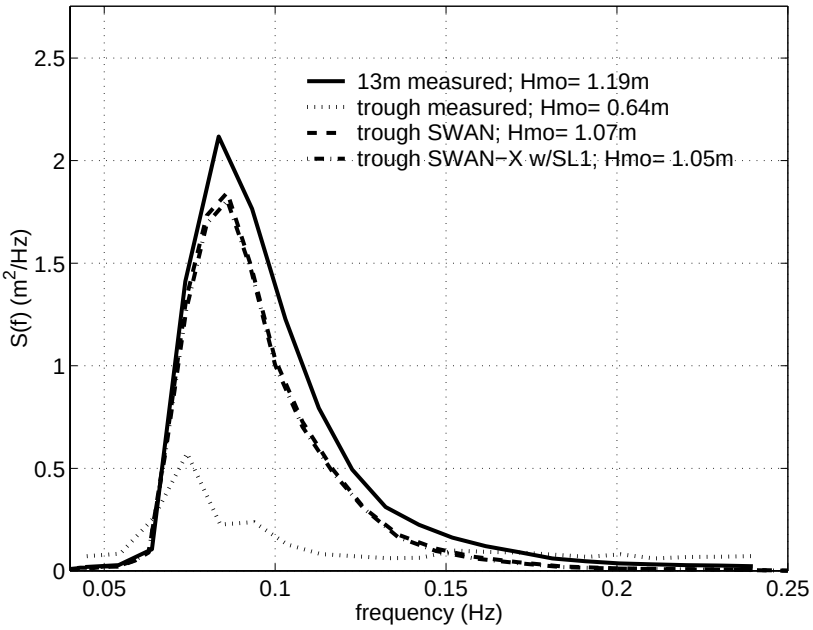

Fig. 45 — Comparison of frequency spectra at the bar trough array for DELILAH simulation of 10-14-90@1900 (EST): data vs the two SWAN models

Although not particularly relevant to a discussion of numerics and diffusion, the effect of triad wave-wave interaction on model results is worth mentioning. Because amplifications of the second harmonic of the spectral peak were observed in the nearshore data, several DELILAH cases were simulated with triads enabled in SWAN. Generally, this resulted in a large improvement in model-data comparisons (e.g., see Fig. 46). However, the model still overpredicts wave energy in the nearshore, particularly at the higher frequencies.

5.7 DUCK94

5.7.1 Introduction

The DUCK 94 experiment (Birkemeier and Thornton 1994) took place in August and October of 1994. The primary purpose was to study sediment transport, morphology, wave transformation, nearshore circulation, and swash processes, as well as to provide a mechanism for collaboration between researchers. Nineteen organizations and over 100 researchers participated. Wave data collected as part of the DUCK94 experiment were used to validate and compare the two SWAN models.

5.7.2 Model Setup and Input

The models were initialized with data collected by the "inner shelf buoy" that had been deployed for the experiment (Jensen 1995). Processed wave spectra at this buoy were available hourly for the time period of 0000 GMT Oct. 10 to 0000 GMT Oct. 22. Wind data, also collected at this buoy, were used for some of the simulations. The buoy was located in approximately 27-m water depth.

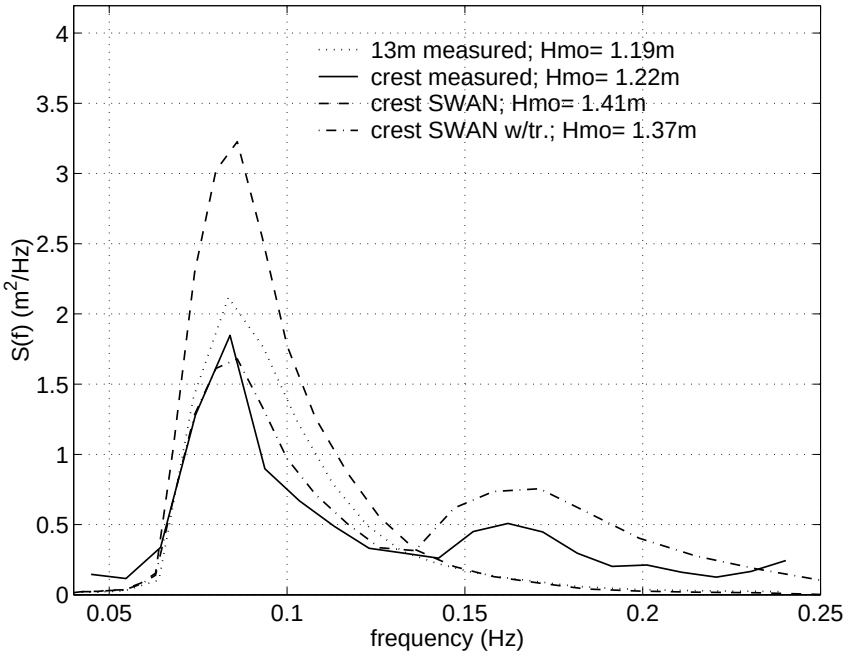

Fig. 46 — Comparison of frequency spectra at the bar crest array for DELILAH simulation of 10-14-90@1900 (EST): data vs SWAN (with and without triads)

Spectral output from the models was compared to data collected at the U.S. Army Corps of Engineers Field Research Facility Linear Array, located in approximately 8-m water depth. Directional wave spectra are calculated from data collected at this permanent array every three hours. During the 12 days that were modeled, there are 89 time periods for which both inner shelf data and Linear Array data exist. Seven simulation sets (each composed of 89 simulations) were conducted. Four are relevant to this study:

- SWAN-X with the BSBT scheme, without wind
- SWAN-X with the SL1 scheme, without wind
- SWAN-X with the BSBT scheme, with wind
- SWAN-X with the SL1 scheme, with wind

These simulations did not include bottom friction.

The Coastal Hydraulics Laboratory, U.S. Army Corps of Engineers, provided a bathymetric grid for the region. This grid was created by Dr. John Dugan (of Arete Associates) using NOS digital bathymetry, DBDB5 bathymetry, and hydrographic surveys conducted during DUCK94. The grid has the following characteristics:

- 40.0 km across in *x* (longitude).
- 107 km wide in *y* (latitude).
- 404 meter resolution in *x.*
- 500 meter resolution in y.
- Low-*x* side of the grid corresponds to the longitude of the Inner Shelf buoy; wave height is specified along this boundary.
- High-*x* side of the grid is land.

Figure 47 shows the bathymetry and the locations of the instruments.

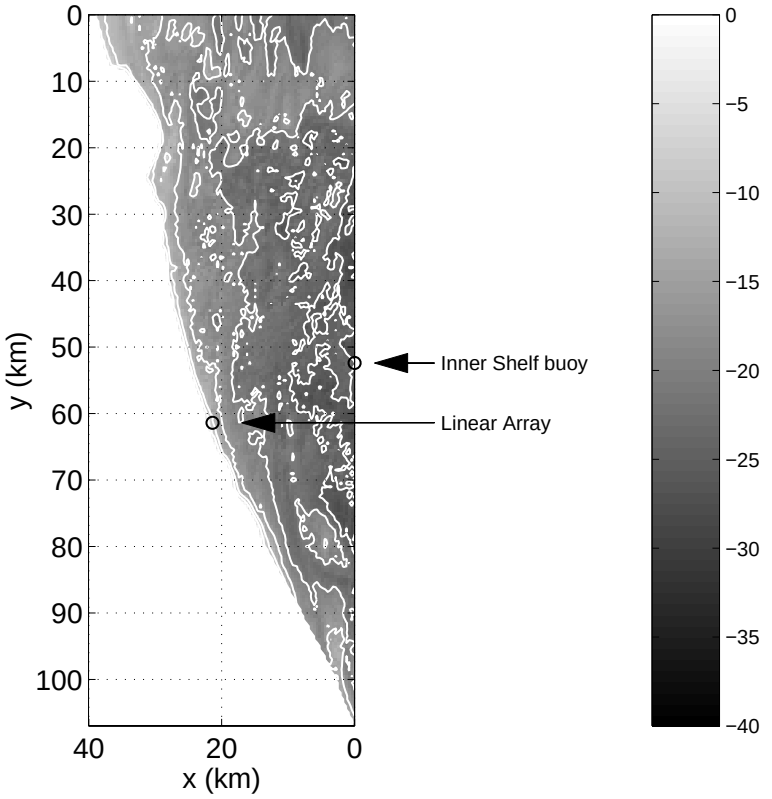

Fig. 47 — Bathymetry used for DUCK94 simulations. Depths are shown in meters.

For the simulations with the higher order scheme, specification of a time step size was necessary. This value was chosen such that the peak wave of a particular spectrum would propagate across the domain four times during the simulation. The approximate travel time of the peak wave was approximated using the direction and group velocity of the wave over an approximated flat bathymetry. The calculated time step sizes resulted in CFLs ranging from 8 to 15.

5.7.3 Comparison: Simulations Without Wind Input

Differences in global waveheights produced by the two models are, for the most part, unremarkable. This is not surprising, as model input is stationary and spatial variability of wave conditions is minimal. Refraction-induced features do exist, however, and diffusion of these features is apparent. Figure 48 shows waveheights in the region of the Linear Array. The more distinctive refraction features in the SL1-based model suggest that the BSBT scheme is artificially diffusing these features.

The impact of the numerical scheme on wave conditions at the location of the Linear Array is minimal. Figures 49 through 52 compare gross wave parameters for both models and data. The two models show similar results; both compare fairly well to the data, though admittedly, these simulations of wave propagation are not difficult tests of model skill.

Directional spectra at the Linear Array (e.g., as in Figs. 53 and 54) were compared, but no clear trends were observed. Error is, in general, evenly distributed across the spectra.

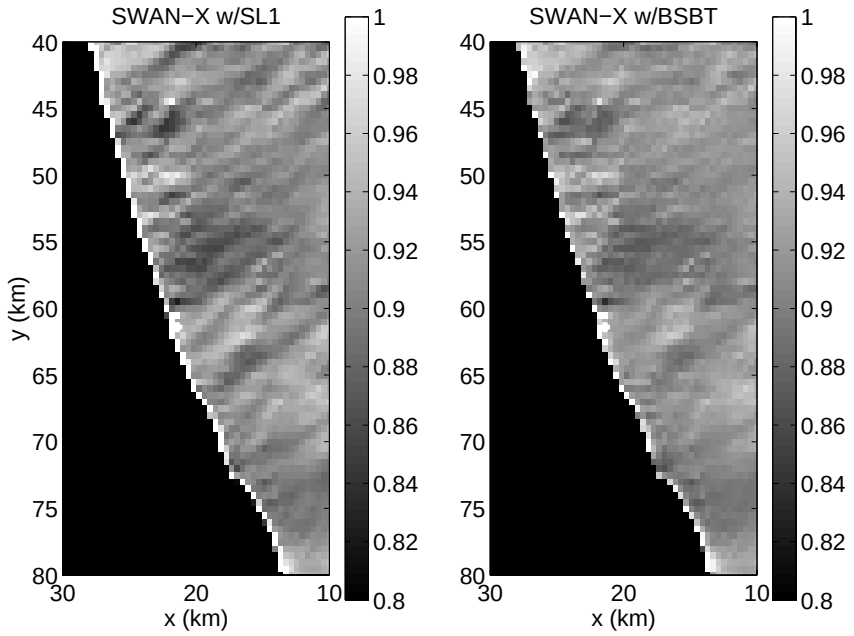

Fig. 48 — Comparison of global waveheights from the two SWAN models on 10-19-1994@0600 EST. Waveheights have been normalized by the waveheights at the Inner Shelf buoy.

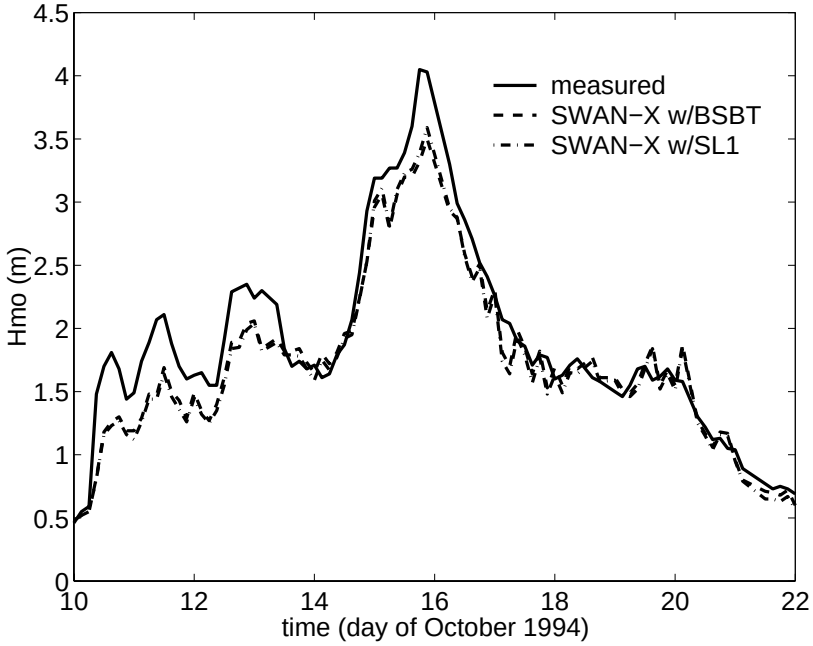

Fig. 49 — Comparison of waveheights from the two SWAN models at the linear array for the 12 days that were modeled (zero moment waveheights in meters)

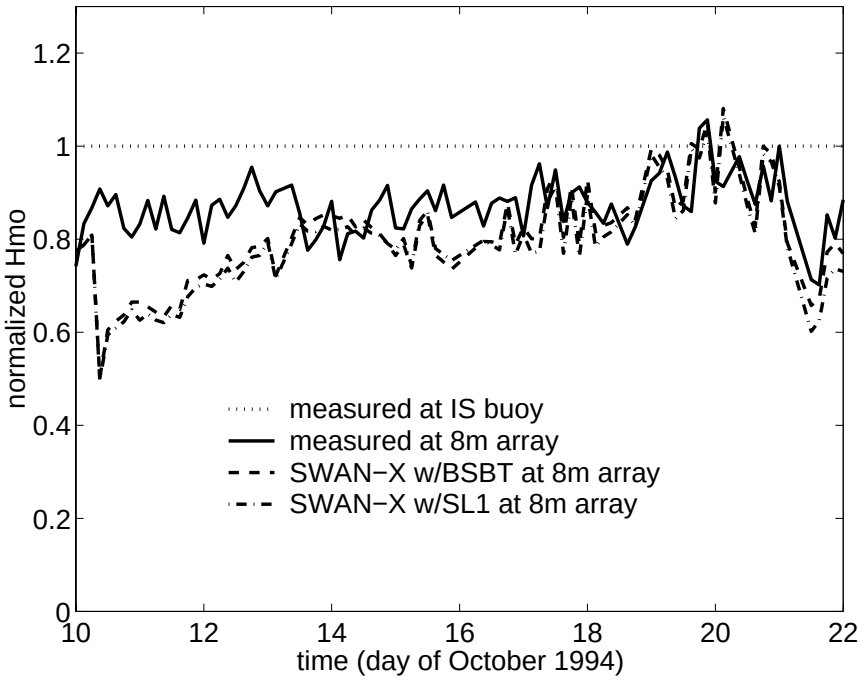

Fig. 50 — Comparison of normalized waveheights from the two SWAN models at the linear array for the 12 days that were modeled. Waveheights have been normalized by the waveheights at the Inner Shelf buoy.

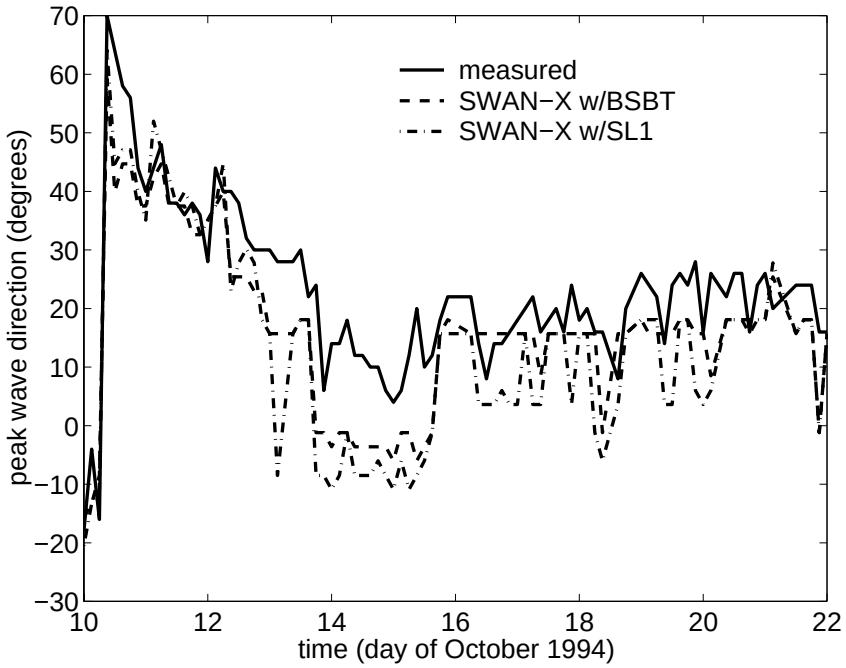

Fig. 51 — Comparison of peak wave angles from the two SWAN models at the linear array for the 12 days that were modeled. Wave angles are in degrees (traveling toward north = –90 degrees; traveling toward south = +90 degrees)

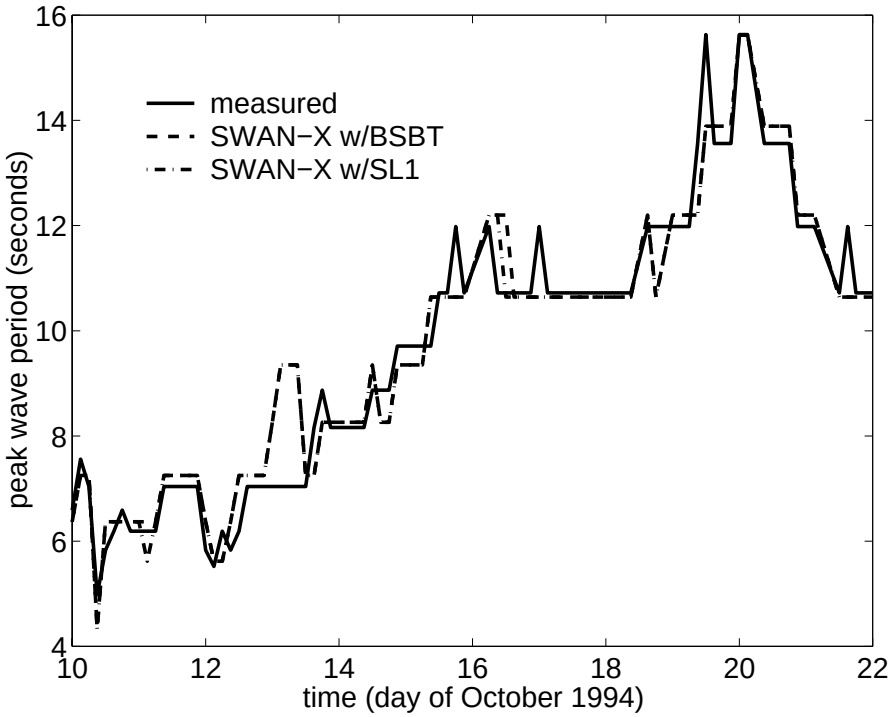

Fig. 52 — Comparison of peak wave periods (in seconds) from the two SWAN models at the linear array for the 12 days that were modeled

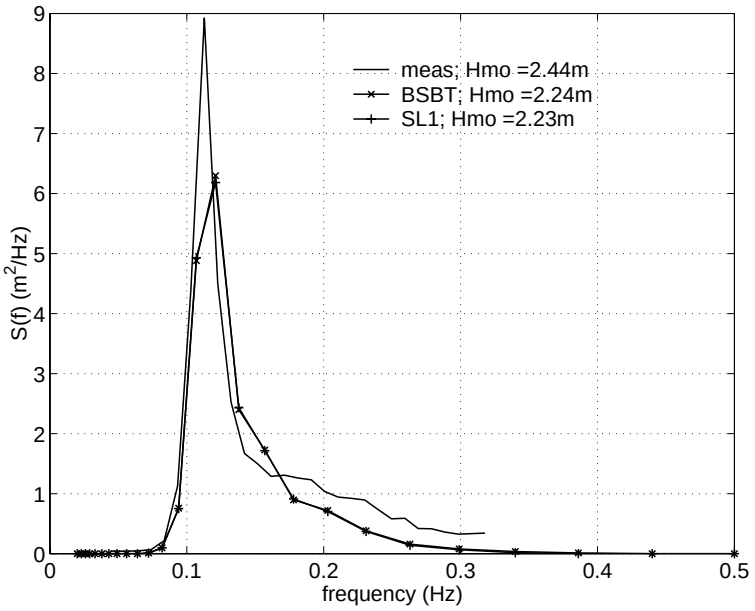

Fig. 53 — Comparison of frequency spectra at the 8-m array: data vs the two SWAN models. Simulation: 10-14-1994@1800 EST.

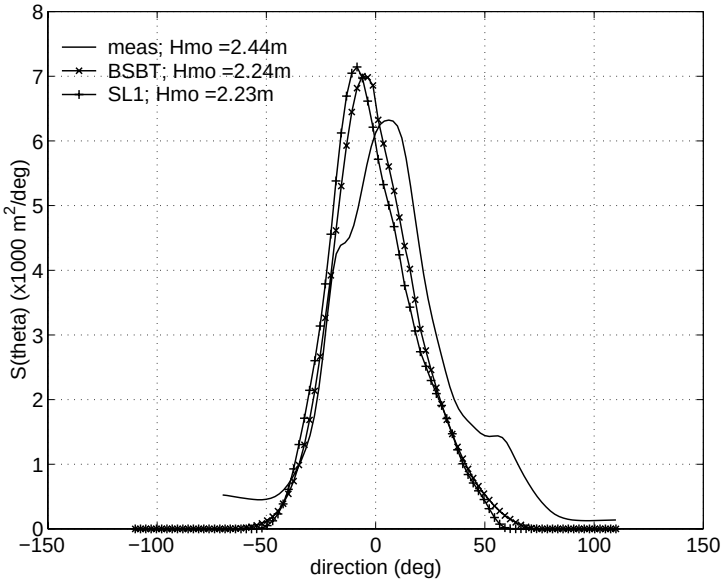

Fig. 54 — Comparison of directional spectra at the 8-m array: data vs the two SWAN models. Simulation: 10-14-1994@1800 EST.

5.7.4 Comparison: Simulations With Wind Input

Comparisons of gross wave parameters to the data are visibly improved with the inclusion of wind for both the SWAN simulations (Fig. 55) and the SWAN-X with SL1 simulations (Fig. 56). Unsurprisingly, the improvement is most noticeable during the first two days of the data set, when local wind sea dominates. As in the simulations without wind, minor differences between the two schemes exist in the global waveheights, but at the linear array, the impact of the reduced diffusion is insignificant.

5.8 Southern California Bight

5.8.1 Introduction

San Miguel and Santa Rosa Islands are located offshore of Ventura, California, in the Southern California Bight. Figure 57 shows their location with respect to the coast. The wave climate in the Southern California Bight (stretching from Point Conception south to the Mexican border) has been actively monitored by the Coastal Data Information Program (CDIP), which is based at Scripps Institution of Oceanography in La Jolla. CDIP is jointly funded by the California Department of Boating and Waterways and the U.S. Army Corps of Engineers.

The California shelf is extremely narrow; it is generally no more than 11 km from shoreline to shelfbreak. The bathymetry in the Bight is mostly planar, with submarine canyons and other features in some areas. The California coastline south of Point Conception generally faces southwest. The presence of Point Conception shelters much of the Bight from waves coming from the northwest, as occurs often during winter storms. During the summer, the wave climate in the Bight is dominated by swell generated by Southern Hemisphere storms. The islands in the Bight potentially shelter much of the coastline from offshore waves.

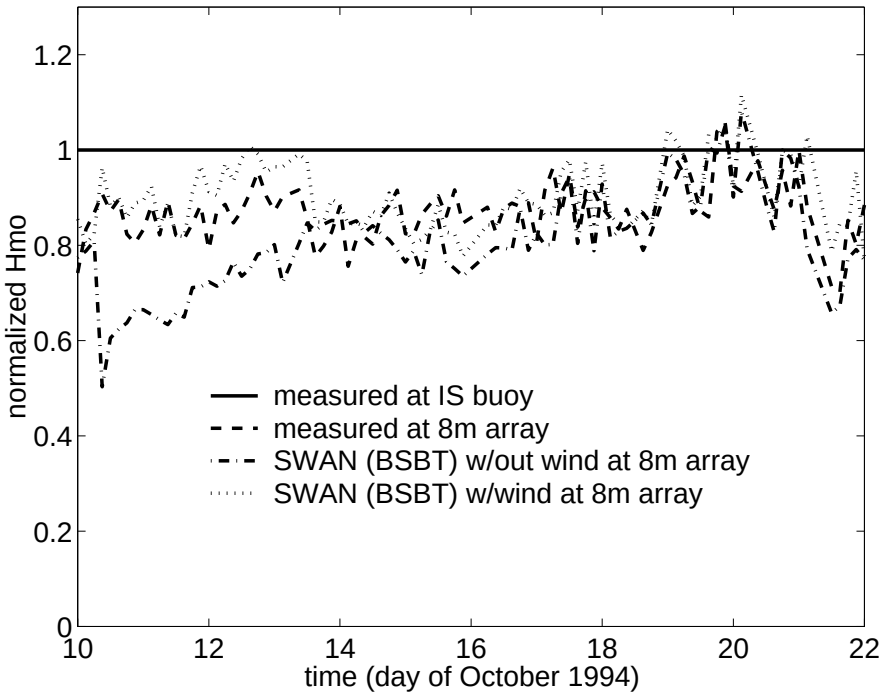

Fig. 55 — Comparison of normalized waveheights from SWAN-X with BSBT scheme (with and without wind) at the linear array for the 12 days that were modeled. Waveheights have been normalized by the waveheights at the Inner Shelf buoy.

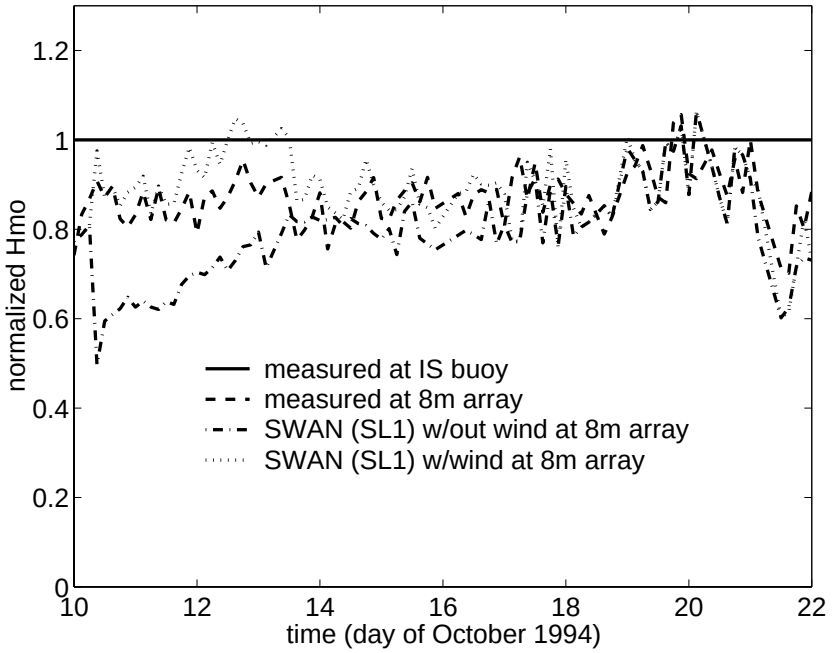

Fig. 56 — Comparison of normalized waveheights from SWAN-X with SL1 scheme (with and without wind) at the linear array for the 12 days that were modeled. Waveheights have been normalized by the waveheights at the Inner Shelf buoy.

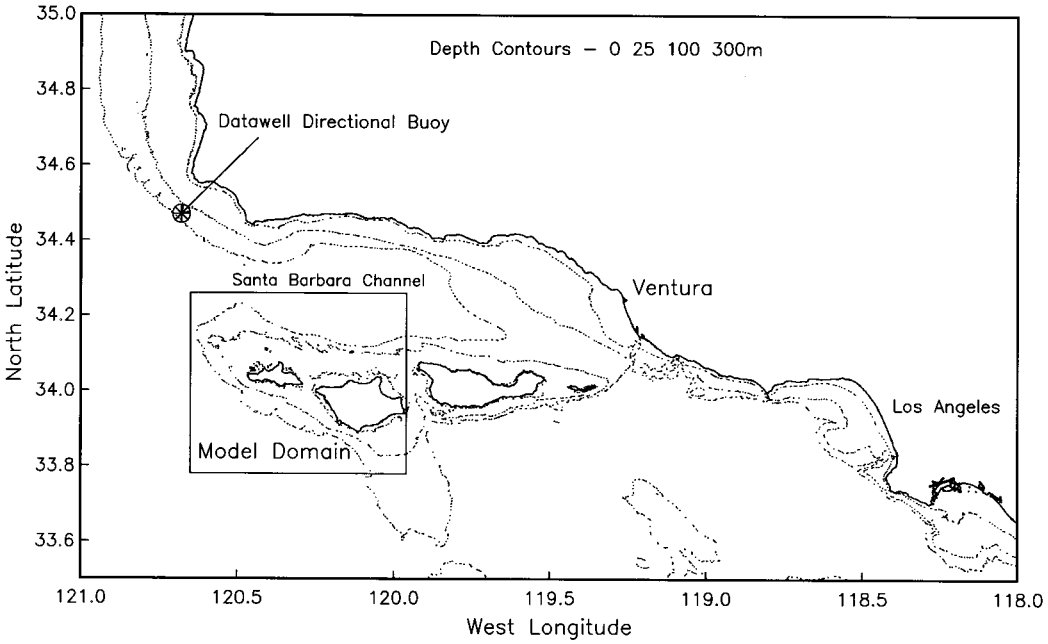

Fig. 57 — Map of San Miguel (left) and Santa Rosa (right) Islands and vicinity

In early 1992, pressure gauges were installed around Santa Rosa Island to measure the wave climate in the area. Figure 58 shows the locations of the gauges and the bathymetry around the islands. We will emphasize comparisons of the data with the model at gauge #10 (located between the islands) and gauge #11 (located on the southwest side of Santa Rosa Island). A Datawell buoy located offshore of Point Conception measured waves as they entered the Bight.

5.8.2 Model Setup

We used the bathymetry depicted in Fig. 58 to simulate swell propagation around the islands. The presence of the islands would tend to exacerbate the diffusion in the geographic propagation terms in SWAN. The bathymetric grid extended 66.7 km by 53.4 km, with a resolution of 100 meters in both directions. This very fine resolution was used to allow direct comparisons to a phase-resolving model; it ensured that the bathymetric variations in the vicinity of the islands would be well resolved in the model (numerical experiments later confirmed a significant dependence on resolution at some locations). Directional spectra measured at the Point Conception buoy during January 1992 were used as model input, with the frequencies limited to the swell range (0.05 to 0.09 Hz). The directional range used comprised waves arriving from due north to due south (37 directions at 5 degree intervals).

5.8.3 Model Results

The stationary SWAN model was run with all January 1992 spectra. Figure 59 compares the energy (in cm^2) from SWAN output with that of the gauge data at gauge #10. Also shown are results from a spectral refraction model (LeMehaute and Wang 1982) and a parabolic refraction/diffraction model (Kirby 1986). The implementation of the latter two models for the Southern California Bight was detailed in O'Reilly and Guza (1993). Finally, the energy level at the Point Conception buoy is also shown. The inclusion of the offshore data in the plot emphasizes the sheltering experienced by gauge #10. In general, SWAN overpredicts

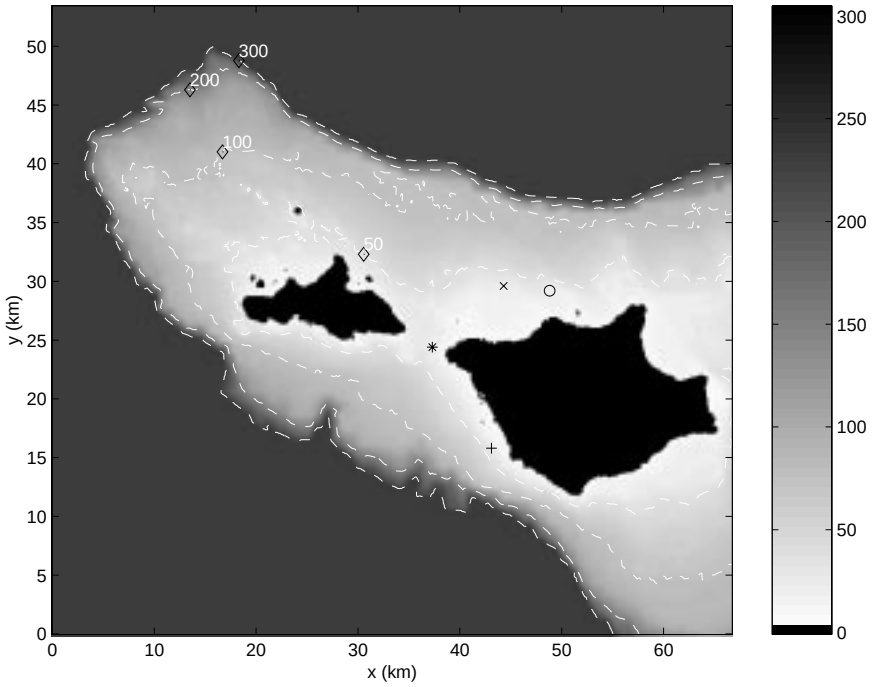

Fig. 58 — Bathymetry and gauge locations around San Miguel and Santa Rosa Islands. Depths are in meters. Gauges shown are: #8 (o), #9 (x), #10 (*), and #11 (+).

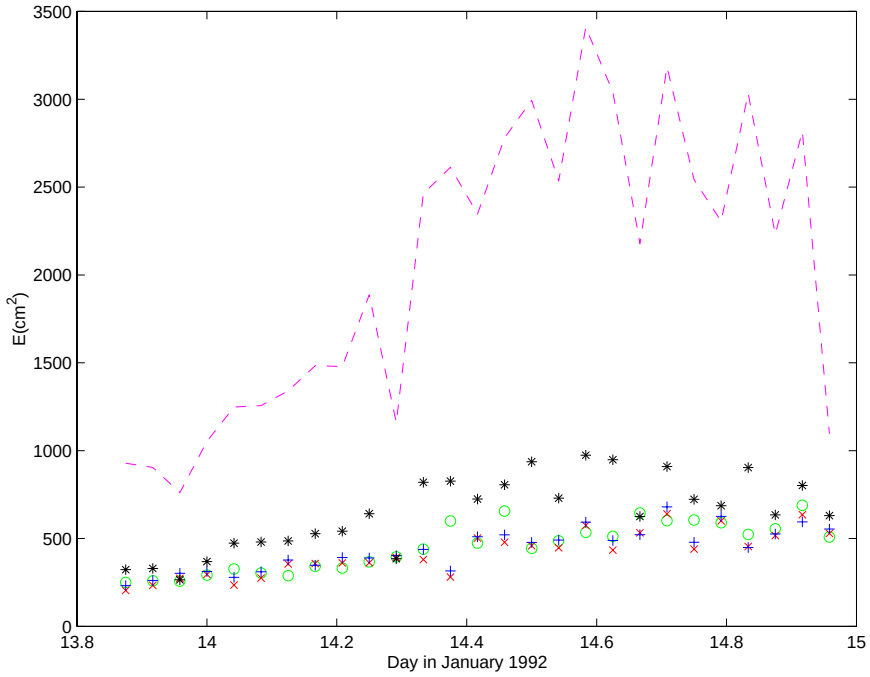

Fig. 59 — Comparisons of SWAN energy predictions (*) at gauge #10 to measured data (o), spectral refraction model (x), and refraction/diffraction model (+). Dashed line is energy level at Point Conception buoy.

the energy at this gauge. This is a consequence of the diffusive numerical scheme leaking energy into heavily sheltered areas. Figure 60 shows a comparison of the models to the measurements at gauge #11. This site is much more exposed to the offshore wave climate. For the most part, the SWAN model does as well as the other models in estimating the wave energy.

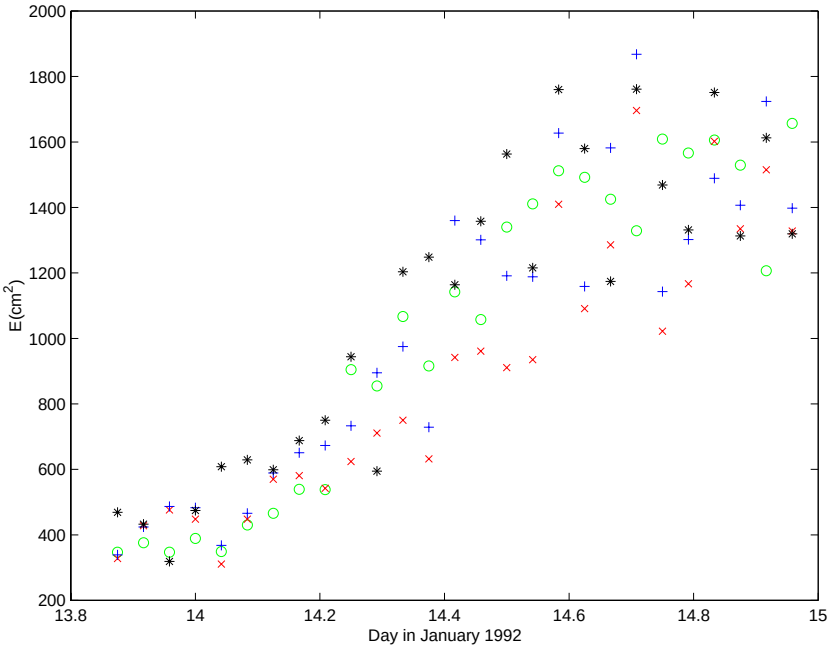

Fig. 60 — Comparison of SWAN energy predictions (*) at gauge #11 to measured data (o), spectral refraction model (x), and refraction/diffraction model (+)

Due to the fine geographic resolution used (with 668×535 grid points), the simulations were expensive computationally. The SWAN runs for the entire January 1992 data set required a total of approximately 2 days of CPU time on a Sun Ultra2300 workstation (300 MHz processor). Each run required approximately 300 MB of RAM. Because of the fine spatial resolution, an equally fine temporal resolution was needed due to CFL considerations: the SWAN-X simulations with the SL1 scheme used a Δt of 10 seconds. With this small time step increment, 1000 time steps were necessary in order to propagate energy to a steady-state condition. Thus, *each* SWAN-X run required almost 2 weeks of CPU time and approximately 600 MB RAM on the same workstation. Clearly, use of the pseudo-stationary SL1 model with a large (100,000+ grid points), high-resolution (less than 200 m spacing) grid is impractical for any present workstation or PC. Fortunately, unlike phase-resolving models, SWAN does not require a minimum spatial resolution, so when the bathymetry does not require high resolution, the size of the SWAN-X simulation can be tailored to computational resources.

The results do look promising in the vicinity of gauge #10. Figure 61 shows frequency and direction spectra at gauge #10 from a SWAN run for January 14, 1992 at 2300 PST. The direction spectra $S(\theta)$ shows two peaks, corresponding to energy propagating around both sides of San Miguel Island. (Zero degrees indicates due east propagation.) The zero moment waveheight H_{mo} = 1.03 m. Figure 62 shows the same result from SWAN-X. The zero moment waveheight is noticeably lower: 0.92 m. Table 2 summarizes the results for this case at gauge #10.

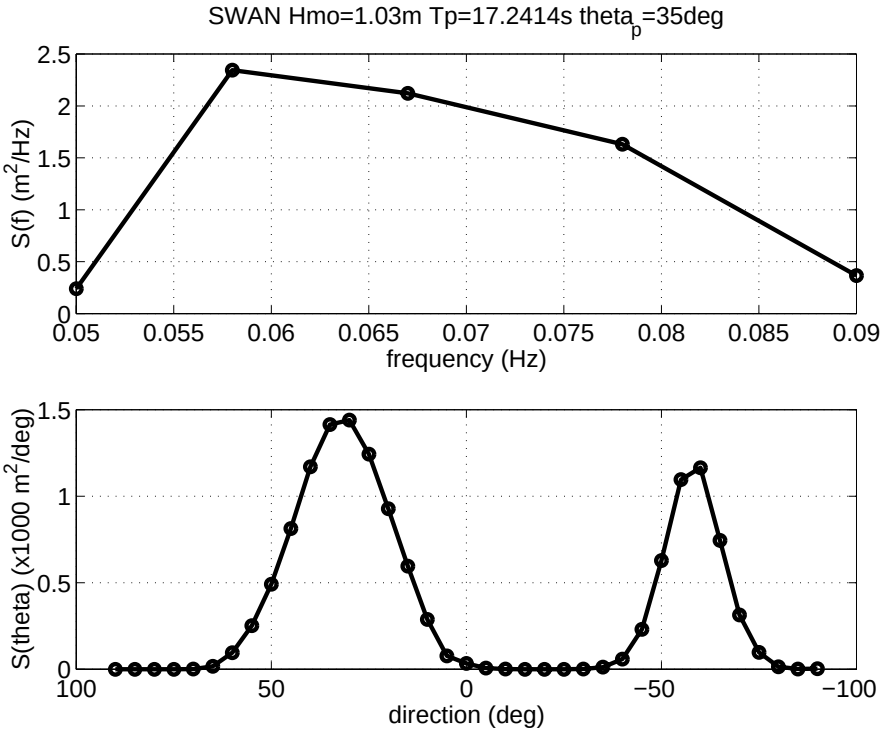

Fig. 61 — Frequency (top) and direction (bottom) spectra from SWAN at gauge #10 for January 14, 1992 at 2300 PST

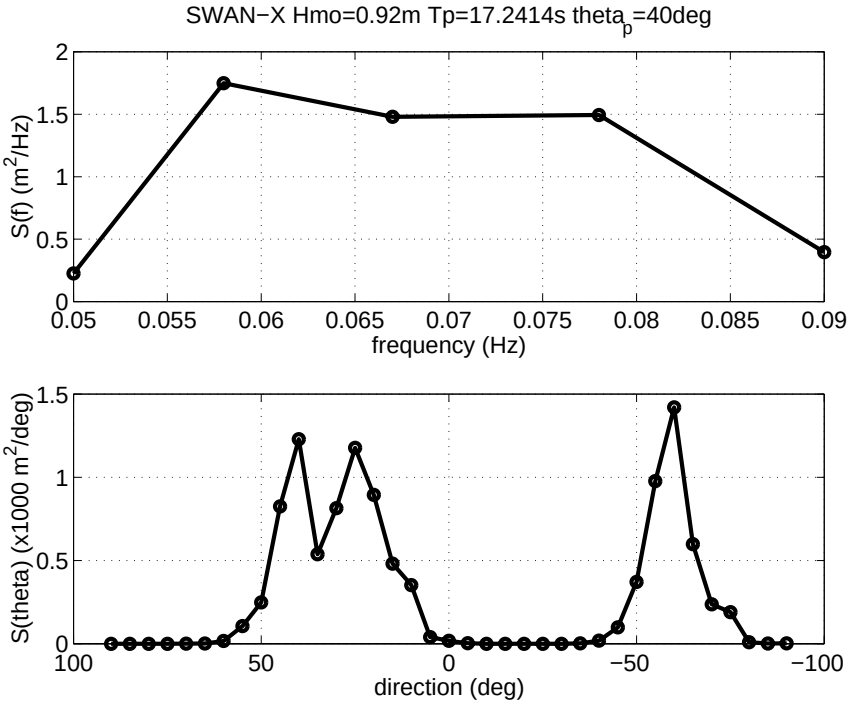

Fig. 62 — Frequency (top) and direction (bottom) spectra from SWAN-X at gauge #10 for January 14, 1992 at 2300 PST

Table 2 — Comparisons of H_{mo} at Gauge #10 for January 14, 1992 at 2300 PST

	H_{mo} at Gauge #10 (m)
Measured	0.89 m
Refraction/Diffraction	0.94 m
Refraction	0.92 m
SWAN	1.03 m
SWAN-X	0.92 m

The reduction in the SWAN-X H_{mo} prediction relative to that of SWAN is due to the reduced numerical diffusion of the higher order scheme. Globally, the effect of this scheme can be seen from the waveheight predictions throughout the domain (Fig. 63). The SWAN prediction shows a fairly smooth waveheight field on the northern side of Santa Rosa Island and between it and San Miguel Island. This smoothness is an artifact of numerical diffusion. In contrast, the SWAN-X prediction shows much more variability in the waveheight patterns around the island, due to the higher-order scheme for geographical propagation.

11. THE GARDEN SPRINKLER EFFECT

The "garden sprinkler effect" (GSE) is a well-known problem whereby an initial spatial distribution of wave energy disintegrates into individual components as the energy propagates, each component corresponding to a particular spectral bin used in the model. The GSE is perhaps most easily described as a problem of spectral resolution: with an extremely fine spectral resolution, energy would disperse evenly and the resulting wave field would be — in most instances — continuous. With a coarse spectral resolution, the resulting energy field is discontinuous due to geographic separation of energy bins (e.g., see Figs. 64 and 65). Typically, computational resources require the use of a relatively coarse spectral resolution ($\Delta\theta \geq 5°$). Because the problem is greater for cases of severe spatial and temporal variability of input, it is generally associated with propagation at large scales.

Numerical diffusion tends to counter the GSE, as it smooths the spatial irregularities in the energy field. Thus, the problem is most noticeable in models that have little numerical diffusion. With the introduction of the new propagation scheme in SWAN-X, there is a greater incentive for incorporating measures to counter the GSE.

Booij and Holthuijsen (1987) created one such tool. It operates by diffusing wave energy a) in the direction of wave propagation (to counter effects of frequency discretization) and b) normal to the direction of wave propagation (to counter effects of directional discretization). The magnitude of the diffusion for each is controlled by a diffusion coefficient—D_{ss} and D_{nn}, respectively. The coefficients are a function of the level of discretization and the propagation characteristics of the wave energy:

$$D_{ss} = \Delta c_i^2 T / 12$$
$$D_{nn} = c_i^2 \Delta\theta_i^2 T / 12 \qquad (62)$$

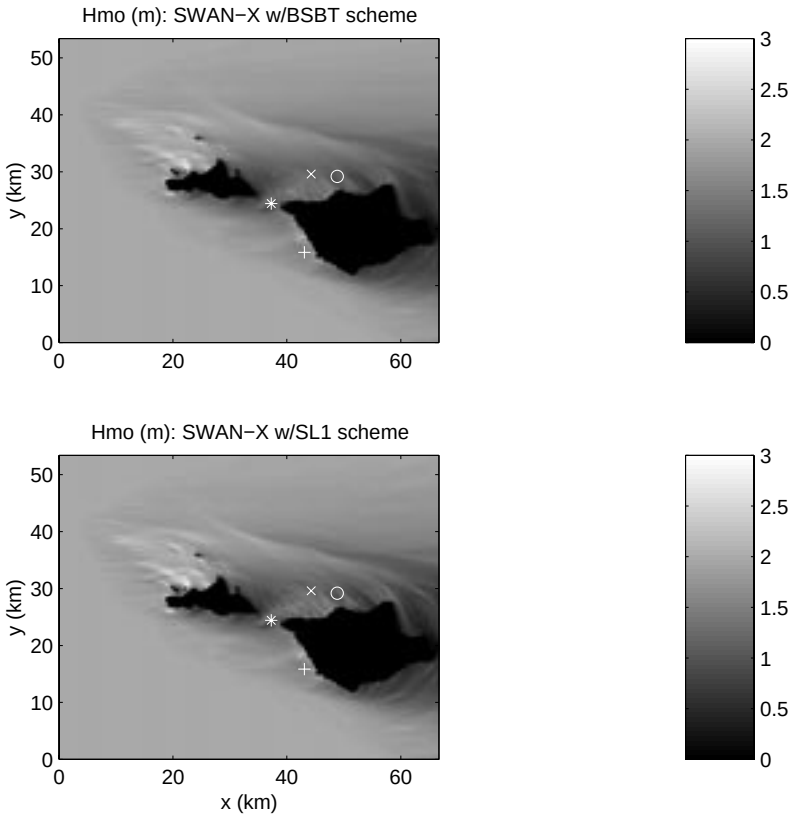

Fig. 63 — Global waveheight results from SWAN (top) and SWAN-X (bottom) for January 14, 1992 at 2300 PST

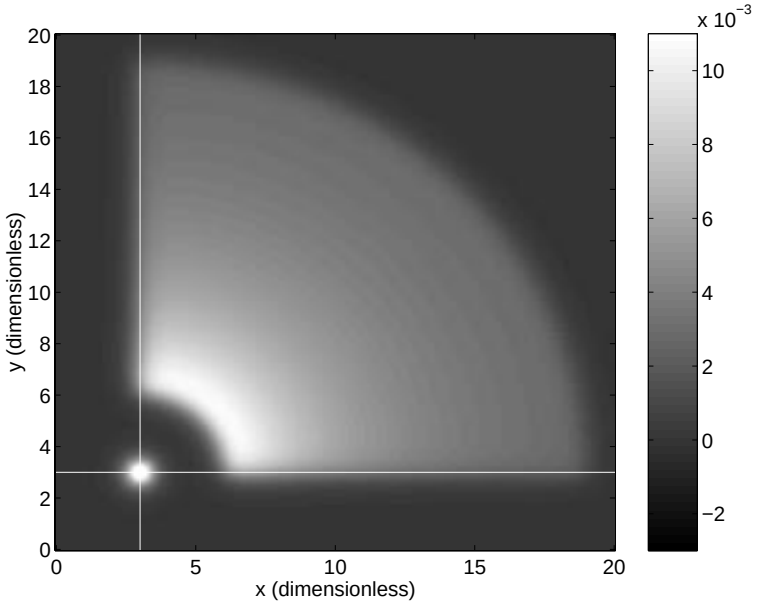

Fig. 64 — An energy field. All energy starts at the same location, shown in lower left corner ($x = y = 3$). Energy disperses as it propagates due to directional and frequency (i.e., speed) distribution of the initial spectra. In this case, the initial spectrum is very finely resolved, so the Garden Sprinkler Effect is insignificant. The resulting energy field is continuous.

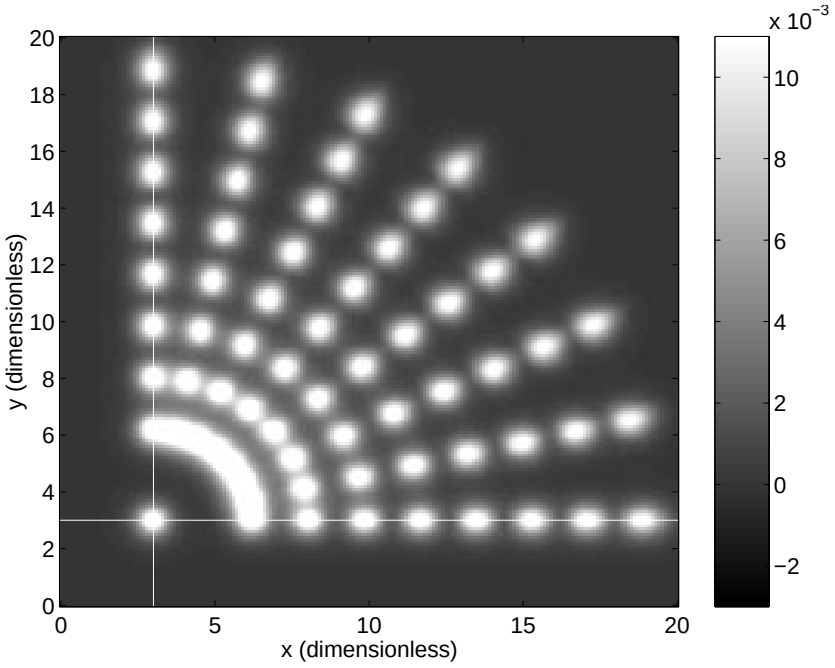

Fig. 65 — An energy field. The discontinuity is a result of the Garden Sprinkler Effect. All energy starts at the same location, shown in lower left corner ($x = y = 3$). Energy disperses as it propagates due to directional and frequency (i.e., speed) distribution of the initial spectrum. In this case, the initial spectrum consists of 8 frequency bins and 8 directional bins.

In polar coordinates, the anti-GSE equation is written as:

$$\frac{\partial}{\partial t}\overline{N}_{ij}(n,s,t)+\frac{\partial}{\partial s}[c_i\overline{N}_{ij}(n,s,t)]-\frac{\partial}{\partial s}[D_{ss}\frac{\partial}{\partial s}\overline{N}_{ij}(n,s,t)]-\frac{\partial}{\partial n}[D_{nn}\frac{\partial}{\partial n}\overline{N}_{ij}(n,s,t)]=0. \tag{63}$$

Converted to Cartesian coordinates (in which SWAN is written),

$$\begin{aligned}&\frac{\partial}{\partial t}\overline{N}_{ij}(x,y,t)+\frac{\partial}{\partial x}[c_{ijx}\overline{N}_{ij}(x,y,t)-D_{xx}\frac{\partial}{\partial x}\overline{N}_{ij}(x,y,t)]+\frac{\partial}{\partial y}[c_{ijx}\overline{N}_{ij}(x,y,t)-D_{yy}\frac{\partial}{\partial y}\overline{N}_{ij}(x,y,t)]\\&-2D_{xy}\frac{\partial^2}{\partial xy}\overline{N}_{ij}(x,y,t)=0,\end{aligned} \tag{64}$$

where

$$\begin{aligned}D_{xx}&=D_{ss}\cos^2\theta+D_{nn}\sin^2\theta\\D_{yy}&=D_{ss}\sin^2\theta+D_{nn}\cos^2\theta\\D_{xy}&=(D_{ss}-D_{nn})\sin\theta\cos\theta\end{aligned} \tag{65}$$

Here, "*s*" denotes frequency discretization, "*n*" denotes directional discretization, $\overline{N}$ is the average action density in a particular action bin, and T is "wave age," or the time elapsed since generation/initialization of the wave energy.

A few options exist for implementing diffusion in SWAN-X:

- use of a weighted mix of BSBT and SL1 schemes,
- use of an explicit diffusion scheme that calculates diffusion from Eq. (64) using information at the previous time level, or
- use of an implicit diffusion scheme that uses Eq. (64) and information at the current time level.

11.1 Use of Numerical Diffusion (BSBT)

This option would involve solving the propagation equations using both the BSBT scheme and the SL1 scheme. The averaging of the two schemes would be governed by a weighting factor that would be chosen based on consideration of the desired diffusion level (D_{xx}, D_{yy}, and D_{xy}) as well as the relative levels of numerical diffusion produced by the two schemes. This would be fairly simple to implement, but the diffusion of Eq. (64) would be impossible to reproduce accurately using numerical diffusion. Indeed, the representation could be quite poor.

11.2 An Explicit Diffusion Scheme

A finite difference representation of Eq. (64) could be added to the SL1 finite differencing in the model. If this finite difference scheme for diffusion is explicit (based on independent variables calculated at the previous time step), then the modification to the model would be minor. This alternative has the disadvantages with regard to accuracy and stability: fully explicit schemes tend to be inaccurate compared to schemes that use information at the current time level (e.g., centered fully implicit schemes); also, fully explicit diffusion schemes are invariably conditionally stable. Several explicit diffusion schemes were tested outside the model. One such scheme is given here. It was derived using Taylor series with the objective of using few points that are outside the numerical stencil used by the SL1 scheme (for the sake of convenience):

$$
\begin{aligned}
&\left\{\frac{\partial}{\partial t}\overline{N}_{ij}(x,y,t)+\frac{\partial}{\partial x}[c_{ijx}\overline{N}_{ij}(x,y,t)]+\frac{\partial}{\partial y}[c_{ijx}\overline{N}_{ij}(x,y,t)]\right\}\\
&-D_{xx}/12\Delta x^2(-N^{n-1}_{ix-3,jy}+4N^{n-1}_{ix-2,jy}+6N^{n-1}_{ix-1,jy}-20N^{n-1}_{ix,jy}+11N^{n-1}_{ix+1,jy})\\
&-D_{yy}/12\Delta y^2(-N^{n-1}_{ix,jy-3}+4N^{n-1}_{ix,jy-2}+6N^{n-1}_{ix,jy-1}-20N^{n-1}_{ix,jy}+11N^{n-1}_{ix,jy-1})\\
&-2D_{xy}/\Delta x\Delta y(N^{n-1}_{ix+1,jy}-N^{n-1}_{ix+1,jy-1}-N^{n-1}_{ix,jy}+N^{n-1}_{ix,jy-1})=0.
\end{aligned}
\tag{66}
$$

Here, the diffusion coefficients for each wave component are assumed uniform in space; this assumption would not necessarily be made in the actual model. Equation (66) was (empirically) found to be somewhat more accurate and stable than a setup that uses traditional lower order formulations for the $\partial^2 N/dx^2$ and $\partial^2 N/dy^2$ terms.

11.3 An Implicit Diffusion Scheme

The third alternative would be the addition of an implicit scheme. The four-quadrant algorithm used by SWAN requires that all computational points used at the current time level must be upwind. Unfortunately, no unconditionally stable, upwind, implicit diffusion schemes are known. Therefore, this option must be ruled out.

12. CONCLUSIONS

The higher order scheme "SL1," taken from Stelling and Leendertse (1992), was successfully implemented in an experimental version of SWAN ("SWAN-X"). The modified model has demonstrated greatly reduced diffusion in cases where diffusion presents problems for the original model. However, for many nearshore simulations, SWAN with the original (BSBT) scheme is more appropriate than is SWAN-X with the higher-order SL1 scheme.

Three primary factors support this argument:

1) The SL1-based model is relatively slow in stationary mode, because the model's system of equations cannot be solved by simply sweeping through the geographic grid points. Thus, the lower-order scheme should be used in stationary simulations for which the higher-order scheme does not offer significant benefit. Most small-scale simulations are conducted in stationary mode.
2) The original SWAN, which uses the BSBT scheme, is relatively inexpensive when used in the nearshore because fine geographic resolutions do not dictate fine temporal resolutions. SWAN-X with the SL1 scheme, though unconditionally stable, does not have this freedom from considerations of Courant number. Thus, when fine geographic resolution is required, smaller time step increments make the SL1-based model more expensive than the BSBT-based model. The time step size must be considered for the SL1-based model in both stationary and nonstationary mode.
3) The diffusion reduction of the SL1-based model is insignificant for many simulations on the continental shelf, because numerical diffusion at these scales tends to be small. The greatest benefit of the higher-order scheme would be felt more at oceanic scales. There are some notable exceptions to this, e.g., in the lee of islands, where diffusion is often a major concern.

Thus, in over-the-shelf simulations, the higher-order scheme can be used when numerical diffusion warrants it. This greater accuracy comes with a significant cost when the simulation is either stationary, or high resolution, or both. Fortunately, it is relatively easy to predict whether a simulation will exhibit high levels of diffusion, so a user can decide whether the potentially high computational cost is warranted.

Numerical diffusion of a geographic propagation scheme is caused by gradients of wave action across geographic grid points. The following factors lead to such gradients:

- nonstationary input,
- nonuniform input,
- obstacles in the model domain, and
- refraction-induced features (which are more severe at locations with rugged bathymetry or spatially varying currents).

Also note that broad wave spectra will tend make diffusion less noticeable in a waveheight field.

At oceanic scales, simulations are nonstationary and relatively nonuniform, making numerical diffusion a real concern. Nonstationary, low-resolution ($\Delta x > 10$ km) simulations can be run with the higher-order

scheme with very little added computational cost. Thus, the implementation of the higher-order scheme as an option in the official version of the model is one major step toward making SWAN a viable ocean-scale wave model.

ACKNOWLEDGMENTS

Thanks to Larry Hsu of the U.S. Naval Research Laboratory for helping to familiarize the first and second authors with the source code of SWAN, and for participating in discussions of the model. The authors would also like to thank Guus Stelling (Technical University of Delft) for suggestions dealing with implementation of his schemes in the model. Thanks to Michael Briggs (Coastal & Hydraulics Laboratory, U.S. Army Corps of Engineers) and Linwood Vincent (Office of Naval Research, ONR) for sharing their W.E.T. data. We are also grateful to Moshe Olim (FSI International) for taking the time to discuss his non-interpolating semi-Lagrangian scheme with us. We appreciate the direction of W.C. O'Reilly (Scripps Institute of Oceanography), the Lead Principal Investigator of this project. Dr. O'Reilly provided the Southern California Bight test case. The ONR Advanced Wave Prediction Program has funded this work.

REFERENCES

Birkemeier, W.A., "DELILAH Investigator's Report (draft)," Technical Report, Coastal Engineering Research Center, U.S. Army Corps of Engineers Waterways Experiment Station, Vicksburg, MS, 1991.

Birkemeier, W.A. and E.B. Thornton, "The DUCK94 Nearshore Field Experiment," *Proceedings of the Conference on Coastal Dynamics '94*, 815-821, 1994.

Berkhoff, J.C.W., N. Booij, and A. C. Radder, "Verification of Numerical Wave Propagation Models for Simple Harmonic Linear Waves," *Coastal Engineering* **6**, 255-279 (1982).

Booij, N. and L.H. Holthuijsen, "Propagation of Ocean Waves in Discrete Spectral Wave Models," *Journal of Computational Physics* **68**, 307-326 (1987).

Booij, N., L.H. Holthuijsen, and R.C. Ris, "The SWAN Wave Model for Shallow Water," *Proceedings, 25th International Conference on Coastal Engineering*, ASCE, Orlando, FL, 668-676, 1996.

Booij, N., R.C. Ris, and L.H. Holthuijsen, "A Third Generation Wave Model for Coastal Regions; Part I: Model Description and Validation," *J. Geophys. Res.* **104**(C4), 7649-7666 (1999).

Bouws, E. and G.J. Komen, "On the Balance Between Growth and Dissipation in an Extreme, Depth Limited Wind-Sea in the Southern North Sea," *J. Phys. Oceanography* **13**, 1653-1658 (1983).

Bretschneider, C.L., in *Shore Protection Manual*, CERC, U.S. Army Corps of Engineers, Tech. Rep. No. 4, 1973.

Fromm, J.E. "A Method for Reducing Dispersion in Convective Difference Schemes," *J. Comput. Phys.* **3**, 176-189 (1968).

Hasselmann, K., T.P. Barnett, E. Bouws, H. Carlson, D.E. Cartwright, K. Enke, J.A. Ewing, H. Gienapp, D.E. Hasselman, P. Kruseman, A. Meerburg, P. Muller, D.J. Olbers, K. Richter, W. Sell, and H. Walden, "Measurements of Wind-Wave Growth and Swell Decay During the Joint North Sea Wave Project (JONSWAP)," *Dtsch. Hydrogr. Z. Suppl.* **12**(A8), 1-95 (1973).

Jensen, R.E., "Interim Report on DUCK94 IOP-2; 3-22 October 1994; Wave Forecasting and Wave Measurement Activities," unpublished report (1995).

Johnson, J.W., "Refraction of Surface Waves by Currents," *Trans. Amer. Geophys. Union* **28**(6), (1947).

Kahma, K.K. and C.J. Calkoen, "Reconciling Discrepancies in the Observed Growth of Wind-Generated Waves," *J. Phys. Oceanography* **22**, 1389-1405 (1992).

Kirby, J.T., "Higher-order Approximations in the Parabolic Equation Method for Water Waves," *J. Geophys. Res.* **91**, 933-952 (1986).

Kirby, J.T. and R.A. Dalrymple, "Combined Refraction/Diffraction Model REF/DIF1, Version 2.5: Documentation and User's Manual," CACR Report 94-22, Center for Applied Coastal Research, University of Delaware, Newark, DE (1993).

Kirby, J.T. and H.T. Ozkan, "Combined Refraction/Diffraction Model for Spectral Wave Conditions: REF/DIF-S, Version 1.1: Documentation and User's Manual," CACR Report 94-04, Center for Applied Coastal Research, University of Delaware, Newark, DE (1994).

LeMehaute, B. and J.D. Wang, "Wave Spectrum Changes on Sloped Beach," *ASCE J. Waterways, Port, Coast. and Ocean Engineering* **108**, 33-47 (1982).

Leonard, B.P., "A Stable and Accurate Convective Modeling Procedure Based on Quadratic Upstream Interpolation," *Computer Methods in Applied Mechanics and Engineering* **19**, 59-98 (1979).

Mei, C.C., *The Applied Dynamics of Ocean Surface Waves* (Wiley, New York, 1983).

O'Reilly, W.C., and R.T. Guza, "A Comparison of Two Spectral Wave Models in the Southern California Bight," *Coastal Engineering* **19**, 263-282 (1993).

Olim, M., "A Truly Noninterpolating Semi-Lagrangian Lax-Wendroff Method," *J. Comp. Phys*. **112**, 253-266 (1994).

Petit, H., *Dissipation and Dispersion of Numerical Schemes for Hyperbolic Problems*, Delft Hydraulics, 1997.

Phillips, O.M., *The Dynamics of the Upper Ocean* (Cambridge University Press, New York, 1977).

Ris, R.C., *Spectral Modeling of Wind Waves in Coastal Areas,* Report No. 97-4, Department of Civil Engineering, Delft University of Technology, 1997.

Roache, P.J., *Computational Fluid Dynamics* (Hermosa, Albuquerque, 1972).

Stelling, G.S. and J.J. Leendertse, "Approximation of Convective Processes by Cyclic AOI Methods," *Proceedings, 2nd International Conference on Estuarine and Coastal Modeling*, ASCE, Tampa, Florida, 771-782, 1992.

SWAMP Group, *Ocean Wave Modeling* (Plenum Press, New York and London, 1985).

Tolman, H.L., "On the Selection of Propagation Schemes for a Spectral Wind-Wave Model," NWS/NCEP Office Note 411, 1995.

WAMDI Group, "WAM Model—A Third Generation Wave Prediction Model," *J. Phys. Oceanography* **18**, 1775-1810 (1988).

Whitham, G.B., *Linear and Nonlinear Waves* (Wiley, New York, 1974).

Wu, J., "Wind-Stress Coefficients Over Sea Surface Near Neutral Conditions: A Revisit," *J. Phys. Oceanography* **10***,* 727-740 (1980).

Wu, J., "Wind Stress Coefficients Over Sea Surface from Breeze to Hurricane," *J. Geophys. Res.* **87**(C12), 9704-9706 (1982).

Young, I.R. and L.A. Verhagen, "The Growth of Fetch Limited Waves in Water of Finite Depth. Part I: Total Energy and Peak Frequency," *Coastal Engineering* **29**, 79-99 (1996).

Appendix A
SWAN-X: CHANGES MADE TO THE MODEL

A1. CHANGES TO CODE

The following changes were made to the code, organized by file and subroutine. Irrelevant changes such as comment statements are not listed.

swanpre1.for:

SUBROUTINE SWREAD

- The code is altered such that the variable "AC1" is always used in "STEL" mode (i.e., when SL1 scheme is used).
- The "SCHEME" command is added to user input (see A2.1 below).
- The "COMPUTE" command is modified to read only Δt when in stationary mode with SL1 scheme.

swanmain.for:

SUBROUTINE SWMAIN

- There are 9 points in the numerical stencil when the SL1 scheme is used.
- The code is altered such that the variable "AC2" is always rolled back to "AC1" when in "STEL" mode.

swancom1.for:

SUBROUTINE SWCOMP

- In stationary SL1 mode, the wave action variable is rolled back after every iteration by calling the new subroutine ST_SNEXTI

SUBROUTINE SWOMPU

- Group velocity at previous time level is added to the variable list.
- Necessary points are added to numerical stencil if SL1 scheme will be used at given grid location.
- If in nonstationary SL1 mode, calculate group velocity at previous time step (unlike action variable, group velocity is not saved in memory, so must be calculated).
- If in stationary SL1 mode, set group velocity at previous time step equal to group velocity at current time step.
- If in SL1 mode, subroutine SPREDT is not called. This modification is not strictly necessary.

SUBROUTINE ACTION

- If in SL1 mode and not near grid boundary, call SANDL instead of STRSXY.

swancom5.for:

SUBROUTINE STRSXY

- When in "STEL" mode, action variable at explicit time level is always "AC1."

SUBROUTINE SANDL (new)

- This new subroutine performs the same function as subroutine STRSXY, but calculates gradients using SL1 scheme.

A2. CHANGES TO USER INPUT

A small number of changes were made to user input (provided to the model by the user in the file "INPUT"):

A2.1 "SCHEME" Command

```
                |—>BSBT     |
SCHEME      <               >
                |  STEL     |
```

With this option, the user specifies the numerical scheme to be used for geographic propagation. "BSBT" indicates that the classic first-order upwind implicit scheme will be used. "STEL" indicates that a higher-order, cyclic scheme will be used — the "$q_o = 0$, $q_1 = 1/6$" scheme of Stelling and Leendertse (1992). (Note: the BSBT scheme will be used at grid boundaries, regardless of this setting.) The STEL scheme is much less diffusive than the BSBT scheme. Thus, it should be used in cases where the wave field is highly non-uniform and/or when the model input is highly nonstationary. The STEL scheme is unconditionally stable and has been used successfully with Courant numbers higher than 50. However, the scheme often produces oscillatory behavior at high Courant numbers (CFL>>1), so it should be used with caution.

A2.2 "COMPUTE" Command

```
                        |—>SEC      |
COMPUTE  ([deltc]           <  MIN       > )
                        |  HR       |
                        |  DA       |
```

This change applies only to the model that uses "MODE STAT" and "SCHEME STEL." With this command, a time step size is specified. The begin and end times are unnecessary; the number of time step increments is specified as "itermax" in the command "NUM ACCUR."

A2.3 "NUM ACCUR" Command

```
NUMERIC ACCUR [drel] [dabs] [dtabs] [npnts] [itermax]
```

Specification of this command is unchanged. However, it should be noted that when in stationary mode while using the "STEL" scheme, the variable "itermax" refers to the number of time steps that the model will allow. Time steps are treated as iterations: at every time step, convergence is checked to determine whether the model has reached steady state. If the user desires multiple iterations at each time step, nonstationary mode should be used (note, however, that convergence is not checked in nonstationary mode).

A2.4 Caveats

When using "MODE STAT" and "SCHEME STEL," the two caveats described below apply.

Stelling, G.S. and J.J. Leendertse, "Approximation of Convective Processes by Cyclic AOI Methods," *Proceedings, 2nd International Conference on Estuarine and Coastal Modeling*, ASCE, Tampa, Florida, 771-782, 1992.

A2.4.1 Caveat #1

In cases where very small time increments are used, the model solution may change very little between time steps; there is a danger that the convergence criterion will pass as a result, causing the model to end prematurely. To avoid this, the user may specify "drel," "dabs," and/or "dtabs" to small values, or specify "npnts" to a high value (or set npnts > 100 to make convergence impossible).

A2.4.2 Caveat #2

When choosing "itermax" and the time step size Δt ("deltc"), the user should be cognizant of the resulting model duration — the wave energy should be given time to fully propagate and wind generation given time to produce a fully arisen sea condition.

Appendix B
DIFFRACTION IN SWAN

B1. INTRODUCTION

As mentioned in Section 2.2, the possibility of modifying SWAN to include diffraction explicitly is currently being considered. The questions central to the debate would be "when does diffraction make a large difference?" and "are these situations common enough to warrant modification of SWAN?" The most obvious examples of diffraction are associated with structures such as jetties, groins, and breakwaters. In these cases, it is clear that diffraction will move energy into the "shadow" region behind the structure. As there are no other physical processes that do this, clearly diffraction is important here. However, one might argue that simulations with structures such as this tend to be at small scale, where more rigorous models such as REF/DIF (Kirby and Ozkan 1994) and CGWAVE (Panchang et al. 1991)—both of which include diffraction implicitly—can be used instead of SWAN.

More common scenarios, such as a case of wave transformation on a nonplanar beach, are also affected by diffraction, as diffraction tends to smooth alongwave variations in waveheight, and create distinctive features in the waveheight field in locations where alongwave variation is especially severe. However, the impact of diffusion in such cases is sometimes not noticeable, due to multidirectional wave conditions "blurring" the effects of diffraction. The sensitivity of diffraction effects to wave conditions is not obvious. Therefore, a test case was used to determine this sensitivity. A lab experiment was available that was well suited for this: the "WET shoal" of Vincent and Briggs (1989).

B2. EXPERIMENT DESCRIPTION

This Vincent and Briggs experiment is a test case of wave transformation over an elliptical mound (with a constant 1.5-ft depth over the rest of the domain). A variety of irregular wave conditions were used. Input wave spectra were well documented, as were waveheights across the interior of the domain (especially within the shoal's region of influence). Figure B1 shows the bathymetry and gauge locations. The "non-breaking" series of the experiment were used for comparison to SWAN. A waveheight of 2.54 cm, a wave period of 1.3 s, and an incident wave direction of 0° were used for all cases in this series; Table B1 shows the spectral wave characteristics.

In this experiment, refraction creates a region of energy focusing directly behind the shoal. Diffraction acts on this refraction-induced feature. To demonstrate the capability of a phase-resolving model to simulate diffraction implicitly, the monochromatic case (M2) and near-monochromatic case (U4) are compared to REF/DIF1 (Kirby and Dalrymple 1993). The model does an extraordinary job of capturing the two diffraction-induced features adjacent to the central refraction-induced feature. The absence of diffraction is apparent in the SWAN result for the near-monochromatic case (Fig. B2). However, the model seems to suffer from the omission of diffraction only for the least realistic, monochromatic cases (Fig. B3).

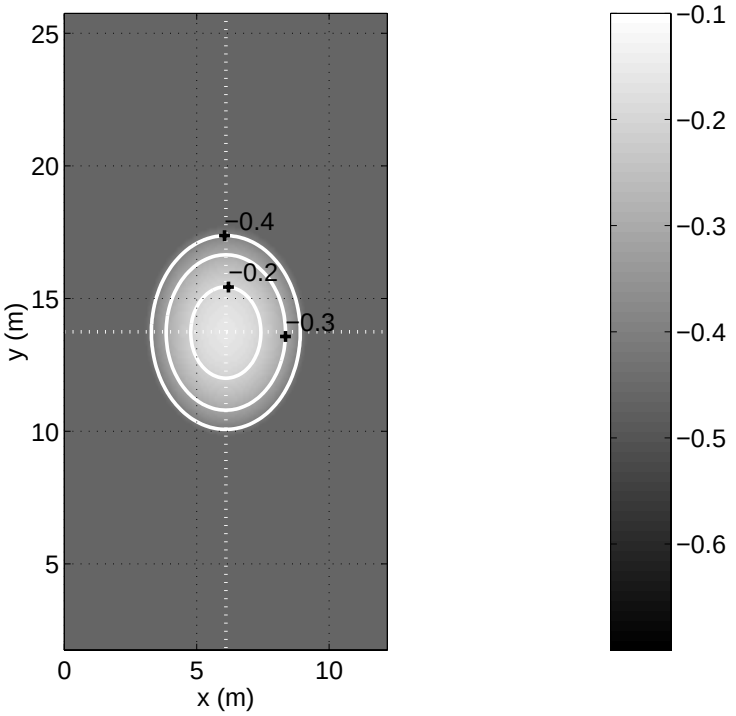

Fig. B1 — Bathymetry and gauge locations for the Vincent and Briggs shoal experiment

Table B1 — Spectral Characteristics of the Nonbreaking Series of Vincent and Briggs (1989)

Case ID	*Directional Spectrum*	*Frequency Spectrum*
M2	Unidirectional	Monochromatic
U3	Unidirectional	Broad
N3	Narrow	Broad
B3	Broad	Broad
U4	Unidirectional	Narrow
N4	Narrow	Narrow
B4	Broad	Narrow

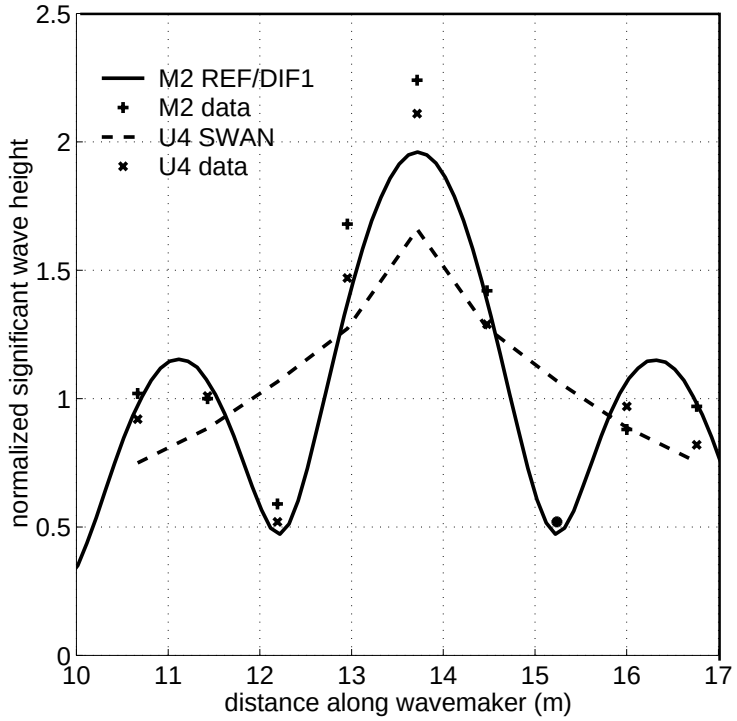

Fig. B2 — Comparison of normalized waveheights along a lateral transect behind the shoal. REF/DIF1 output is compared to the monochromatic case and SWAN output to the near-monochromatic case.

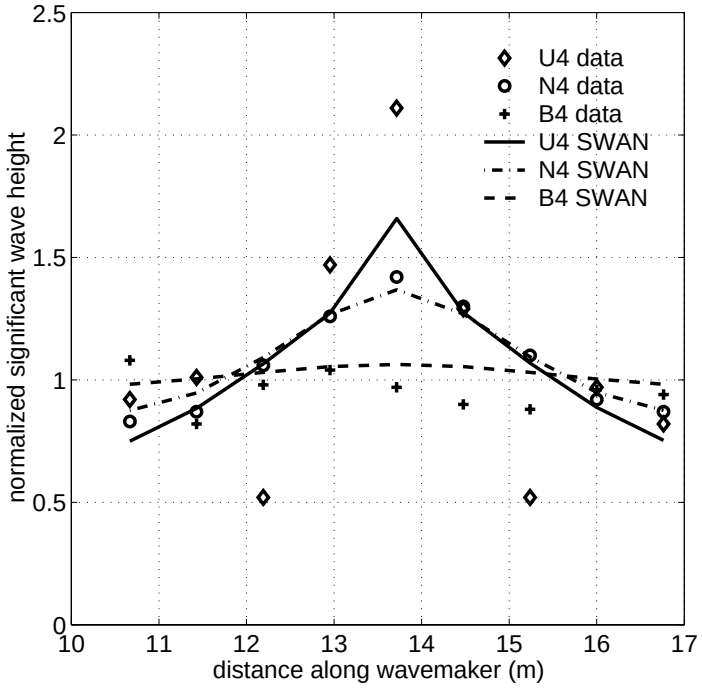

Fig. B3 — Comparison of normalized waveheights along a lateral transect behind the shoal. SWAN output for the six of the nonbreaking wave conditions are compared to corresponding data.

B3. CONCLUSION

This is merely a single, simple experiment of diffraction on a nonplanar bathymetry. However, it suggests that under realistic, multidirectional wave conditions, and in the absence of wave-blocking structures, diffraction has only a minor impact on gross energy estimates.

When information is needed beyond simple energy estimates, the inclusion of diffraction may be a serious consideration. One would expect the impact of diffraction on directional distributions of wave energy to be nontrivial in many cases. Also, if phase-related information is needed, e.g., wave asymmetry, the use of a phase-resolving model that includes diffraction is clearly necessary.

REFERENCES

B1. Kirby, J.T. and R.A. Dalrymple, "Combined Refraction/Diffraction Model REF/DIF1, Version 2.5: Documentation and User's Manual," CACR Report 94-22, Center for Applied Coastal Research, University of Delaware, Newark, DE (1993).

B2. Kirby, J.T. and H.T. Ozkan, "Combined Refraction/Diffraction Model for Spectral Wave Conditions: REF/DIF-S, Version 1.1: Documentation and User's Manual," CACR Report 94-04, Center for Applied Coastal Research, University of Delaware, Newark, DE (1994).

B3. Panchang, V.G., W. Ge, B. Cushman-Roisin, and B.R. Pearce, "Solution to the Mild Slope Wave Problem by Iteration," *Applied Ocean Research* **13**, 187-199 (1991).

B4. Vincent, C.L. and M.J. Briggs, "Refraction-Diffraction of Irregular Wave Over a Mound," *Journal of Waterway, Port, Coastal, and Ocean Engineering* **115**(2), 1989.

Appendix C
RECENT DEVELOPMENTS — STATIONARY HIGHER-ORDER SCHEMES

C1. INTRODUCTION

Although a pseudo-stationary mode for SWAN-X w/SL1 was successfully implemented (Section 4.3.1), it is clear that the SL1 scheme is not suited for stationary computations. Due to the downwind point in its numerical stencil, the scheme, operating at a single time level, cannot simply sweep through the geographic grid. The pseudo-stationary method of time-stepping until steady state is impractical due to the large number of time steps typically required. Iterative methods for a stationary SL1 scheme have proven unreliable. Thus, we have endeavored to find a scheme more suited for stationary calculations.

C2. TESTS OF STATIONARY SCHEMES OUTSIDE OF SWAN

Because we wanted to avoid the use of iterative methods, we imposed a requirement on the new scheme: it would need to be entirely upwind. We compared the results of simple models based on various upwind schemes to exact solutions for the case of a submerged breakwater with gap (since we were not interested in nonstationary calculations, a large set of test cases was not necessary). Tests were similar in setup to those shown in Figs. 1 and 24 of the body of this report. Results were compared to the exact solutions along the "high-x" open boundary.

Some of the more notable contenders:

1) the implicit half (i.e., the upwind stage) of the SL1 scheme,
2) a scheme derived from Taylor Series, with three upwind points in the stencil,
3) the Box scheme,
4) the Second ORder UPwind Implicit scheme (Section 3.1.2.2), "SORDUPI,"
5) the one-dimensional NISL scheme (Section 3.1.2.10), made two-dimensional and stationary by replacing the time dimension with a second space dimension, and
6) same as (5), but using the SL1 scheme.

Of schemes (1) through (4), scheme (4) displayed the least severe numerical oscillations and the most severe numerical diffusion (see Fig. C1). As numerical oscillations were deemed to be more of a concern than diffusion (given the fact that all four were much less diffusive than the BSBT scheme), scheme (4) was judged the most favorable of these four schemes.

Of the two "traded" schemes (5 and 6), the NISL scheme is clearly more accurate (e.g., Fig. C2); in fact, it was the most accurate scheme tested. However, there are potential difficulties associated with the NISL scheme:

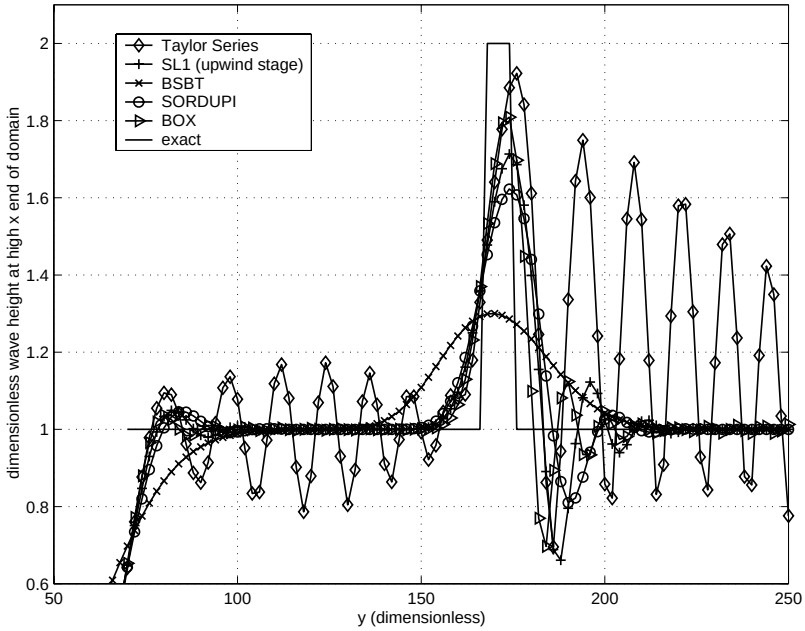

Fig. C1 — Result from several stationary models of the submerged breakwater with gap test case, compared to exact solution. Six propagation angles were tested; the result for theta = 35 degrees is shown here. Distance is nondimensionalized by Courant number.

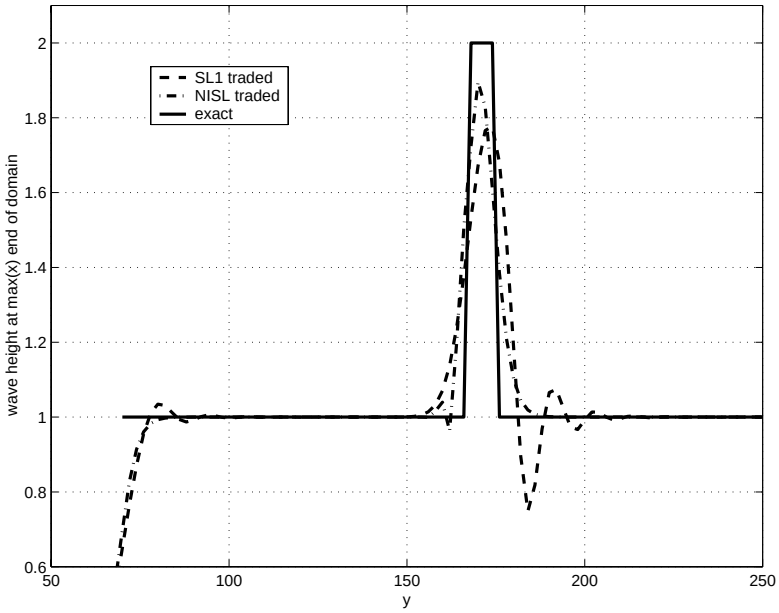

Fig. C2 — Result from two stationary models of the submerged breakwater with gap test case, compared to exact solution. These two models are based on the two "traded" numerical scheme. Six propagation angles were tested; the result for theta = 35 degrees is shown here. Distance is nondimensionalized by Courant number.

a) The variable numerical stencil of the NISL scheme is dependent on the "traded" Courant number (e.g., CFL = $(C_{gx}\Delta y)/(C_{gy}\Delta x)$). The subroutine structure of SWAN does not presently allow for this, so nontrivial changes to the code would be necessary. Also, at a given geographic grid location, the numerical stencil for geographic propagation varies in spectral space. NISL would require considerably more RAM, due to the need to store C_{g_x} and C_{g_y} for every stencil (note that with the dynamic memory of Fortran90, this would be less of a concern).
b) It is uncertain how well NISL would perform for large Courant numbers when C_g varies along the characteristic used by this semi-Lagrangian scheme. Numerical experiments suggest serious problems with mass conservation for such cases.

In contrast, the SORDUPI scheme appeared simple to implement in SWAN, with no potential drawbacks. Therefore, a second experimental version of SWAN ("SWAN-XX") was created that uses the SORDUPI scheme. Implementation of NISL in SWAN is still a possibility, but has not yet been undertaken.

As of this writing, there are four schemes that are either already in SWAN or still being considered for inclusion in SWAN. Based on the breakwater tests described above, the four schemes were scored based on average amplitude preservation (note that this scoring does not take phase error into account) as shown in Table C1.

Table C1 — Stationary Breakwater with Gap Test: Amplitude Preservation

Scheme	Amplitude Preservation (%)
BSBT	28
SORDUPI	55
SL1 (nonstationary; with a small time step)	69
NISL	76

C3. SOUTHERN CALIFORNIA BIGHT

The SORDUPI-based model was applied to the Southern California Bight test case (Section 5.8). Computation times for this model were encouraging. The SORDUPI scheme uses the same simple sweeping technique as that used by the BSBT-based model. No iterations are required for geographic propagation (although some are required for spectral propagation). The additional math operations used by the second-order scheme increased computation time by approximately 10% per iteration. However, in the 100-m-resolution case, this was offset by the slightly lower average number of iterations required by the SORDUPI model. Table C2 compares the total computation times on an Ultra60 (360 MHz) Sun workstation with the different schemes and geographic resolutions.

Outputs of the models were compared at the locations of the four pressure gauges. Error in the SWAN model results at gauge 10 (the gauge in the lee of San Miguel Island) is dominated by diffusion effects and, therefore, provides a good indication of relative diffusivity of the models. The results are as expected: at equivalent resolution, the SL1 scheme is somewhat less diffusive than the SORDUPI scheme, which is in turn much less diffusive than the BSBT scheme (Fig. C3).

Table C2 — Southern California Bight: SWAN Computation Times

Scheme	**Resolution (Δx and Δy)**	**Total computation time***
BSBT	100 m	27 hours, 34 minutes
SORDUPI	100 m	27 hours, 27 minutes
SL1	100 m	Approximately 5 months (this set was not completed)
BSBT	200 m	7 hours, 7 minutes
SORDUPI	200 m	8 hours, 7 minutes
SL1	200 m	Approximately 19 days
BSBT	400 m	1 hour, 51 minutes
SL1	400 m	55 hours, 15 minutes

* Durations given are totals: 27 simulations were performed with each model

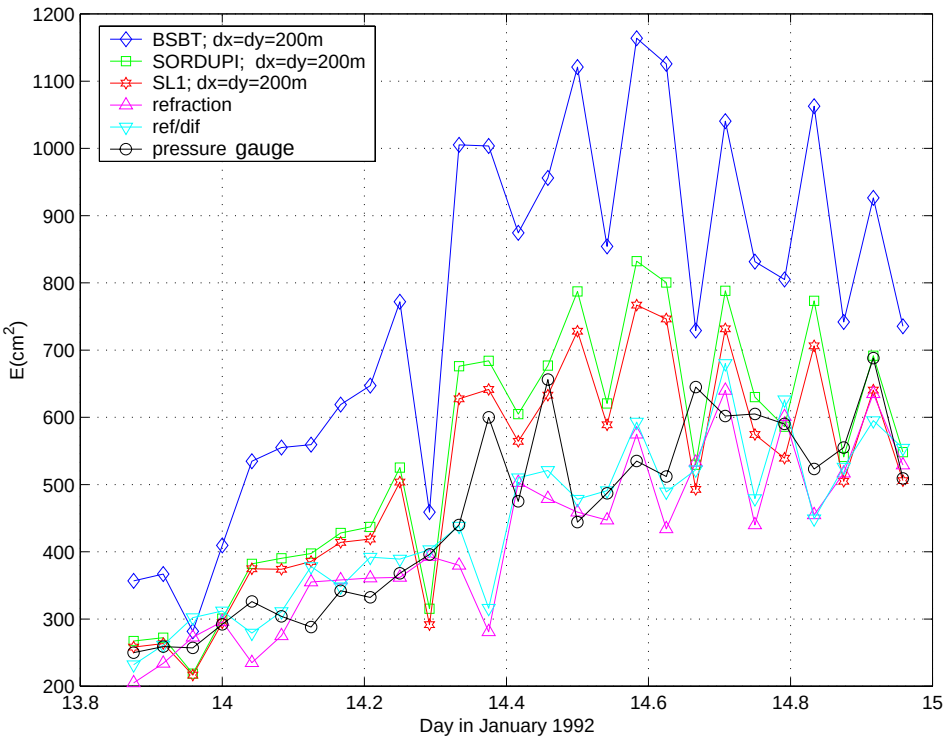

Fig. C3 — Time series comparisons of models to data for the Southern California Bight case. Here, SWAN models of equivalent geographic resolutions are compared.

When models of approximately equivalent computation time are compared, the SORDUPI scheme is most accurate (Fig. C4). The SL1-based model had to be run at a grid resolution of $\Delta x = \Delta y = 400$ m in order to finish within a reasonable time period. At this resolution, the SL1-based model suffered from significant diffusion (and perhaps other resolution-related effects).

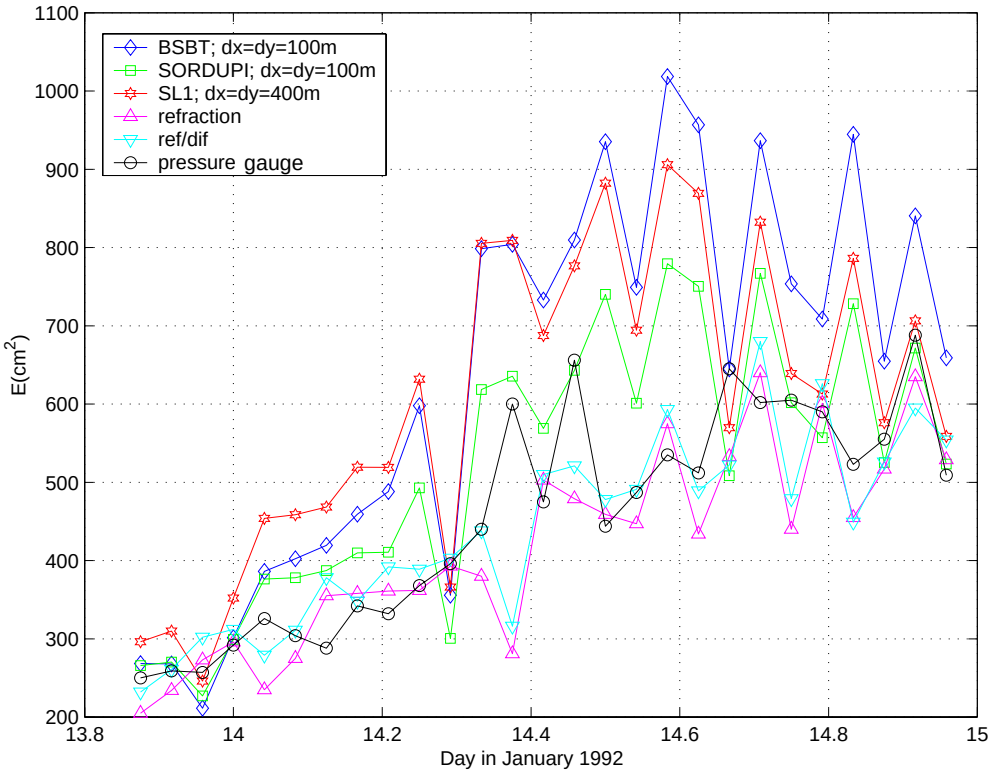

Fig. C4 — Time series comparisons of models to data for the Southern California Bight case. Here, SWAN models of approximately equivalent computational requirements are compared.

C4. CONCLUSION

The current version of SWAN-X has two schemes available for geographic propagation: the BSBT scheme (which is very diffusive) and the SL1 scheme (which is not suited for stationary computations). Thus, for stationary, diffusion-prone simulations, a second alternative is needed. The second-order upwind implicit (SORDUPI) scheme was tested and results look promising.

A model using the SORDUPI scheme would be much less diffusive than the BSBT-based model. It would be somewhat more diffusive than the SL1 model, but unlike the SL1 model, is economical. In fact, it is probably no more expensive than the BSBT model. Nonphysical oscillation with the scheme appears to be well within acceptable levels. Thus, the SORDUPI model is a much better choice for a large majority of stationary computations than either the BSBT scheme or the SL1 scheme.